2009

The mechanics of defect detection in vibrothermography

Jeremy Blake Renshaw
Iowa State University

The mechanics of defect detection in vibrothermography

by

Jeremy Blake Renshaw

A dissertation submitted to the graduate faculty

in partial fulfillment of the requirements for the degree of

DOCTOR OF PHILOSOPHY

Major: Materials Science and Engineering

Program of Study Committee:
Stephen D. Holland, Co-major Professor
R. Bruce Thompson, Co-major Professor
Theodore J. Heindel
Ralph E. Napolitano
Ersan Ustundag

Iowa State University

Ames, Iowa

2009

DEDICATION

I would like to dedicate this dissertation to my wife Rachel, who has been my support and companion, my children who have been my inspiration, and my parents who have been the motivation for this work. Without all of their support, I would not have been able to complete this work.

TABLE OF CONTENTS

LIST OF TABLES

LIST OF FIGURES

LIST OF SYMBOLS

a - half of semielliptical surface crack length (crack length from -a to +a)

+a/-a - location of crack tips

$\hat{a}$ - vibrational test specimen reference x direction

A - area

b - thermal parameter ($\sqrt{\rho c_p k}$)

$\hat{b}$ - vibrational test specimen reference y direction

c_p - specific heat

$\hat{c}$ - vibrational test specimen reference z direction

C - degrees Celsius

E - Young's Modulus

f - body force

F - degrees Fahrenheit

F_{clamp} - Clamping force

i - imaginary number (square root of negative 1)

I - second moment of area

k - thermal conductivity

K - degrees Kelvin

K_I^t - Stress intensity factor for Mode I crack growth

$\hat{l}$ - vector direction of the laser in the laser vibrometer

L - characteristic length

m - meters

mm - millimeters

M_b - bending moment

n_i - unit normal to the surface

ρ - density

r - radius

R - equivalent radius of contact

R_a - roughness parameter - average height of profile

R_c - roughness parameter - mean height of profile irregularities of primary profile

R_{max} - roughness parameter - maximum peak to valley height of primary profile in sampling length

R_p - roughness parameter - maximum peak height of primary profile

R_q - roughness parameter - RMS height of profile

R_t - roughness parameter - maximum peak to valley height of primary profile

R_v - roughness parameter - maximum valley height of primary profile

R_z - roughness parameter - mean peak to valley height of primary profile

s - second

σ_{xx} - stress on x face in the x direction

$\sigma_{xx}(y)$ - stress between crack faces along the crack surface (assumed to be in y-direction)

$\sigma^p_{xx}(y,0)$ - surface plastic closure stresses along a crack

σ_{pp} - peak to peak vibrational stress

t - time

T_f - maximum asperity flash temperature

T_{VMF} - temperature of VMF synthetic defects

τ_{ij} - stress tensor

$\tau^{G:X}_{ij}$ - Greens function stress with an impulse applied at X

u_j - displacement in the j direction

$\ddot{u}_j$ - acceleration in the j direction

$u_{j:k}^{G:X}$ - Greens function displacement in the j direction due to an impulse force at X

μ - coefficient of friction

μm - micrometers

ν - Poisson's ratio

V - volume

V_1 / V_2 - velocities of sliding contacts

ω - angular frequency

W - load

x - x-axis coordinate

$\hat{x}$ - x-axis coordinate of table reference in vibrometry scans

X - location of impulse force

y - y-axis coordinate

$\hat{y}$ - y-axis coordinate of table reference in vibrometry scans

y_t - location(s) of heat generation along a crack

z - z-axis coordinate

$\hat{z}$ - z-axis coordinate of table reference in vibrometry scans

ACKNOWLEDGEMENTS

This material is based upon work supported by the Air Force Research Laboratory under Contract #FA8650-04-C-5228 at Iowa State University's Center for NDE.

I would like to thank my major professors, Drs. Stephen D. Holland and R. Bruce Thompson, who have guided this work and provided valuable insights and ideas to help my research progress. I would like to thank my program of study committe, Drs. Theodore Heindel, Ralph Napolitano, and Ersan Ustundag, who have have helped to shape this dissertation. I would like to thank Christopher Uhl who provided many important contributions and suggestions throughout this work. I would like to thank Jake Auliff who provided significant materials processing and analysis equipment as well as advice for this research. Finally, I would also like to thank the many other CNDE staff and students who have helped this work along the way, though they are too numerous to name and a partial list would not suffice. Without their help, this research would not have been possible.

ABSTRACT

Vibrothermography is a nondestructive evaluation (NDE) technique that is used to detect surface and sub-surface defects such as cracks, disbonds, and delaminations through observations of vibration-induced frictional heat generation at defects. Frictional heating is observed using an infrared (IR) camera and is used to determine the presence and location of defects. There is a large industrial interest in vibrothermography due to its ability to rapidly detect defects over a large area. Another motivation for using this technology is its ability to find defects, such as tightly-closed cracks, that can be missed using other common NDE techniques. A major hindrance to the widespread application of vibrothermography has been an inability to quantify the reliability and capability of the inspection due to insufficient knowledge of the underlying physics of vibrothermography.

The purpose of this work is to further understand the physics controlling defect detection in vibrothermography. The influence of vibration was studied through the use of synthetic defects and noncontact measures of vibration. Numerous samples of aluminum, brass, titanium, and carbon fiber-reinforced polymer composites were used to study the physics of heat generation to isolate the different sources of heat generation in metals and composites. The effects of crack closure on heat generation were studied and a method was developed to accurately measure crack closure stresses using vibrothermography. Finally, the effect of friction and heat generation on rubbing crack faces was observed using techniques such as profilometry, optical microscopy, and scanning electron microscopy. This work describes some of the fundamental parameters affecting

heat generation and methods to improve defect detection reliability. This research provides a foundation for creating statistical models to improve the defect detection process using vibrothermography.

CHAPTER 1. OVERVIEW

Vibrothermography is a nondestructive evaluation (NDE) technique that is used to detect surface and sub-surface defects such as cracks, disbonds, and delaminations through observations of heat generated when these defects vibrate. Vibrating interfaces, such as crack faces, rub together and generate frictional heat. An infrared (IR) camera observes the heat generated on the surface of the structure to determine the presence and location of defects. There is a large industrial interest in this technique due to its ability to rapidly detect defects over a large area in timescales on the order of a few seconds Han, X. (2004A). Another reason driving the interest in this technology is its ability to find defects that can be missed using other common NDE techniques, such as fluorescent penetrant inspection (FPI) DiMambro, J. (2007); Renshaw, J. (2009B). Another advantage of vibrothermography is that inspected parts often do not need to be cleaned or have coatings stripped off for the method to be effective. Vibrothermography is sensitive to cracks, disbonds, and delaminations while being largely insensitive to many surface features such as scratches, high surface roughness, etc. that may cause false indications when using other NDE inspection methods. For a defect to produce a distinguishable heat signature, the defect must have a contacting interface that can rub when the structure containing the defect is vibrated. Vibrothermography, therefore, is not sensitive to certain types of defects, such as porosity, pitting, and corrosion as well as most types of synthetic defects (i.e. flat-bottom holes or EDM notches) since they do not have a contacting surface.

A major hinderance to the widespread application of vibrothermography is a lack of

repeatability. Repeatability is vital for any NDE inspection technique to be considered accurate and reliable. This dissertation first details a process developed to manufacture synthetic defects that can be used for vibrothermography. Synthetic defects are useful in nondestructive evaluation for simulating the presence of defects in structures. The research conducted using synthetic defects shows the importance of the vibrational profile (mode shape) for crack detection. Next, the different sources of heat generation in vibrothermography are presented along with experimental evidence of each source. The effect of crack closure on heat generation is shown in addition to a method to measure crack closure using vibrothermography. Finally, it is shown that excessive levels of vibrational stress applied to crack faces can irreversibly alter rubbing crack faces which reduces the repeatability of the vibrothermographic signal.

1.1 Introduction

Thermography is the process of imaging the surface temperature of an object. An infrared (IR) camera is generally used to measure and image the surface temperature of the object(s) under investigation. In the world of science and engineering, thermography has many uses. IR cameras can be used for energy auditing to image regions of a house or building that have poor or insufficient insulative properties. Thermography can be used in medicine to image certain types of tumors or detect the early onset of a disease. IR cameras are also used for night vision applications in addition to having many other potential applications. The examples above are of passive thermography, or observing an object without interacting with it. Vibrothermography is a form of active thermography which combines thermography with a vibrational stimulus applied to the object under observation where the vibration is intended to generate heat at defects.

Vibrothermography was originally developed by Henneke et al. Henneke, E. G. (1986) in the 1970's to inspect composite materials for delaminations. Large tempera-

ture variations were observed and measured around delaminations in composites due to both the heat generated at the delaminations and the low thermal conductivities of the polymer-based materials. An important discovery of this early work was that heat was most efficiently generated when the structure was vibrated at resonance. Due to the limitations of infrared sensing technology, only large temperature variations could be observed. This meant that materials with high thermal conductivities, such as metals, could not be accurately inspected because they quickly diffuse heat away from any heat generation source, such as a vibrating defect, preventing the large temperature differences needed for contemporary IR cameras. Therefore, this method was not widely used for many years since most contemporary engineering materials were metals.

Advances in IR cameras in the 1990's brought new capability for remotely sensing minute variations in surface temperatures and brought about a renewed interest in vibrothermography. A research group at Wayne State University Han, X. (2004A) began researching applications for vibrothermography. Instead of relying on resonant excitation, they used single frequency (20 or 40 kHz) ultrasonic generators or welders, originally designed for welding plastics, to generate high-amplitude vibrations. Their research focused on improving defect detection by intentional nonlinear contact to generate hammering between the specimen and excitation system to generate resonant vibrations throughout a structure. Such nonlinear, and potentially chaotic, excitation methods have been effective in finding defects in many materials, including metals Morbidini, M. (2006).

The first major concern with using chaotic excitation methods is that chaos is, by definition, not repeatable. The non-repeatability of chaos only exacerbates the problems with repeatability. Though ultrasonic welders have proven to be effective in finding cracks in many different structures, this excitation method can often miss cracks when the necessary structural resonances are not excited Lively, J. (2008); Renshaw, J. (2009A). To better understand the relationship between vibration and heat generation,

Morbidini et al. have developed a method to estimate the amount of heat generated by a crack when the structure containing the crack is vibrated Morbidini, M. (2006). These estimates are based on measures of vibration damping of an undamaged structure compared to the additional vibration damping in a damaged structure due to the presence of a crack in the structure. Such measures have provided quantitative numbers that reasonably predict the amount of heat generated by a specific crack based on the excitation parameters and measures of vibration.

The second major concern with the ultrasonic welder excitation system is the potential for vibrothermography to transition from a nondestructive to a destructive testing method where the excitation can actually induce additional bulk damage and reduce the fatigue life of a structure. The high amplitude vibrations of the ultrasonic welder have been shown to cause plastic deformation at the contact point between the welder and the sample Lively, J. (2008) and even crack growth Chen, J. C. (2007); Lively, J. (2009).

To prevent bulk structural damage from vibration, a different excitation system has been developed and implemented at Iowa State University. This system uses a broadband piezoelectric stack transducer Holland, S. D. (2007A) capable of exciting vibrations over a broad range of frequencies (from about 0.1 to 32 kHz) to increase the number of structural resonances that can be excited in inspected structures. This system allows the user to tune the vibrational source to excite specific structural resonances as was done in the early work of Henneke. Excitation at resonance couples energy more efficiently into a structure and allows for lower power consumption and reduced risks of damage to the excited structures. To date, no cracks have propagated using the Iowa State University transducer system Renshaw, J. (2009D).

A typical experimental setup for the vibrothermographic experiments conducted as part of this research is shown in Figures 1.1 and 1.2. The piezoelectric transducer is used to excite a broad range of frequencies in a structure. A pneumatic cylinder is

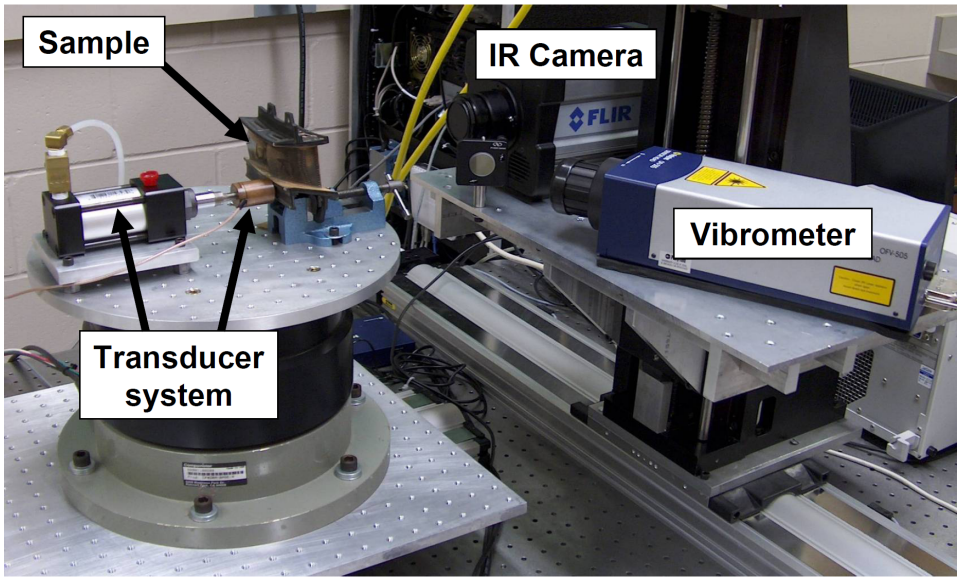

Figure 1.1 General experimental test setup used for vibrothermographic experiments.

used to press the piezoelectric transducer against a specimen to maintain contact during the duration of an excitation pulse. This prevents hammering action on the specimen's surface and harmonic generation. Paper, typically a business card or piece of cardstock, is used as a coupling material between the piezoelectric transducer and the specimen to maintain linear contact between the two and prevent surface damage to the specimen. The laser vibrometer is used to measure the motion of the specimen using the Doppler shift of the reflected beam from the specimen's surface while an infrared camera observes the surface of the specimen. A 640 X 512 pixel infrared camera is used to observe the sample surface with a frame rate of 91.5 Hz. The IR camera pixels have a sensitivity of 20 mK. Clamps are used to hold the specimen in place during excitation and inspection. Rubber mounts are used between the specimen and the clamps to minimize the effect of the mounting on the structural vibrations of the specimen.

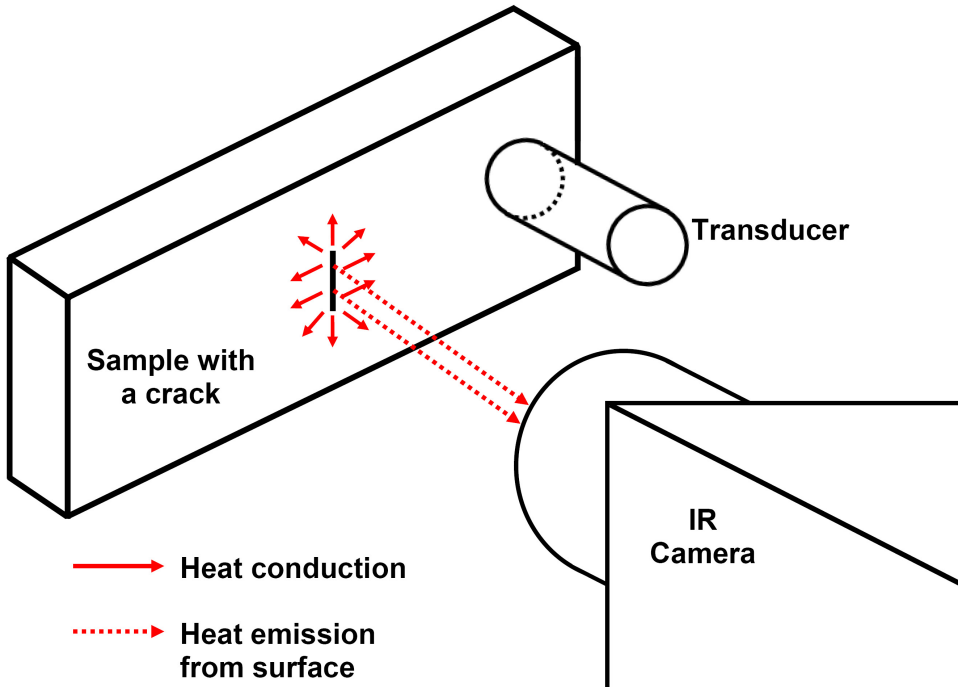

Figure 1.2 The heat generation process in vibrothermography. First, the part is vibrated causing crack faces to rub and generate heat. Heat diffuses away from the crack and is emitted from the sample surface(s). An infrared camera is used to observe any changes in surface temperature to detect the presence of defects.

1.2 Process of Vibrothermographic Measurements

The process of taking measurements using vibrothermography includes three primary steps. They are vibration, heat generation, and heat detection. Figure 1.3 shows an overview of these three steps of vibrothermographic measurements and their influence on defect detection in vibrothermography. Energy, in the form of motion or vibration, must be input to the system to interact with any defect present in the structure. Next, heat is generated at the crack or flaw due to friction or some other heat-generating mechanism. Heat generation will depend on many factors associated with the vibration and the crack or flaw itself. Once heat is generated, it will diffuse away from the source via conduction and radiate from any external surface where it can then be detected using an IR camera.

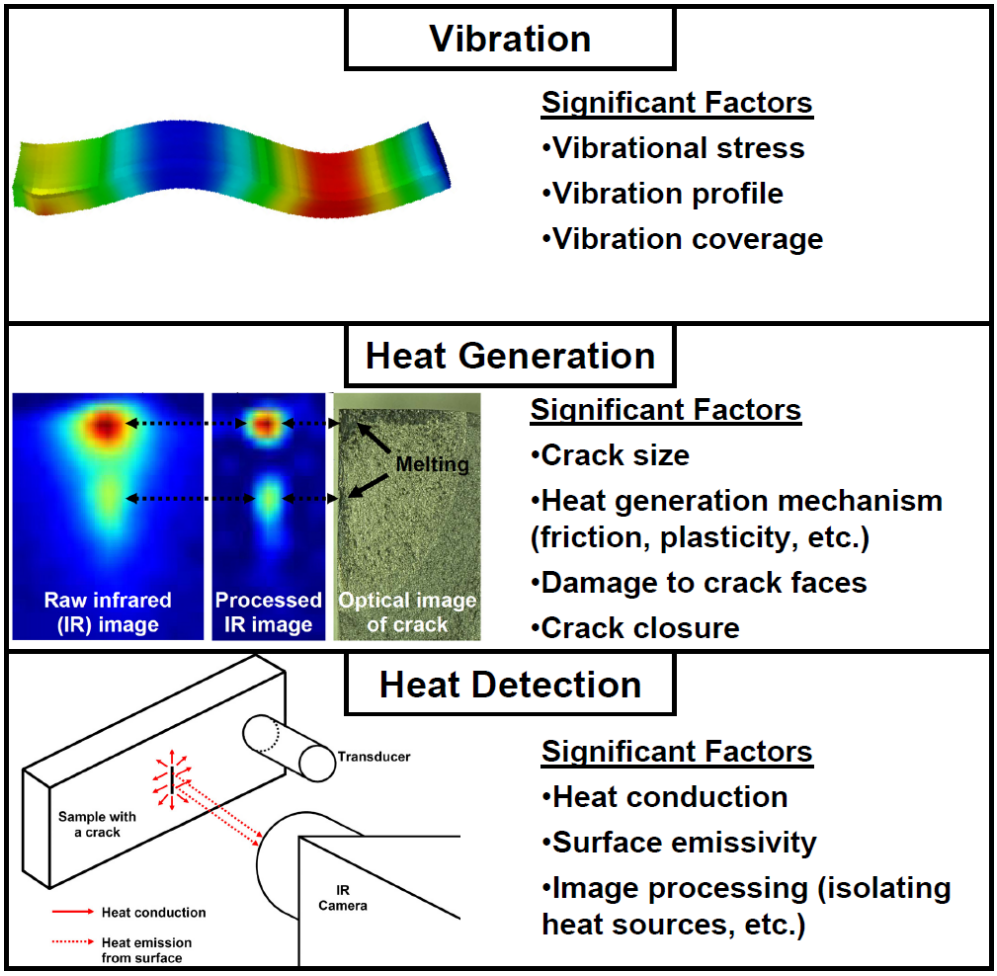

Figure 1.3 Figure showing the primary physical mechanisms (vibration, heat generation, and heat detection) controlling defect detection using vibrothermography. Each mechanism section also details its primary controlling factors as related to vibrothermography.

All three steps (vibration, heat generation, and heat detection) must operate together. If there is any disconnect between steps then defects present in the structure will not be observed. Each step has a significant impact on the observed heating. For example, defect surfaces must rub together for frictional heating to occur. Without vibration, no relative movement will occur, so no heat will be generated. Larger defects have larger surfaces available to rub together, and therefore will generate more heat than smaller defects. If the rubbing surfaces are too small, then the heat that the defects gen-

erate will be below the IR camera's detection threshold. Finally, the thermal properties of the sample are also important. Thermal properties, such as a low surface emissivity (generally evidenced by a shiny or reflective surface), can mask even significant heat generation in a structure. A high thermal conductivity will diffuse heat away from a defect rapidly, requiring a higher heat generation rate in materials with high thermal conductivities, such as metals, than in materials with a low thermal conductivity, such as polymers and ceramics. Thus, many factors, including those mentioned above, are important to consider when studying vibrothermography.

1.3 Vibration

Vibration is the first factor that controls frictional heat generation in vibrothermography. Simply stated, friction requires both contact and relative motion between two bodies. Vibration is used to supply the required motion to generate frictional heating.

The ISU transducer system allows the user to specify the frequency or range of frequencies to use during testing. By tuning the transducer properly, the user can focus on specific sample resonances. It is best to use natural sample resonances for testing since the mode shape (profile of vibration) is either known or can be easily measured. Second, structures "like" to vibrate at resonance, meaning that the energy conversion efficiency between the transducer and the structure is highest at resonance. Next, resonances will have specific nodes (minima of vibration) and antinodes (maxima of vibration). By placing mounts (i.e. clamps) at the nodal points, the mounting itself will have a minimal effect on the overall specimen vibration.

The excited vibrational mode shape also controls heat generation in a structure. A defect located at or near a location with high vibrational stress, such as a vibrational stress antinode has a higher probability to be detected than an identical defect located near a vibrational stress node. This is demonstrated through the use of synthetic, or

artificial, defects. By creating an array of synthetic defects across a structure, coverage analysis can be performed to understand which modes of vibration will give adequate detection coverage in a structure.

1.3.1 Synthetic defects

Synthetic defects are widely used to characterize NDE techniques since they are easier, cheaper, and more repeatably manufactured than natural defects, such as cracks; however, no suitable synthetic defects existed for vibrothermography. Chapters 2 and 3 detail a method developed to create and characterize viscous material-filled (VMF) synthetic defects for use with vibrothermography. These synthetic defects rely on viscoelasticity to generate heat and can be easily and repeatably manufactured in a wide variety of materials for vibrothermographic testing Renshaw, J. (2009A). The heating response of these defects was measured and compared to that of cracks. Additionally, application examples are shown to highlight both the usefulness of these synthetic defects and to show how vibration controls heat generation in vibrothermography.

1.3.2 Vibration measurement

Crack detection using vibrothermography is dependent on the location of the defect within the vibration profile of the excited mode shape(s) in a structure. If a crack is located at a nodal point of a resonant mode, the lack of motion at the nodal point prevents motion, and therefore heat generation at the defect. Thus, it is important to understand the complete vibration profile of resonant modes of a structure and how the vibration profile of each resonant mode influences the heat generation and detection of defects throughout the structure. This means that for a defect located at the node of one excited resonant mode, a different excitation frequency is needed to excite other resonant modes where the defect is no longer located at a vibrational node Uhl, C. J. (2008).

Chapter 4 outlines the process of measuring the 3-Dimensional stresses, strains, and displacements of a vibrated sample by using measurements of the 3D vector surface velocities of a sample Holland, S. D. (2007B); Renshaw, J. (2009B). Similar experiments have been done to measure the stresses and strains normal to rubbing crack faces and then relate them to crack heating Holland, S. D. (2008). Using the measured vibrations, it is possible to evaluate the resonant mode shapes and resonant frequencies of a structure. Using this data, it is possible to determine which resonance(s) must be excited in a structure to detect defects at specific locations within a structure.

1.4 Heat Generation

Heat generation in a crack has long been assumed to be a result of friction, though no experimental evidence has been shown to substantiate this claim. Chapter 5 presents experimental evidence of three primary mechanisms of heat generation. Chapters 6, 7, and 8 deal with different parameters that affect the heat generation of cracks, including crack closure stresses, the level of applied vibrational stress, and minute modifications (tribological damage) to contacting regions within the crack.

1.4.1 Heat generation mechanisms

Though frictional heat generation has been presumed to be the primary mechanism of heat generation in vibrating cracks, no previous experimental evidence has been presented to conclusively support this theory. Current published research in the field of vibrothermography simply assumes friction to be the source of vibrothermographic heating without careful experimental or theoretical validation. The work presented in this dissertation shows that while friction between rubbing asperities on opposing crack faces is the dominant source of heat generation in vibrating cracks, plasticity and viscoelasticity can be contributing factors to defect heat generation under certain circumstances

Renshaw, J. (2009C).

Experimental results have shown that friction is the dominant source of heat generation in vibrothermography. This is evidenced by the fact that crack closure determines which regions along a crack will generate heat. Also, experimental evidence shows that the regions along a crack that generate heat are the most likely to be modified (or tribologically damaged) due to friction as observed using a scanning electron microscope (SEM) of the crack faces.

1.4.2 Crack closure

A key issue affecting the heat generation process is crack closure. Crack closure refers to the premature contact (closure) of crack faces even while under tensile loads and is an important parameter governing both crack propagation Suresh, S. (1998) and NDE inspection accuracy Buck, O. (1983); Clark, R. (1987). Crack closure can be caused by a number of mechanisms, including plasticity-induced closure and roughness-induced closure, due to the roughness mismatch between asperities on opposing crack faces. Numerous other closure mechanisms are possible, such as oxide-induced closure, closure due to a phase transformation, viscous fluid, etc. Suresh, S. (1998) but only plasticity and roughness-induced closure contributed significantly to the closure stresses in the cracks used for this research.

The dominant form of closure for most cracks in metals is plasticity-induced closure, where the plastically-stretched material that surrounds the crack forces crack faces into contact when external loads that grew the crack are released. The plastic stretching of the material around the growing crack is forced back into roughly the same volume as the pre-stretched material once the external loads are released. This means that the stretched material on the crack faces forced back together by the surrounding material, which can give rise to very high contact, or closure, stresses on the crack faces. Roughness or mismatch between opposing crack face asperities along the crack can give rise to

additional closure stresses and is referred to as roughness-induced closure. These and other closure mechanisms force crack faces into contact and to carry load from the bulk structure. Higher closure stresses press crack faces together more tightly, lowering the crack opening displacement (COD) and often masking the crack to NDE inspections. NDE inspections tend to rely on the presence of open regions along cracks to be effective. For example, a larger opening in a crack creates a larger reservoir for a fluorescent penetrant inspection or a larger interruption in the electromagnetic fields for an eddy current inspection. Thus, high closure stresses result in more tightly closed cracks and reduce both the crack opening displacement and the probability of detection (POD) of closed cracks. One driving motivation for the use of vibrothermography is its ability to detect tight cracks with high closure stresses Renshaw, J. (2009B).

As vibrothermography relies on the contact and motion between crack faces, an understanding of crack closure is equally, if not more, critical in vibrothermography than with other NDE techniques. Chapters 6 and 7 deal with understanding the effects of closure stresses and present a new method developed in conjunction with this research used to measure both crack opening stresses and crack closure stress profiles of cracks.

1.4.3 Tribological damage (modifications) to fracture surface morphology due to vibrothermography

It is well known that, regardless of the material, fracture surfaces are delicate and should not be handled or touched if possible Wulpi, D. J. (1999) to avoid irreparable damage to the asperities on the surface. Vibrothermography intentionally rubs contacting asperities of crack faces (fracture surfaces) directly against one another, sometimes violently. These vibrations are sometimes strong enough to generate bulk heating of several degrees Kelvin. The temperature rise at the actual rubbing asperities of any rubbing surface is much higher than the bulk temperature rise Bowden, F. P. (1950); Cowan, R. S. (1992). Likewise, the stresses applied to individual pairs of contacting,

rubbing asperities between two contacting surfaces are also very large Bowden, F. P. (1950). Thus, it is obvious that some micro-scale damage, herein referred to as 'tribological damage,' will occur on the rubbing crack surfaces due to the effects of the applied vibration and subsequent heat generation.

It is important to understand what happens to the fracture surfaces due to the large number of cycles at high stresses that are applied to the cracks during each inspection. For experiments performed at Iowa State University, vibrations are generally well controlled in all experiments to minimize or prevent such problems, but many excitation systems currently in use elsewhere apply very high amplitude, uncontrolled vibrations which have been shown in some cases to not only damage crack faces, but also grow cracks Chen, J. C. (2007). It is therefore necessary to understand how tribological damage to the fracture surfaces due to a vibrothermographic inspection will affect the heat generation in subsequent vibrothermographic inspections of a crack as well as how the tribological damage to the crack may affect subsequent crack propagation rates. If fracture surfaces change in such a way that continuously reduces heat generation with subsequent excitations on a short timescale, then this exposes an important weakness of vibrothermography. If the tribological damage on the fracture surfaces relieve crack closure stresses, this creates another problem in which the crack may propagate faster than expected if the structure containing the crack returns to service and could result in premature failure of the structure. If the amount of heat generation of a crack and its fracture surfaces remain relatively unchanged or slowly change over very long timescales, then vibrothermography can be considered a truly nondestructive technique. Chapter 8 explains how crack faces are tribologically damaged due to vibrothermographic excitation and some guidelines on how to minimize causing tribological damage on crack faces to improve the repeatability of vibrothermographic experiments.

1.5 Heat Detection

The third step in vibrothemography is on heat detection. As with vibration and heat generation, an inadequate heat detection process can result in a flawed inspection. For example, the instrument used to detect heat in nearly all vibrothermographic experiments is an IR camera. The IR camera user must be cognizant of both the inspected material's bulk thermal properties, surface thermal properties, and image processing techniques to be able to obtain accurate and reliable heating data.

1.5.1 Thermal properties

The IR camera relies on detecting the thermal emission of heat from a surface, which means that it is influenced by the surface emissivity, or thermal radiation efficiency of the surface. In other words, heat detection can be significantly different for two different surfaces with the same temperature if their surface emissivities are different. Thus, an understanding of the heat detection process and limitations is necessary.

Though surfaces with low emissivities can cause problems, such as reflecting heat or not efficiently emitting generated heat, these problems are generally easy to resolve. Simple black spray paint coatings can be used to raise the surface emissivity if it is too low. Problems arise when it is not feasible or possible to apply a coating or when a coating cannot be applied uniformly (i.e. on a surface with a very complex geometry). For the research presented in this dissertation, the surfaces where heating data were measured were coated with a flat, black spraypaint to obtain nearly identical values of emissivity between experiments.

Other thermal properties that influence the heat detection process are the thermal conductivity, density, and specific heat of the material under inspection. These three material properties can be combined and expressed as the thermal diffusivity, which relates the rate of thermal conductivity to the volumetric heat capacity. In other words,

the thermal diffusivity relates how quickly a material can reach a thermal equilibrium. This also affects the temperature rise at a defect. Defects in materials with low thermal diffusivities, such as polymers, may have large thermal gradients. In contrast, materials, such as aluminum with a very high thermal diffusivity, may wick away the heat generated at a defect so quickly that it will not produce a measurable temperature rise at the defect. Thus, an otherwise identical crack that is detectable in one structure may not be detectable in another similar structure with different thermal properties.

1.5.2 Infrared imaging and image processing

Imaging using an IR camera requires some understanding of the physics of thermal radiation. The energy radiated from a surface is proportional to the fourth power of the absolute temperature, in Kelvins. Thus, camera calibration is an important factor to consider long before any measurements are taken. The IR camera is generally calibrated using a blackbody source at a known temperature. Generally, the IR camera is only calibrated for a narrow temperature range to be used for experiments. When calibrated correctly, research grade IR cameras, such as the one used in this research, can achieve temperature sensitivities of 20 mK.

Once calibrated, infrared images can be recorded. Due to varying emissivity values and geometry considerations of inspected surfaces, simple image processing techniques, such as background subtraction, are often used. The principle of background subtraction is that the initial measured temperature value (or average of some number of initial values) is used as a reference for each pixel. After the excitation is turned on, the initial value for each pixel is subtracted from that pixel at every subsequent time period to obtain a difference from the initial state. This can result in a large increase in sensitivity of thermal imaging using an IR camera.

An additional image enhancement technique Holland, S. D. (2009) was developed to eliminate the blurring effects of heat diffusion and pinpoint locations of heat generation.

This technique was based on the physics of heat diffusion and takes a filtered second-order spatial derivative combined with the time derivative of the measured heating data to eliminate heat diffusion and isolate regions of heat generation. Implementing such image enhancement techniques is useful for understanding more about the physics of heat generation.

The final important characteristic associated with infrared imaging is the defect detection depth of vibrothermography. Surface defects directly radiate heat to the IR camera whereas subsurface defects cannot. Heat from these defects must diffuse through the material until reaching the surface and then radiate from the surface. Thus, due to the effects of heat diffusion, the heat signature from a subsurface defect compared to an otherwise identical surface defect is delayed in time, lower in temperature, and more diffuse.

CHAPTER 2. VISCOUS MATERIAL-FILLED SYNTHETIC DEFECTS FOR VIBROTHERMOGRAPHY

A paper published in NDT&E International[1]

Jeremy Renshaw [2], Stephen D. Holland, and Daniel J. Barnard

2.1 Abstract

This paper describes a method to create viscous material-filled (VMF) synthetic defects for vibrothermography that, like cracks, delaminations, or disbonds, generate heat when exposed to vibration. Standard synthetic defects used in nondestructive evaluation, such as EDM notches and flat-bottom holes, are not suitable for vibrothermography since they do not generate a measurable amount of heat when vibrated. An array of viscous material-filled synthetic defects can be used to evaluate the vibration field in a structure due to a specific source to determine if local vibration amplitudes are sufficient to detect cracks or other defects in different locations in a structure. These synthetic defects can be used to resolve the long-standing problem of testing vibration coverage in a specimen for vibrothermography. Such defects can be manufactured in a wide range of materials and can aid in probability of detection studies.

[1]Reprinted with permission from Elsevier, 2009
[2]Center for NDE, Ames, IA 50011

2.2 Introduction

Vibrothermography is a nondestructive evaluation (NDE) technique that is used to find cracks, delaminations, and disbonds in structures through vibration-induced heat generation Reifsnider, K. L. (1980). An infrared (IR) camera detects cracks due to heat generation at the crack resulting from frictional rubbing or other heat-generating processes. Vibrothermography, sometimes referred to as sonic IR when performed at sonic or ultrasonic frequencies Chen, J. C. (2007), has shown significant ability in finding defects that may not be detected using other NDE methods Renshaw, J. (2009B). Defect detection using vibrothermography has been shown in some cases to have better inspection accuracy than fluorescent penetrant inspection DiMambro, J. (2007); Renshaw, J. (2009B) while having a lower instance of false calls DiMambro, J. (2007). These and other results have generated significant interest in vibrothermography; however, many fundamental questions have remained unanswered, such as the physical mechanisms of heat generation.

One critical problem that has not been adequately addressed is the variation of defect detectability in different regions of a structure due to single or multiple frequencies of excitation. Due to resonance effects, the vibration applied to a structure is never uniform throughout the structure. Therefore, in order to predict defect detectability, or how much heat a defect in a particular location would generate, the excited mode shape or shapes (vibration profiles) of the structure must be known. Synthetic defects that generate heat in response to an applied vibration could be used to map out the vibration field and predict defect detectability. Thus, a robust inspection method must quantify the vibrational amplitude as a function of position within a structure to determine whether a defect at a particular location is likely to be detected using a given vibrational excitation source. Using a single frequency excitation will inherently have nodes and antinodes of vibration throughout the structure. Quantifying stress and strain

contributions from a combination of two or more frequencies, resulting in two or more mode shapes, can improve defect detection, particularly when the antinodes of one mode shape correspond with nodes of another excited mode shape and vice versa. Chaotic, or nonlinear, excitation has not been used since it is not repeatable Morbidini, M. (2006) and would introduce undesired subharmonic and superharmonic vibrations into the structure.

Synthetic defects are widely used in other NDE techniques to estimate defect detectability and probabilities of detection (POD) for real defects. Typical synthetic defects for other NDE techniques are:

1. Electrical discharge machining (EDM) notches that are used as a substitute for cracks in fluorescent penetrant inspection as well as for eddy current and magnetic particle inspections.

2. Flat-bottom holes that are used to simulate voids or cracks for ultrasonic testing.

3. Foreign material inserts in composites, such as teflon tape and teflon tape pillows, that are used to simulate delaminations for ultrasonic inspection.

To be useful for vibrothermography, a synthetic defect must generate heat when exposed to vibration. EDM notches and flat-bottom holes do not generate a detectable amount of heat when vibrated unless they are stressed to the point of yield Luong, M. P. (1998); Rabiei, A. (2000). This is because notches and holes do not have contacting surfaces that can generate frictional heat. Likewise, simple material inserts in composites do not generate a detectable thermal response when vibrated since no actual disbond is present to create friction. However, when the insert material is folded over on itself and sealed at the edges such that no adhesive can penetrate, an artificial disbond with a rubbing surface is created. Disbonds with this type of rubbing surface may generate sufficient heat to be detected using vibrothermography Reifsnider, K. L.

(1980). These folded, sealed material inserts (pillows), however, are only suitable as simulated delaminations in composite laminates.

Though it is well known that cracks heat when vibrated Morbidini, M. (2006); Uhl, C. J. (2009), it is not feasible or possible to create a series of identical, regularly-spaced cracks in a structure. The nature of the crack growth process prevents cracks from being repeatably grown under precisely controlled conditions in close proximity to one another. Thus, conventional synthetic defects are ineffective and real defects are impractical when attempting to study vibration coverage and crack detectability in vibrothermography. This paper describes a viscous material-filled synthetic defect that uses viscoelasticity as a source of heat generation. These defects have the potential for providing a reliable means of testing the vibrational coverage of vibrothermography.

2.3 Methods

Mechanical waves in a viscous material generate heat Reifsnider, K. L. (1980) due to irreversible viscous flow. Therefore, a defect containing a viscous material would generate heat when vibrated. There are several possible ways to apply a viscous material to a specimen to create such a defect. The viscous material may be spread across the surface of a specimen as a coating, but since the viscous material has the ability to flow, such a coating does not create a robust, stable, or long-term synthetic defect. However, if the viscous material is confined to small pockets, such as drilled holes, and not allowed to flow by covering the holes with a coating, then it is possible to create individual, separated synthetic defects. An array of such viscous material-filled holes in a specimen could provide a useful test for infrared heating detection coverage of defects over an area that could be used to help assess POD's and vibrational coverage in a sample resulting from different vibrational excitation frequencies.

The test setup used for experiments is shown in the top half of Fig. 2.1. This figure

shows an elevated view of the test setup and how a typical sample was mounted in the clamps. A piezoelectric stack transducer Holland, S. D. (2007A) was used to excite vibrations at specific frequencies corresponding to flexural resonances of a sample. A laser vibrometer was scanned across the surface of the sample to measure vibration velocities and verify flexural mode shapes.

Several materials were tested as candidates to create effective synthetic defects. The bottom half of Fig. 2.1 is an infrared image of the heat generation due to applied vibration at a series of drilled holes filled with different viscous materials: honey, CA9 glue (superglue), and 3M adhesives #75 and #77. The bright circular areas indicate heat generation at the drilled holes. It can be clearly seen that the holes filled with honey generate more heat than the other materials used in this test. A similar test was performed using ultrasonic shear couplant and other adhesives; however, the shear couplants and adhesives did not adequately fill the holes to be able to repeatably generate a detectable amount of heat. Therefore, honey was used as the viscous material for subsequent testing.

Honey was able to fill the drilled holes more completely than any other material tested and also generated heat more efficiently. Of the materials tested, honey was superior in its ability to fill the drilled holes, ease of application and cleaning, and had a good heat generation efficiency. None of the other materials tested were able to both sufficiently fill the drilled holes and generate detectable amounts of heat. Honey is non-toxic, inexpensive, and generates heat when vibrated, making it an excellent substance for this application and the best overall material used to date for creating VMF synthetic defects. However, honey can crystallize during months in storage; therefore, long-term stability of honey-filled VMF defects needs to be addressed. If crystallized, honey may be decrystallized when heated to 60° C (140° F) for 30 minutes White, J. W. (1980).

To test the utility of these synthetic defects for vibration coverage analysis, a 21 X 3 array of defects was manufactured in a titanium test specimen (153.6 mm X 25.2 mm

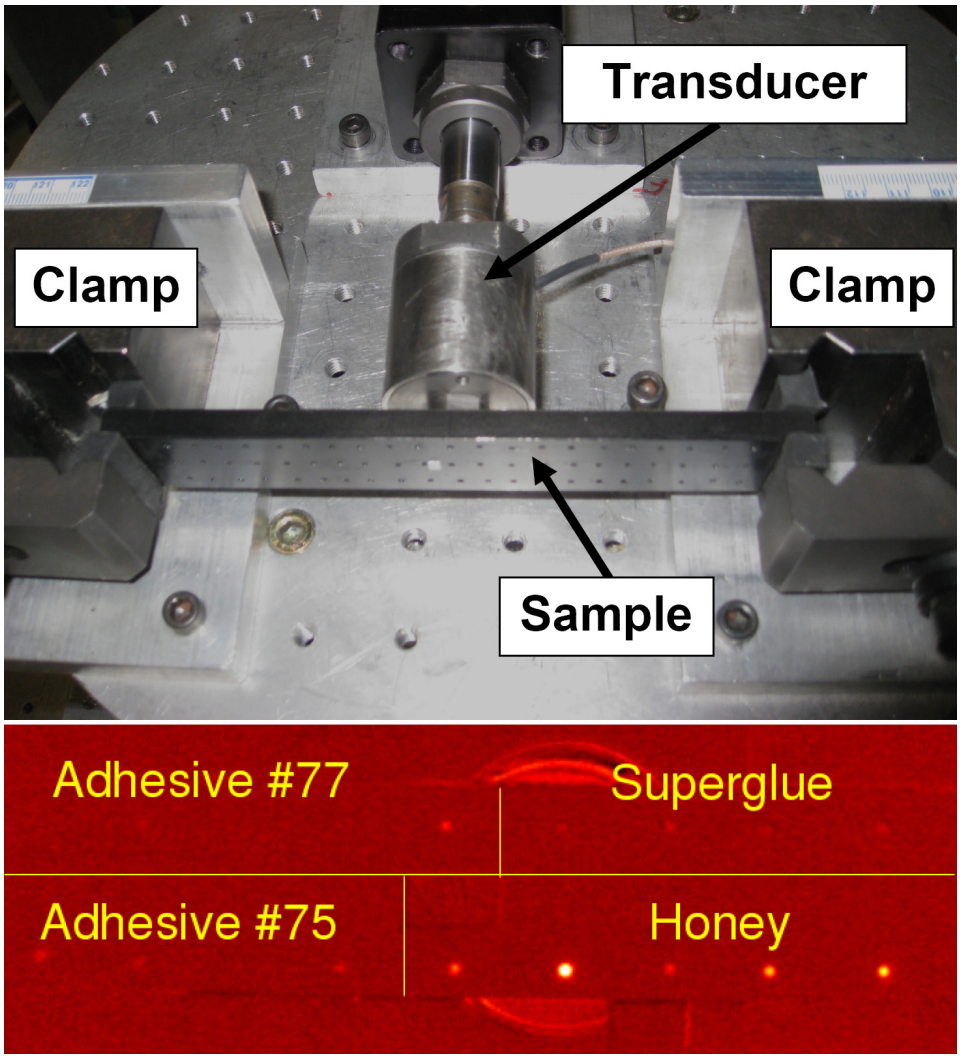

Figure 2.1 Top: elevated view of the experimental setup used for vibrothermographic testing of samples containing VMF synthetic defects. Bottom: infrared observation of the heat generation of several candidate materials considered for creating synthetic defects.

X 7.3 mm) with a horizontal spacing of 6.5 mm, a vertical spacing of 8 mm, and hole diameters of 1.17 mm (0.0460 in). A method was developed for filling arrays of holes with a viscous fluid. First, the holes were covered in a layer of the viscous fluid, in this case, honey. The honey, being a viscous material, did not flow into the holes on its own, so the bar was placed in a vacuum to pull the air out of the holes through the layer of honey. After the air bubbles traveled through the layer of honey and began to burst, the vacuum was released. The force of the returning air pressure drove the honey into the drilled holes, creating an array of VMF defects. Finally, the surface was cleaned and painted with a coating that served both to trap the honey in the holes and to increase the emissivity of the sample surface. After the coating dried, the sample had an array of viscous material-filled pockets that generated heat when vibrated and had a highly emissive coating to efficiently radiate any heat generated in the synthetic defects.

For testing, the samples were mounted in an apparatus Uhl, C. J. (2009) using 5 mm wide rubber pins placed at the right and left edges of the samples to maximize the observable area for the laser vibrometer and infrared camera used to measure the vibration and heating profiles, respectively, of the sample surface. This means that vibration and heating data could be measured across nearly the entire sample surface. Rubber pins were used since they could hold the sample securely in place while minimizing the effect of the mounting configuration on the sample vibration.

2.4 Results

Figs. 2.2a and 2.2b show the measured vibration profile (top) and pattern of VMF defect heating (bottom) for the titanium sample when vibrated for 1 s at its fourth and fifth order flexural resonances, respectively. Vibration data were measured with a scanning laser vibrometer and infrared data shown were measured at the end of the 1-s excitation pulse. Light areas (yellow and light blue in color) in the vibration data

indicate vibrational nodes while dark areas (blue and red in color) indicate antinodes. The VMF defects shown in Fig. 2.2 were filled with honey. VMF defects located in regions near antinodes heated significantly, indicated by bright patterns in the heating data, while regions near nodes barely heat, and remain dark. By comparing the VMF defect heating to the measured vibration profile, the effect of the vibrational mode shape is clearly seen. Synthetic defects located at vibrational antinodes heat up significantly while those located near vibrational nodes do not. Thus, the heating profile of the VMF defect array shows that heat generation is dependent on the local vibration at each synthetic defect. Fig. 2.2 also illustrates how these synthetic defects can be used to determine coverage analysis for vibrothermography. Cracks located in regions where the VMF defects generate heat would likely be detectable while cracks located in regions where the VMF defects did not heat (dark regions) would not be detectable.

When vibrating in resonant modes, such as shown in Figs. 2.2a and 2.2b, a laser vibrometer can be used to measure stresses, in this case using flexural wave theory Holland, S. D. (2008); Elmore, W. C. (1985), and the displacement velocity of a known mode shape while temperature changes are measured using an infrared camera. Fig. 2.3 plots the temperature rise of the VMF defects as a function of the local vibrational stress (measured using the laser vibrometer) at the defects as the applied vibrational stresses at the defects were varied. The variation shown in the heating data is typical for the set of VMF defects tested. Fig. 2.3 shows that increasing stresses at a VMF defect generate larger temperature rises and that the temperature versus stress data follow a definite trend. Similar temperature versus stress data have been shown for cracks Holland, S. D. (2008); Homma, C. (2006). This means that higher vibrational stresses applied to a crack also lead to larger temperature rises at the crack.

The solid line shown in Fig. 2.3 is a curve fit to the temperature rise versus dynamic stress data. The heating response of the VMF defects used in this experiment was

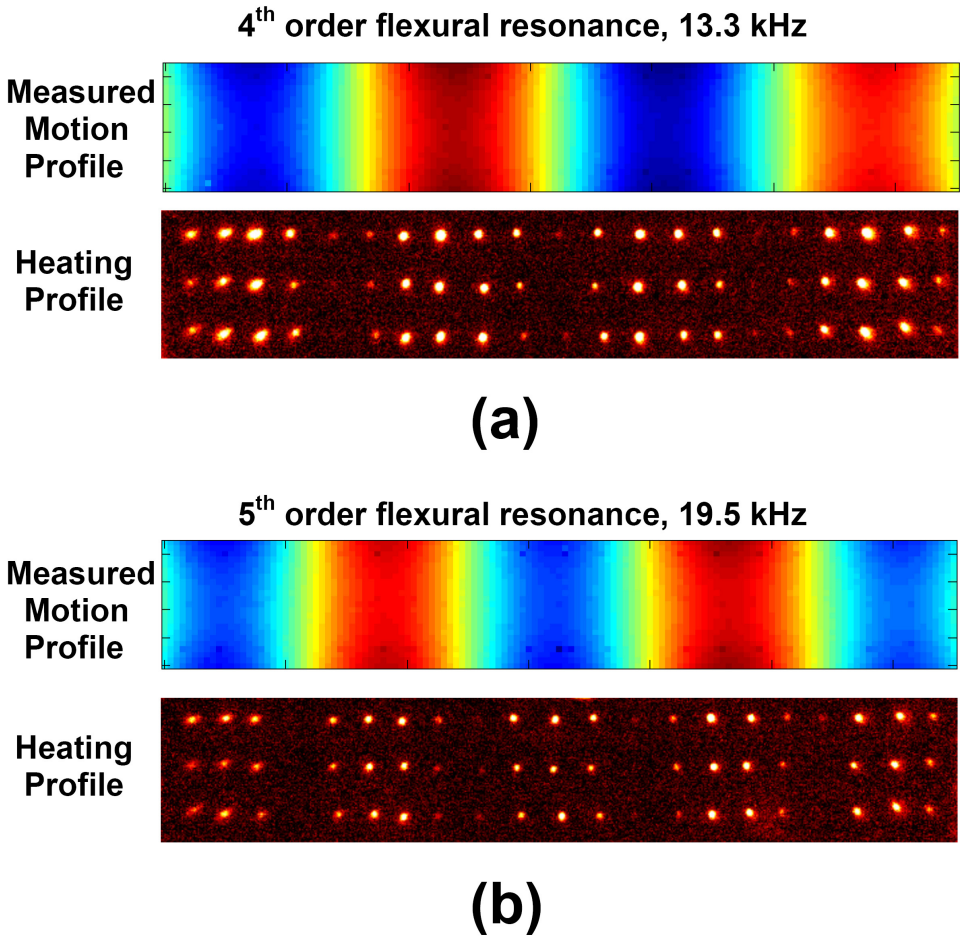

Figure 2.2 (a) Experimental measurement of the vibration profile (upper image) and the heating profile (lower image) from the fourth order flexural resonance of the specimen and (b) for the fifth order flexural resonance. Light areas (yellow and light blue in color) indicate vibrational nodes while dark areas (blue and red in color) indicate antinodes. Light areas in the heating profile indicate heat generation. (For interpretation of the references to color in this figure legend, the reader is referred to the web version of this article.)

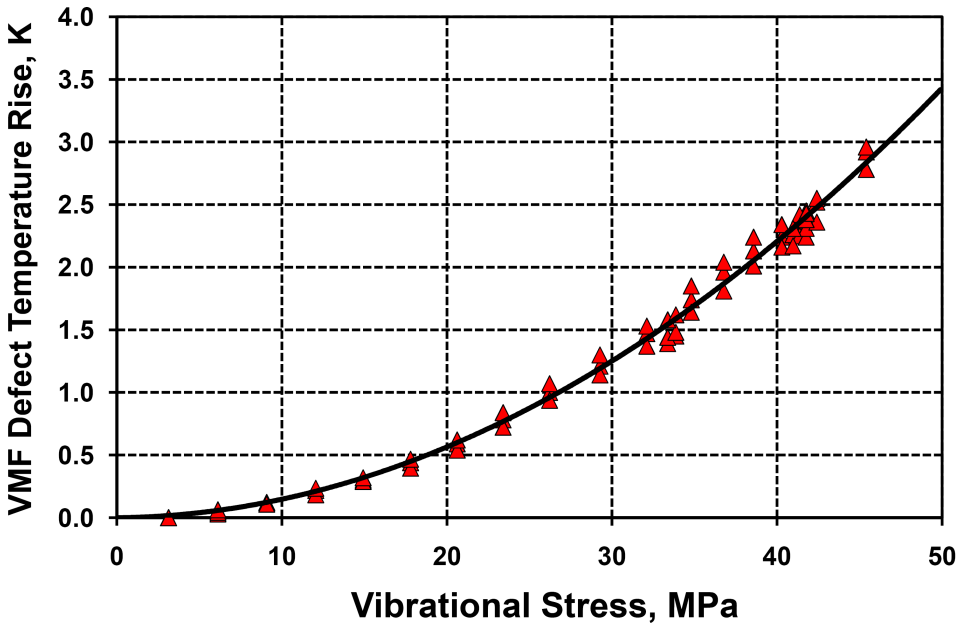

Figure 2.3 Experimental measurement of VMF defect heating as a function of the local vibrational stress at the defects. The superimposed line is the curve fit from Equation 2.1.

$$T_{VMF} = 0.0013\sigma_{pp}^2 + 0.0013\sigma_{pp}, \tag{2.1}$$

where σ_{pp} is applied peak-to-peak vibrational stress in MPa and T_{VMF} is the temperature rise in degrees Kelvin of the VMF defects. The noise level of the infrared camera used to record the data was 0.020 K and the detectability threshold was assumed to be 0.030 K. This means that the synthetic defects used in this study began to be visible above about 2.2 MPa of vibrational stress amplitude (4.4 MPa peak-to-peak vibrational stress). Thus, these synthetic defects easily generated heat and were very sensitive to applied vibrational stresses.

A direct comparison of heat generated at VMF defects and heat generated at cracks has not yet been developed. Heat generation in cracks is related to the vibrational stress, the crack size, and other factors such as crack closure Homma, C. (2006); Renshaw, J. (2009B); Uhl, C. J. (2009). Additionally, cracks have an orientation within a structure and rely on rubbing between crack faces to generate heat. The applied vibration must cause the contacting crack faces to rub together to generate heat, whereas synthetic defects are isotropic and rely on viscous flow to generate heat. More research regarding crack heating processes is needed to determine the relationship between VMF defect heating and crack heating.

Synthetic defects will be critical in determining vibration coverage for vibrothermography for complex parts such as turbine blades. Synthetic defects could be created across the surface of a turbine blade and used to determine the vibrational coverage of an excitation source. By relating the heating of synthetic defects to the heating of cracks, VMF synthetic defects could also help to determine the probability of detection of cracks. This would help to determine how a specimen must be vibrated to obtain optimal vibrational coverage of the specimen and maximize crack detectability.

The resolution obtained using these synthetic defects is related to the size and spacing

of the defects. Smaller synthetic defect sizes and spacings will give enhanced resolution, but may not generate as much heat as larger defects. It is also important to keep the size of the defects small enough to avoid significant changes to the vibrational mode shapes or frequencies of the inspected part since material removal in the part will alter the mechanics of the vibration process increasingly as more material is removed.

An alternative method to create synthetic defects would be to use removable coatings that generate heat when vibrated to achieve similar vibration and heat coverage results. Such coatings would improve the ability to determine critical vibrational frequencies and would not require material removal.

Synthetic defects have been instrumental in characterizing different NDE techniques. Using synthetic defects for vibrothermography will improve understanding of its advantages and limitations which will, in turn, help vibrothermography to become a more widely used technique in industry.

2.5 Conclusions

This paper presents a method for creating and characterizing a new type of synthetic defect to be used with vibrothermography. Viscous material-filled (VMF) synthetic defects are suitable for simulating cracks in vibrothermographic studies. Since these defects are not real cracks and have a different mechanism of heat generation, careful judgment is required when relating VMF defect heating to actual defect heating of cracks, disbonds, or delaminations.

Unlike typical synthetic defects designed for other NDE applications, VMF defects generate significant heat when vibrated. Heat generation of these synthetic defects is a function of the local stress at the defect. VMF defect heating for an array of defects is dependent on the location of the defect within the vibrational profile of the structure containing the defect array. VMF defects located in regions of high vibrational stress

(antinodes) generate more heat, whereas, those located in regions of low vibrational stress (nodes) generate less heat, often below the detection threshold of the IR camera. Thus, VMF defects are very useful not only for simulating cracks in structures but also for testing and verifying vibration coverage for vibrothermography.

2.6 Acknowledgements

This material is based upon work supported by the Air Force Research Laboratory under Contract #FA8650-04-C-5228 at Iowa State University's Center for NDE.

CHAPTER 3. SYNTHETIC DEFECTS FOR VIBROTHERMOGRAPHY

A paper to be published in Revew of Progress in Quantitative Nondestructive Evaluation [1]

Jeremy Renshaw [2], Stephen D. Holland, R. Bruce Thompson, and David J. Eisenmann

3.1 Abstract

Synthetic defects are an important tool used for characterizing the performance of nondestructive evaluation techniques. Viscous material-filled synthetic defects were developed for use in vibrothermography (also known as sonic IR) as a tool to improve inspection accuracy and reliability. This paper describes how the heat-generation response of these VMF synthetic defects is similar to the response of real defects. It also shows how VMF defects can be applied to improve inspection accuracy for complex industrial parts and presents a study of their application in an aircraft engine stator vane.

3.2 Introduction

Vibrothermography is a nondestructive evaluation (NDE) technique that uses structural vibrations to detect defects via vibration-induced heat generation that occurs at

[1] Reprinted with permission from the American Institute of Physics, 2009

[2] Center for NDE, Ames, IA 50011

defects. An infrared (IR) camera is used to observe surface temperature changes of a structure to locate defects within the structure. Since defects tend to heat most when the structure containing the defects is vibrated at resonance Henneke, E. G. (1986), a major issue that must be addressed is the coverage analysis of vibrothermography, especially when one or more specific resonances are excited. It is not possible to create a fine array of identical, natural defects, such as cracks, across a structure that are suitable for coverage analysis. Synthetic defects must be employed for an accurate evaluation of coverage.

Synthetic defects have been developed that are suitable for vibrothermography since they generate heat when vibrated Renshaw, J. (2009A). This paper compares the behavior of synthetic defects to cracks and demonstrates the ability of synthetic defects to map vibrothermographic test coverage over the surface of a real part, in this case, a stator vane from an aircraft engine. It is shown that different excitation frequencies excite different resonances which, in turn, produce variations in defect detection coverage.

3.3 Theory

For a defect to be useful for vibrothermography, it must be able to generate heat when vibrated and should be easily and repeatably manufactured. Typical synthetic defects used for NDE applications, such as electrical discharge machining (EDM) notches and flat-bottom holes are not suitable for vibrothermography since they do not generate a measurable amount of heat when vibrated. Folded, sealed teflon tape pillows Reifsnider, K. L. (1980); Renshaw, J. (2009A) have been used as synthetic defects in vibrothermography, but are only appropriate for composite laminates, limiting their widespread use. Viscous material-filled (VMF) defects, however, are applicable for vibrothermography in a wide range of materials since they rely on viscoelasticity to generate heat. They are also easily and repeatably manufactured and have a repeatable heating response as

well.

VMF defects are created by filling a drilled (or pre-existing) hole with a viscous fluid, typically honey Renshaw, J. (2009A). The sample containing the viscous material-filled hole is then covered with an emissive coating that serves both to increase the radiated heat from the outer surface of the defect and to prevent the viscous material from exiting the hole. A defect created using this method generates significant heat when exposed to vibration.

3.4 Methods

The dimensions of the VMF defects used in the test sample in this study were 1.18 mm in diameter and 5.0 mm in depth. They were manufactured in a titanium (Ti 6-4) test sample in a 21 X 3 array across the sample with dimensions 153.6 mm X 25.2 mm X 7.3 mm. Honey was used as the viscous material of choice. Figure 3.1 shows a schematic side view of a typical synthetic defect with the top side of the image representing the outer surface of the material that is observed using an IR camera.

The sample bar was mounted using rubber-tipped clamps located at nodal points of vibration on each end of the bar to minimize the influence of the clamps on vibrational modes. We used a tunable piezoelectric stack transducer Holland, S. D. (2007A) to excite the sample. Using a tunable piezoelectric transducer allowed us to isolate individual, heat-generating resonances for further study. All vibrational mode shapes and frequencies were confirmed using a scanning laser vibrometer. All infrared data were recorded using an IR camera with a 640 X 512 focal plane array with a pixel noise-equivalent temperature difference of 0.02 degrees Kelvin.

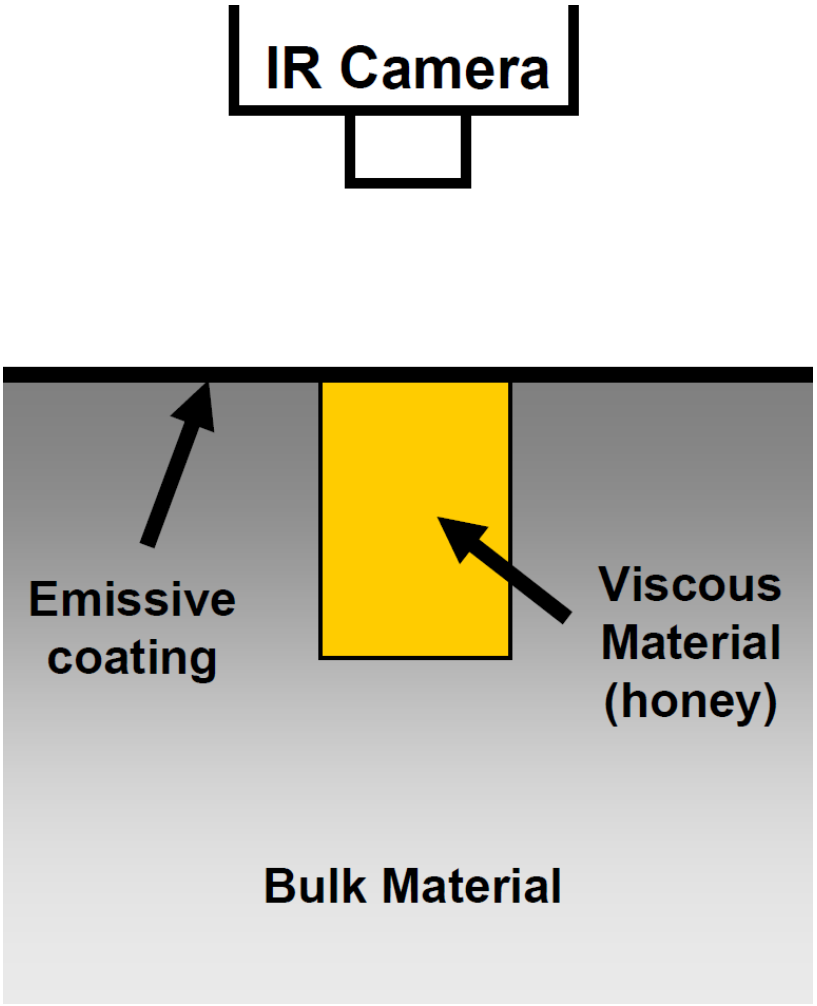

Figure 3.1 Side view of a typical synthetic defect used for this study. A circular hole is drilled in the titanium sample and filled with honey. The outer surface is covered with an emissive coating to increase the heat emitted from the outer surface and prevent the honey from leaving the hole.

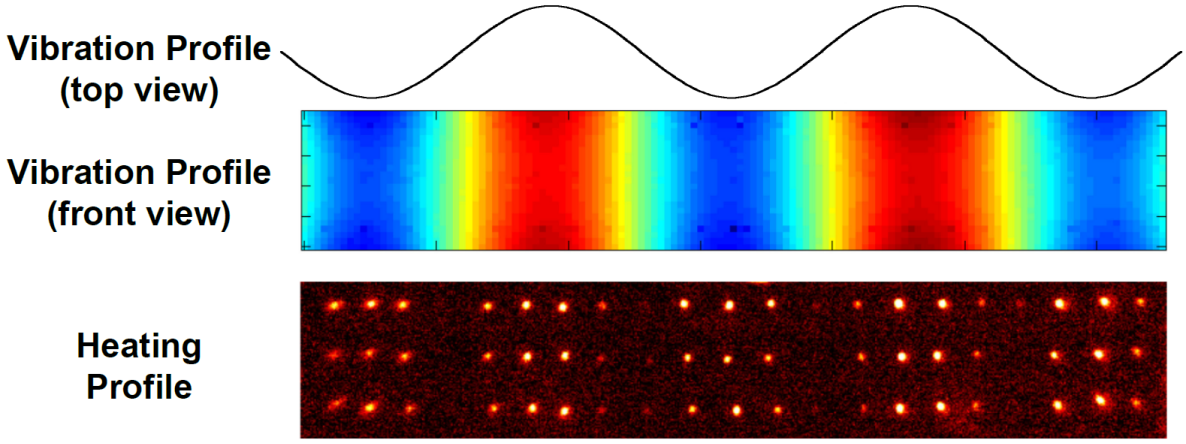

Figure 3.2 (top) top view of the 5^{th} order flexural resonance mode shape of the test sample, (middle) front view of the experimental measures of the vibrational mode shape of the test sample using a laser vibrometer (light areas (light blue and yellow in color) indicate vibrational nodes while dark areas (blue and red in color) indicate antinodes), and (bottom) the heat generation, indicated by lighter colored regions, of the synthetic defects following the measured mode shape of the titanium test sample, with increased heating at vibrational antinodes.

3.5 Results

The sample containing the synthetic defects was vibrated at its 5^{th} order flexural resonance as shown in Figure 3.2. Figure 3.2 shows both a top view (top) and a front view (middle) of the 5^{th} order flexural resonance of the bar. The bottom image of the figure shows the heat generation in the synthetic defects that results from this flexural mode. Heat generation of the defects, indicated by bright regions, directly correlates to the vibrational antinodes of the mode shape (vibrational profile). Defects located at or near antinodes heated significantly while those located near nodes generated little to no heat.

Using a known mode shape and flexural wave theory, vibrational stresses can be calculated from measures of surface motion Elmore, W. C. (1985); Holland, S. D.

(2008). The temperature rise of the VMF defects was recorded as a function of the local vibrational stress at the defects, taken at room temperature. These data are plotted in Figure 3.3. Figure 3.3 also shows a heating curve from a surface fit to data based on the experimental heating data collected by Uhl et al. Uhl, C. J. (2008, 2009). These data resulted from the heat generation of over 60 different fatigue cracks in titanium (Ti 6-4) samples with varying crack length, a range of local vibrational stress levels at the cracks, and using different excitation setups. The VMF defects in this study heated to a temperature similar to what would be anticipated for a typical crack of length 6.35 mm (0.250 in) in the previous study. The use of smaller VMF defects would generate less heat due to the smaller volume of viscous material available to flow and the diffusion of the generated heat into the base structure.

Though the physics of viscoelastic heat generation in synthetic defects Renshaw, J. (2009A) is different from friction in cracks Homma, C. (2006), the trends of the temperature rise versus local vibrational stress graphs are surprisingly similar, leading to the conclusion that VMF defects are both useful and appropriate synthetic defects that can be utilized to improve inspection coverage using vibrothermography.

Several factors may influence the heat generation properties of honey. First, since honey is an organic compound, honey from different sources and of different ages will have some variation in chemistry and physical properties. Second, contamination of the honey will alter its purity and can alter heat generation properties. Finally, the ambient temperature can alter the viscosity of the honey which can, in turn, affect the heat-generating properties of the honey and the resulting temperature rise in the synthetic defects. To minimize the change in viscosity with honey temperature, all heating data taken using VMF synthetic defects were taken on the same day with the same setup with identical room temperatures. The defects were allowed to cool for at least one minute in between excitations to ensure that the initial temperature of the honey was the same for each experimental test.

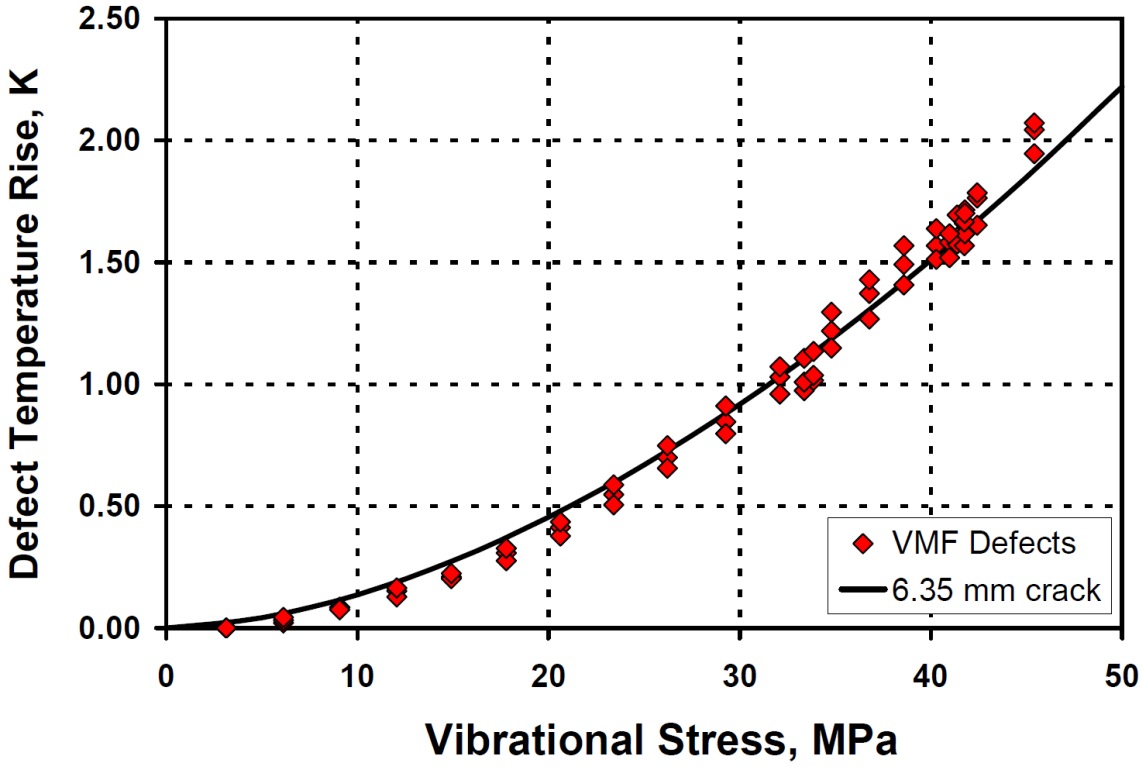

Figure 3.3 Experimental measures of heat generation of the VMF synthetic defects as a function of local applied stresses on the defects (diamond points) compared with the heat generation of typical cracks (based on data taken from Renshaw, J. (2009A); Uhl, C. J. (2009)).

Though these tests may show that VMF synthetic defects are useful for vibrothermography in a laboratory setting, this does not directly translate to a useful synthetic defect for non-laboratory specimens. Industrial parts may have complicated geometries, surface coatings, joints, welds, etc. that significantly complicate the NDE inspection process. For this reason, it is important to test the utility of these defects using industrial parts with complex geometries that would otherwise be difficult to inspect.

A stator vane is a common component in aircraft engines and has a particularly complicated geometry that makes inspections of nearly any kind difficult due to its curved geometry and many cooling holes. For this reason, a stator vane was used as a test piece to evaluate the usefulness of VMF defects in a complicated geometry.

The cooling holes on the stator vane were filled with honey. Honey was again used as the viscous material of choice due to its efficiency in heat generation and ease of application and removal without the need for harsh chemicals or cleaning processes. Once the cooling holes were filled with honey, the vane was covered with an emissive coating. Figure 3.4 shows an infrared image of the stator vane used in the test setup.

The stator vane was then excited at different excitation frequencies and the results are shown in Figure 3.5. The first excitation frequency was 20.1 kHz, similar to the typical excitation frequency of most ultrasonic welders commonly used for vibrothermography or sonic IR inspections. Only a few small regions of VMF defects generated heat, meaning that the local vibrational stresses throughout the vane were relatively low. Two stronger resonances were excited in the sample (12.5 and 13.6 kHz) using the piezoelectric transducer, but again only a few regions across the vane generated measurable amounts of heat. For this vane, the most effective single frequency to generate large local vibrational stresses was found to be 14.4 kHz, as shown by the large area that generated heat (became brighter) in Figure 3.5. Different stator vanes (different sizes and geometries) will have different resonant frequencies and will require experimental testing using synthetic defects to determine effective vibrational frequencies and stress

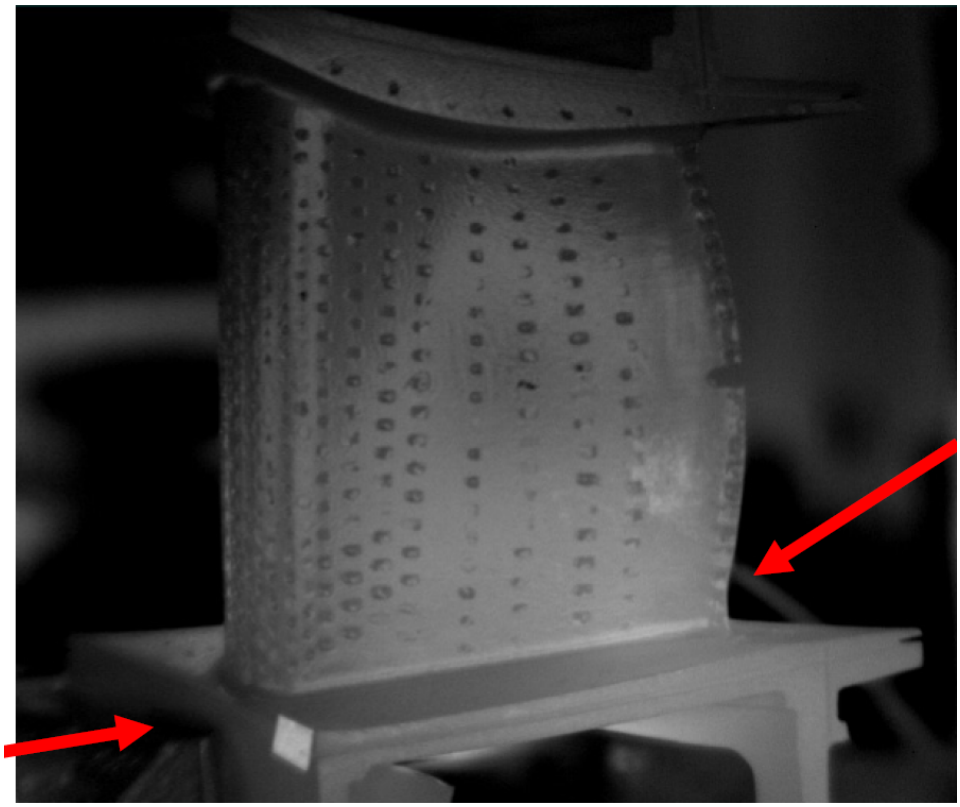

Figure 3.4 Infrared image of the stator vane used for testing the applicability of VMF synthetic defects. The front face of the vane is shown. The array of cooling holes across the front face have been filled with honey and covered with an emissive coating. Since both the coating and honey are easily removed, these synthetic defects were created and removed with no damage to the sample.

levels to assess coverage analysis. However, VMF synthetic defects have proven to be a very useful resource in determining effective resonances for heat generation. Certainly, numerous resonances must be excited to avoid the potential for defects located at vibrational nodes of any single resonance to be missed, but VMF defects can be a useful means of determining the best set of resonances to provide the highest level of inspection coverage for complicated parts and geometries.

3.6 Conclusions

Synthetic defects are important in understanding advantages and limitations of NDE techniques. Viscous material-filled (VMF) synthetic defects have been developed to better understand the mechanics of heat generation in vibrothermography. These synthetic defects can be manufactured more easily and repeatably than cracks and can be spaced close together for fine resolution of defects in particular locations across a sample. Since vibrothermography is dependent on excited mode shapes of a structure, an array of VMF synthetic defects can also be a useful tool in determining excited structural resonances and performing coverage analysis.

VMF synthetic defects have a similar heat generation response to applied vibrational stresses as real cracks. VMF defects have been applied to real world parts and found to be very helpful in determining the best vibrational frequencies to use for improved inspections. A study is presented where VMF defects are created across the surface of a stator vane and provide a means of determining the best vibration frequencies to use for inspecting that particular stator vane design.

3.7 Acknowledgements

This material is based upon work supported by the Air Force Research Laboratory under Contract #FA8650-04-C-5228 at Iowa State University's Center for NDE.

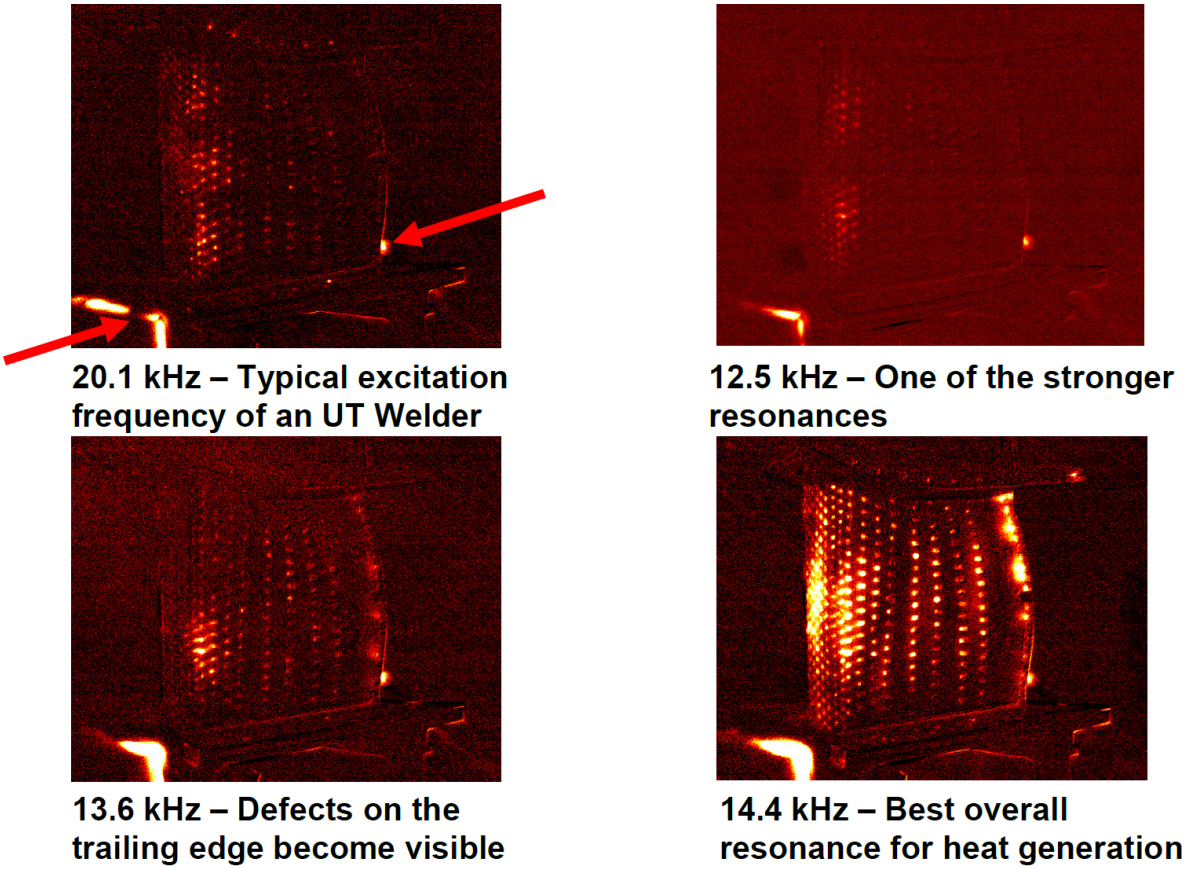

Figure 3.5 Four images of heat generation (heat generation indicated by bright regions) in VMF synthetic defects in a stator vane showing the detection coverage on the vane for each frequency. The arrows in the top left image point to the regions of heat generation that appear in each figure, but are unimportant (i.e. due to mounting, etc.).

CHAPTER 4. FULL-FIELD VIBRATION MEASUREMENT FOR VIBROTHERMOGRAPHY

A paper published in Review of Progress in Quantitative Nondestructive Evaluation [1]

Jeremy Renshaw [2] and Stephen D. Holland

4.1 Abstract

Vibrothermography is a nondestructive technique for finding defects through vibration-induced heating imaged with an infrared camera. To model the crack heating process in vibrothermography, it is essential first to understand the vibration that causes heat generation. We describe a method for calculating internal motions from surface vibrometry measurements. A reciprocity integral and Gauss's law allow representation of internal motion by a surface integral of boundary motion times the Green's Function. We present experimental results showing internal motions calculated from measured surface motions of a vibrating sample. This will ultimately allow estimation of the detectability of a hypothetical crack at an arbitrary location in a specimen.

4.2 Introduction

We demonstrate a method that measures internal stresses and strains of a vibrating part Burger, C. P. (1987) through surface velocimetry. This allows for a direct calcula-

[1] Reprinted with permission from the American Institute of Physics, 2009

[2] Center for NDE, Ames, IA 50011

tion of the internal stresses and strains at any point within an object. The mathematics involved in this process are similar to those of the Boundary Element Method (BEM). Understanding the internal vibration around a crack may lead to a relation between the stresses and strains around the crack and the observed heating in vibrothermography. The ultimate goal of this research is to understand the physics of the crack heating process.

4.3 Theory

The equation of motion governing a solid body is given as Kobayashi, S. (1987)

$$\tau_{ij,i} + f_j = \rho \ddot{u}_j \tag{4.1}$$

with stress tensor τ_{ij}, a body force f_j, density ρ, and displacement u_j. Following the notation used in Achenbach Achenbach, J. D. (2003), the time-harmonic Green's Function with stress $\tau^{G:X}_{ij:k}$ and displacement $u^{G:X}_{j:k}$ Kame, N. (1999) is the solution to Equation 4.1 given a time harmonic impulse body force in the k'th direction.

$$\tau^{G:X}_{ij:k,i} + \delta(\underline{x} - \underline{X})e^{-i\omega t}\delta_{jk} = \rho \ddot{u}^{G:X}_{j:k}, \tag{4.2}$$

The body force is applied at $x = X$ and it is expressed as $f_j = \delta(\underline{x} - \underline{X})e^{-i\omega t}\delta_{jk}$. The reciprocity formulation of Equation 4.1 is given as Equation 4.2 multiplied by u_j minus Equation 4.1 multiplied by $u^{G:X}_{j:k}$.

$$\tau^{G:X}_{ij:k,i}u_j - \tau_{ij,i}u^{G:X}_{j:k} = (\rho \ddot{u}^{G:X}_{j:k} - \delta(\underline{x} - \underline{X})e^{-i\omega t}\delta_{jk})u_j - \rho \ddot{u}_j u^{G:X}_{j:k}. \tag{4.3}$$

Equation 4.3 can be simplified due to symmetry and integrated over the specimen volume. Several of the terms in the equation can be grouped and represented as a divergence. Then, these terms can be transformed through the divergence theorem into a surface integral. The remaining terms are the volume integral of a spatial Dirac delta

$$\int_V (\delta(\underline{x} - \underline{X}) e^{-i\omega t} \delta_{jk} u_j) dV = -\int_S (\tau_{ij:k}^{G:X} u_j - \tau_{ij} u_{j:k}^{G:X}) n_i dA, \tag{4.4}$$

where n_i is the normal to the part surface at a given location. The surface tractions for this experimental setup are assumed to be zero; therefore, $\tau_{ij} u_{j:k}^{G:X} = 0$ and the equation can be written as

$$\int_V (\delta(\underline{x} - \underline{X}) e^{-i\omega t} \delta_{jk} u_j) dV = -\int_S (\tau_{ij:k}^{G:X} u_j) n_i dA, \tag{4.5}$$

Solving the volume integral thus allows us to calculate the displacement at any given point X as

$$u_k|_{\underline{x}=\underline{X}} = \frac{1}{e^{-i\omega t}} \int_S (-\tau_{ij:k}^{G:X} u_j) n_i dS. \tag{4.6}$$

Equation 4.6 shows us that the internal displacement at a point is calculated from a surface integral of the boundary displacement times the Green's Function stress. As the laser vibrometer measures velocity, not displacement, the displacement can be obtained simply through a time integral of the measured velocity. Once the internal displacements are known, the strain can be calculated from the spatial derivative of the displacements. Stress can then be calculated through the use of Hooke's Law. Therefore, the strain and displacement at any point within a part can be calculated from a knowledge of the vector surface velocity of the part. Stress can then be calculated given the material properties of the part in question. A major benefit of this method is that the Green's Function drops off as 1/r in the far field, so the effect of areas that cannot be measured is limited to the immediate vicinity of the missed points.

4.4 Experimental Procedure

The vector surface velocity of the specimen is needed to calculate its internal stresses and strains. The vector surface velocity is determined by measuring surface velocity

with a laser vibrometer from three linearly independent incident directions. The laser vibrometer measures one-dimensional vibration using the doppler shift in the direction of the beam reflected back from the specimen surface; thus three measurements are needed to obtain the complete vibration of a point. Two in-plane measurements are obtained by rotating the sample by means of a motion control system. A third, out-of-plane measurement is obtained using the motion control system and a carefully-aligned mirror to redirect the beam. The motion control system is programmed to scan the measurement beam across the entire surface of the part. As some points - namely those near the transducer - are shadowed and not possible to measure, a few points will always be missed.

A titanium bar 152.4 mm (6.0 in.) long, 25.4 mm (1.0 in.) wide, and 12.7 mm (0.50 in.) thick was fastened to a piezoelectric transducer. We covered the bar in retroreflective tape to maximize the reflected optical signal returning to the laser vibrometer. To minimize shadowed areas, the attachment to the transducer was the bar's only means of support. We positioned the bar on a carefully-aligned motion control system and vibrated it using a 100-20000 Hz frequency sweep at low amplitude ensuring repeatable vibration and stresses well within the linear elastic regime. The bar was tesselated into 5mm by 5mm areas and scanned from three selected linearly independent incident directions. The measured data were numerically integrated using Equation 4.6 to calculate the internal motion of the sample.

4.5 Results

The full stress tensor, τ_{ij}, for any point within the bar can be determined using the derivative of Equation 4.6 and Hooke's Law. For any frequency, an Inverse Fourier transform gives the stress as a function of time instead of frequency for a given point within the bar. For example, the cross-sectional shearing stress, τ_{yz}, at a selected point

within the test bar is shown in Figure 4.1. Any component of the stress tensor at any location inside the bar can be accurately calculated and expressed quantitatively, with the exception of the shaded areas near the transducer.

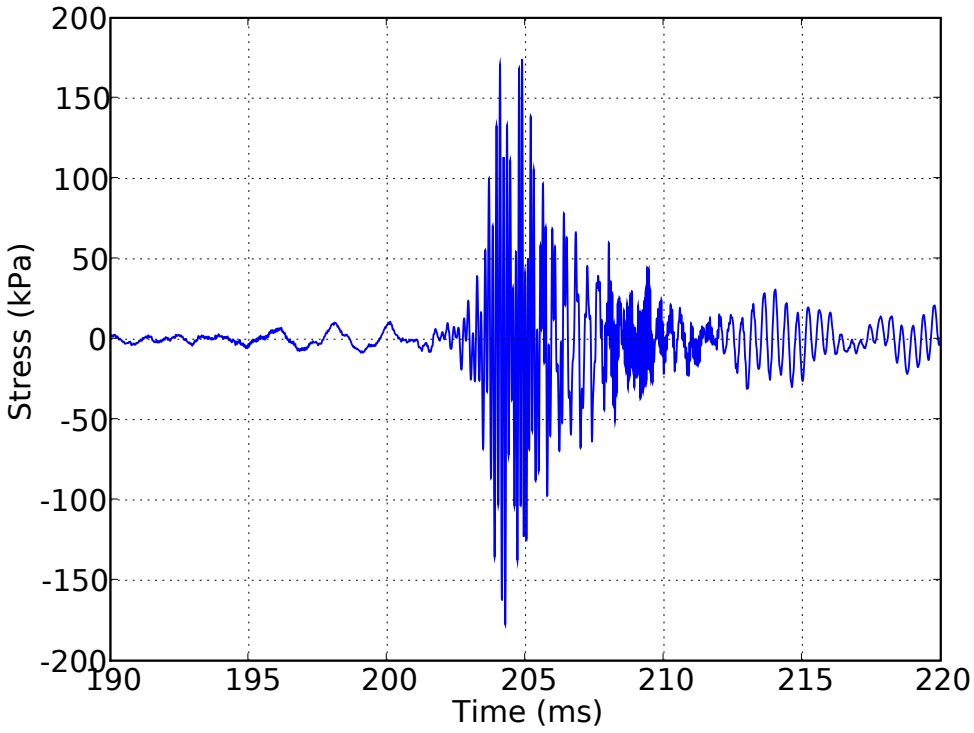

Figure 4.1 Stress as a function of time at a point in the bar using spatial differentiation and Hooke's Law.

The test bar exhibited several resonances at frequencies within the sweep. One such resonance, a flexural resonance occurring at 7.40kHz, will be examined in more detail. The mode shape of this resonance is shown in Figure 4.2 with the values of stress mapped to color. The region of the bar that appears flat was the area that was shadowed by the transducer. All other parts of the bar appear to follow a flexural wave mode shape and can be fit to the flexural wave solution. Flexural wave theory allows four parameters to fit the displacement profile of a mode. The allowed parameters are coefficients of sin(kx), cos(kx), sinh(kx), and cosh(kx) where k is the wave number and x is the longitudinal

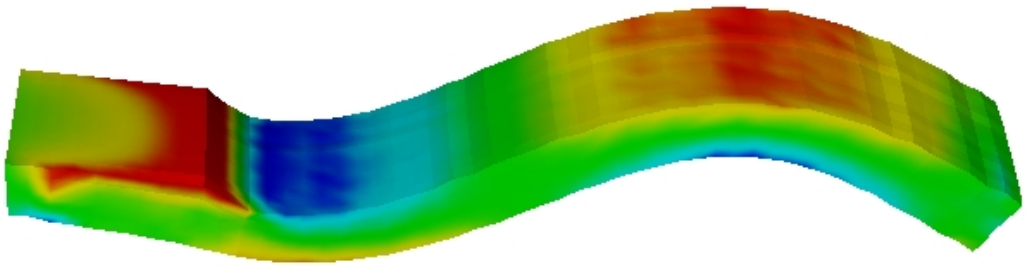

Figure 4.2 7.4 kHz resonant mode shape measured with the laser vibrometer. The τ_{xx} stress of this mode has been mapped to color.

position along the bar. These four parameters were fit to the observed shape of the 7.40kHz mode. The velocity profile and the four parameter fit to flexural wave theory are shown in Figure 4.3.

The four parameters obtained from the best fit to flexural wave theory can be used to evaluate the stress profile in the bar. The τ_{xx} stress is given for the cross-sectional slice of the bar and mapped to color in Figure 4.4. These values match to within 5% for all areas not shaded by the transducer or its immediate vicinity, corresponding to $x < 35$ mm on the lower left-hand side of the upper bar in Figure 4.4.

One major advantage of this method for determining stress is shown in Figure 4.5. This figure shows two missed data points, one on the upper part of the specimen and another near the lower edge. Though these points have a zero velocity, their effects on the surrounding areas quickly drop off as 1/r.

4.6 Conclusions

We have demonstrated a method to calculate the dynamic stress tensor at all points within a vibrating object through the use of surface vibrometry. These results were found to compare to within 5 percent - except in the immediate vicinity of shaded regions -

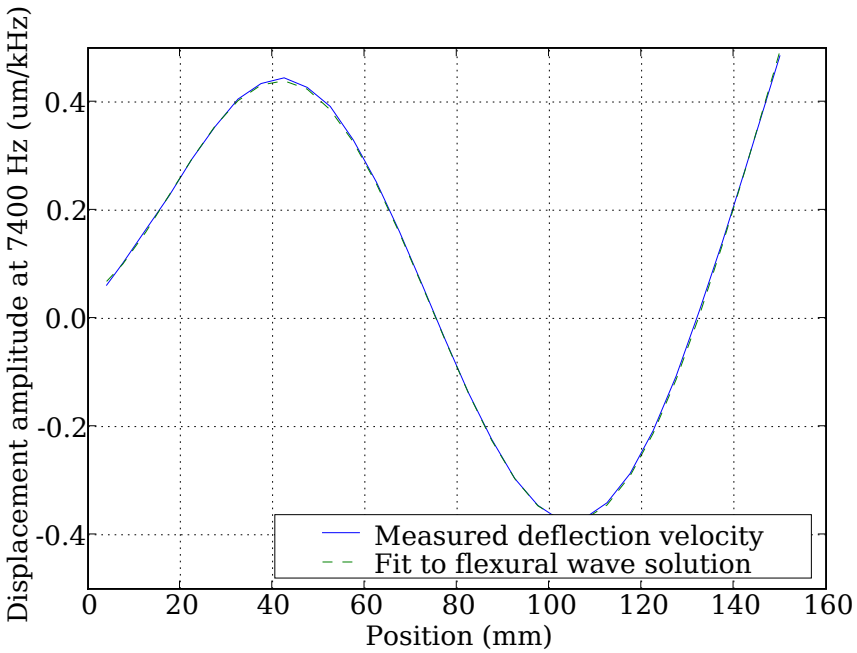

Figure 4.3 Mode profile of the 7.4 kHz resonant mode and the best-fit flexural mode shape. The curve fit is: $y = -.272\sinh(\kappa x) + .272\cosh(\kappa x) + .337\sin(\kappa x) - .226\cos(\kappa x)$ μm/kHz. The two curves are superimposed nearly on top of one another.

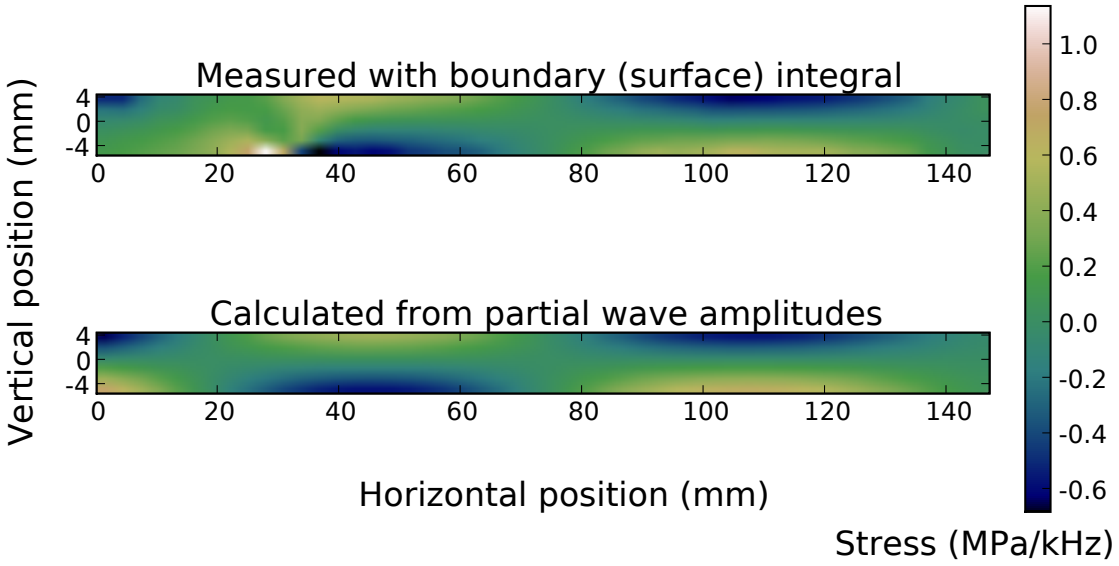

Figure 4.4 Color mapped images of the measured and calculated stresses.

of those calculated based on flexural wave theory using the four parameters shown in Figure 4.3. The use of the Green's Function and the reciprocity integral formulation allow the measurement to be done even when one or more faces of an object are not measurable, since the influence of missed points or areas dies away with a 1/r dependence from such locations. This method shows promise to accurately correlate internal stresses and strains at a crack face to the observed heating in vibrothermography.

4.7 Acknowledgements

This material is based upon work supported by the Air Force Research Laboratory under Contract #FA8650-04-C-5228 at Iowa State University's Center for NDE

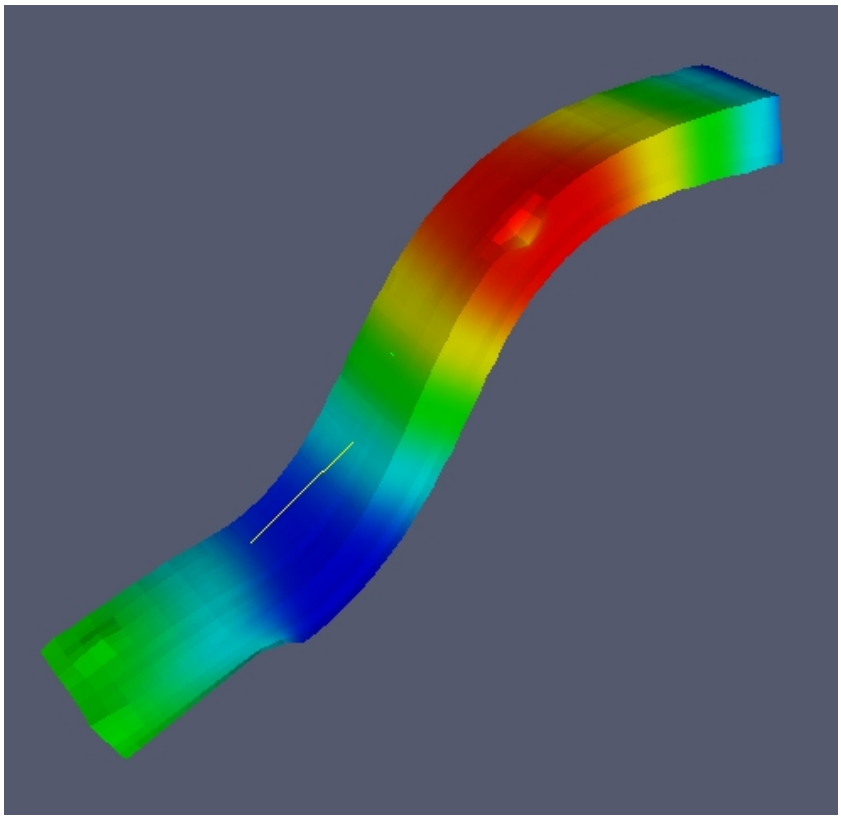

Figure 4.5 Effect of missed data points on surrounding areas. The bar is color mapped to velocity.

CHAPTER 5. THE ORIGINS OF HEAT GENERATION IN VIBROTHERMOGRAPHY

A paper under review at the Journal of Applied Physics

Jeremy Renshaw [1], Stephen D. Holland, John C. Chen, R. Bruce Thompson, and Christopher Uhl

5.1 Abstract

Vibrothermography, or sonic IR, is a nondestructive evaluation technique used to find surface and near surface defects, such as cracks and delaminations, through observations of vibration-induced heat generation. This method has significant interest as an industrial inspection method, however, a lack of understanding of the fundamental physics governing the heat generation process has limited its application in industry. This paper presents experimental observations of vibration-induced heat generation in samples that correlate to specific heat-generating mechanisms. Experimental evidence shows that the primary source of heat generation for typical industrial vibrothermography is frictional rubbing. If vibrational stresses are large enough to cause material degradation, such as crack propagation, additional heat is also generated due to plastic deformations around the crack tip. In some materials, significant heat can also be generated due to viscoelasticity.

[1]Center for NDE, Ames, IA 50011

5.2 Introduction

Vibrothermography is a nondestructive evaluation technique used to find surface and near surface defects. Also known as thermosonics and sonic IR Morbidini, M. (2006), vibrothermography finds cracks, disbonds, or delaminations using the heat generated at these defects when they are vibrated. The generated heat diffuses away from the defects and radiates from the outer surfaces. Radiated heat is detected and measured using an infrared (IR) camera observing the surface of the structure. There is significant industrial interest in vibrothermography due to its ability to rapidly and accurately detect the presence and locations of defects in structures DiMambro, J. (2007); however, it has been hindered by issues such as repeatability Morbidini, M. (2006), due in part, to a lack of understanding of the physics governing the heat generation of vibrating defects Han, X. (2004B).

Reifsnider, Henneke, and Stinchcomb Reifsnider, K. L. (1980) observed heat generation at vibrating artificial delaminations in composites. They noted that heat generation at the delaminations increased when samples were vibrated at certain resonant frequencies. Through these and other observations, they suggested that the sources of heat generation in their artificial delaminations resulted primarily from friction, plasticity, and viscoelasticity in and around the defects. Subsequently, many similar experiments have been performed on samples containing cracks Han, X. (2004B); Morbidini, M. (2006); Renshaw, J. (2008). It has been shown that regions of heat generation along a crack correspond to contacting regions in the crack and the location of these regions changes as the crack is opened with an external load Renshaw, J. (2008, 2009B). Lu et al. Lu, J. (2007) showed that increasing compressive stresses on a crack can terminate heat generation, presumably by locking crack face asperities together with static friction, giving additional evidence that heat generation in cracks appears to be related to friction. Frictional rubbing between contacting asperities has long been assumed to

be the dominant source of heat generation in vibrothermography Morbidini, M. (2006); Shepard, S. M. (2004); Zhang, W. (1999). However, there is controversy over this claim since it has also been argued that frictional rubbing between crack faces is not responsible for heat generation or energy dissipation, but that crack heating is entirely due to interactions in the elastoplastic region of a crack Bovsunovsky, A. P. (2004). No conclusive experimental validation of either theory has been presented and no single theory has been universally accepted to date to explain the sources of heat generation in vibrothermography.

This paper presents experimental evidence correlating observations of heat generation in vibrothermography to specific heat-generating mechanisms. Crack heating in these experiments is generated primarily due to frictional rubbing of contacting regions (asperities) on crack faces. When cracks begin to propagate, additional heat may be generated due to plastic deformations. Viscoelastic losses can also generate significant heat in some materials and these losses are larger in regions of stress concentration Homma, C. (2006), such as around delaminations or other defects Reifsnider, K. L. (1980).

5.3 Theory

Heat generation in cracks is primarily generated from one or a combination of three mechanisms: friction, plasticity, and viscoelasticity/material damping.

Spatially isolating regions of heat generation provides a means to determine contributions from heat-generating mechanisms on the total heat generation of a defect. In cracks, frictional heat generation occurs due to rubbing of contacting regions (asperities) along crack faces. Frictional rubbing may also induce plastic deformation of rubbing asperities, evidenced by plow marks on the asperities Blau, P. J. (2009); Bowden, F. P. (1950). Such deformations are classified here as "friction," first because they are friction-induced and, second, to avoid confusion with plastic deformations near

the crack tip associated with crack propagation. Frictional heat generation cannot occur past the crack tips in vibrothermography since there is no surface available to rub. Crack growth, however, can cause heat generation in the plastic zone beyond a crack tip due to plastic deformations in the crack's plastic zone. Viscoelastic heating is negligible in most metals, but can be a significant heat source for polymer-based materials Homma, C. (2006); Reifsnider, K. L. (1980). Viscoelastic heating is evidenced by bulk heating of the structure from the vibrational stress with additional heating at regions of stress concentration, so it is generally possible to distinguish between plasticity-induced and viscoelastic heating. Measurements of vibrational stresses further aid in distinguishing between heating from plasticity, which only begins to occur above a specific threshold stress, and viscoelasticity, which is linearly related to the vibrational stress level.

Thermoelastic heating and cooling can be significant in some circumstances, but are averaged out of the heating data by setting the integration time of each IR camera frame to be many times longer than the period of vibration.

Observing heat generation of a crack while modifying its closure state (the regions of contact along the crack) also helps to determine whether friction or viscoelasticity is dominant. Both heating mechanisms depend on the local vibrational stress and strain at the defect, though frictional heating also depends on the contact between crack faces and the level of the stress pressing crack faces together. Varying closure stresses can separate crack faces from contact or lock them together. Both actions can prevent frictional heating, though neither action would entirely eliminate viscoelastic heating.

5.4 Experimental Procedure

The experimental setup used for the tests performed in this study is shown in Figure 5.1. A cracked sample is held in place using clamps and vibrated using a broadband piezoelectric transducer excitation system Holland, S. D. (2007A). Samples are vibrated

at resonance to improve energy coupling into the sample and more effectively generate heat at defects. Surface vibrations of the sample are measured using the laser vibrometer, whose beam is reflected through a mirror to obtain normal incidence to the measured surface while surface heating of defects is observed and measured using the IR camera Renshaw, J. (2009A). Sequences of calibrated IR images are recorded for subsequent processing to extract heat generation and diffusion information.

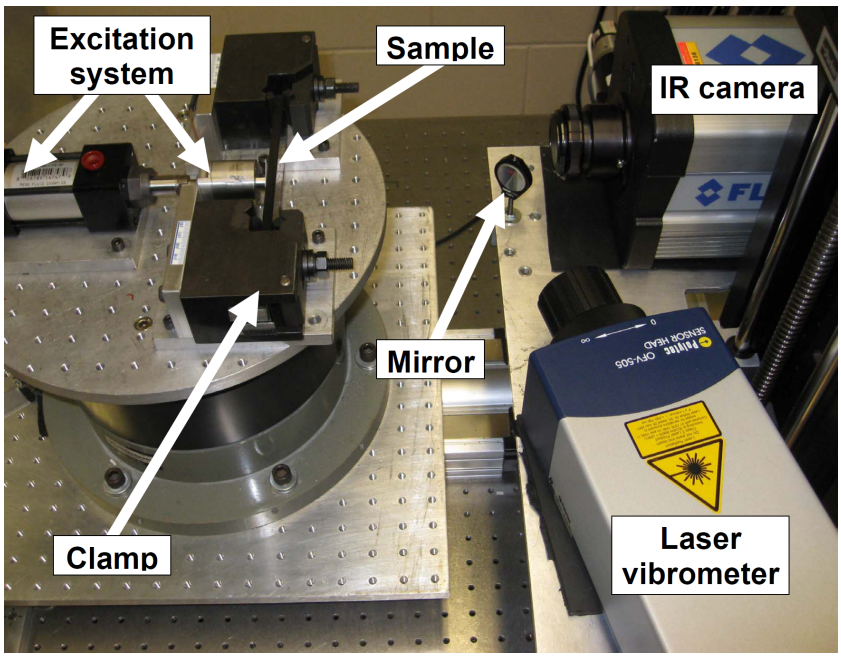

Figure 5.1 Experimental setup used for exciting the test specimens and observing heat generation.

The vibrational stresses used for most experiments were small in comparison to the fatigue limit of the material to avoid causing additional damage to the specimen, such as crack growth, which has been observed at high vibrational stress levels Chen, J. C. (2007).

After testing was completed on each sample, the cracks were observed and their lengths carefully measured to check for crack growth. After a surface examination, the cracks were broken open to observe the rubbing crack faces using optical and scanning

electron microscopy to check for friction-induced damage to the rubbing surfaces.

5.5 Results

5.5.1 Frictional heating

Previous work Lu, J. (2007); Renshaw, J. (2008, 2009B) shows that friction is a dominant source of vibrothermographic heating in metals since high closure stresses on crack faces can terminate heat generation, but these stresses would not have had such a significant effect on the heat generation of a crack were viscoelasticity or plasticity primarily responsible for heat generation in these cases. The work of Homma et al. Homma, C. (2006), however, shows that viscoelastic heating can also be significant in polymer-based materials.

Figure 5.2 shows a hypothetical schematic of how heat is generated by friction in a semielliptical surface crack. View A in Figure 5.2 shows heat generation due to vibration at the surface of a semielliptical crack in titanium (Ti 6-4) with the crack length (dotted line) superimposed on top of the heating profile. View B in Figure 5.2 shows a schematic side view of the semielliptical crack, correlating to the observed heat generation in View A, including open, heating, and locked asperity regions as well as the plastic zone past the crack tips. The heating profile in View A shows that heat is not generated near the crack tips in this crack and demonstrates that, in this crack, frictional heating appears to be the primary source of the observed heat generation.

Figures 5.3 and 5.4 show IR crack heating and microscopy images for cracks in titanium (Ti 6-4) samples. These cracks were grown to a length of 8.0 mm in three-point bending with an R-ratio (min/max stress) of 0.5 and maximum stress of 772 MPa.

If present, friction can cause modifications (damage) to rubbing asperities on surfaces such as fretting, plastic deformation, melting, etc. Bowden, F. P. (1950). Figures 5.3 and 5.4 show a correlation between the heat generated from two cracks and the

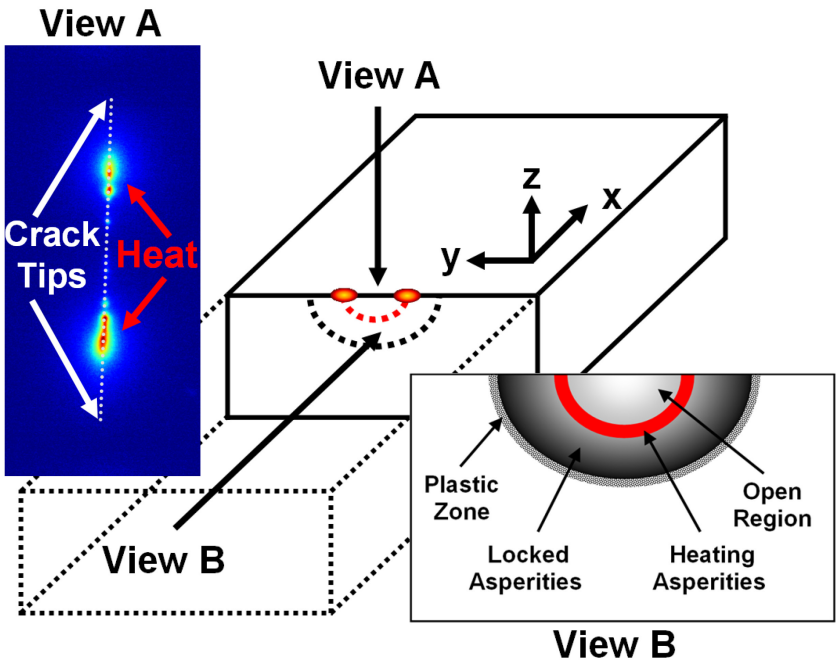

Figure 5.2 Hypothesized schematic of how heat is generated in a semielliptical surface crack based on previous studies Renshaw, J. (2008). View A shows the cross-section of the crack and View B shows the measured surface heating of the crack. The superimposed dotted line shows crack length and the white arrows point to the crack tips.

damaged regions on the crack faces caused by intense frictional rubbing. An image processing algorithm, based on the physics of heat conduction Holland, S. D. (2009), was used to eliminate effects of heat diffusion and isolate regions of heat generation on the sample surface by taking a filtered, second-order spatial derivative and first-order time derivative of a series of calibrated surface temperature measurements from the IR camera. Thus, Figures 5.3 and 5.4 compare regions of heat generation on the sample surface to regions within the crack that were damaged due to frictional rubbing as a result of the vibration. The crack in Figure 5.3 sustained fretting damage in a band that mirrors the schematic presented in Figure 5.2, providing evidence that the schematic is accurate for this particular crack geometry. Once grown to a length of 8.0 mm, the crack in Figure 5.4 was sliced in half. One half, shown at the top of Figure 5.4, was

kept as a pristine reference sample and the other half, shown directly below the pristine half in Figure 5.4, was vibrated at resonance to generate heat and compare against the pristine reference half for evidence of frictional rubbing. The reduced cross-section and additional free surface of the crack in Figure 5.4 allowed for intense vibrations to be applied, which generated sufficient frictional heat to cause oxidation and melting on the rubbing crack face asperities. These results clearly show that friction is a primary mechanism of heat generation in vibrothermography.

5.5.2 Plasticity-induced heat generation

Planar cracks were grown in 2024 aluminum eccentrically loaded single edge tension (ESET) samples as described in Chen et al. Chen, J. C. (2007). An annealing heat treatment was used to relieve closure stresses along the cracks. These cracked samples were then loaded into the mounting apparatus and vibrated using an ultrasonic welder. The welder can provide high vibrational amplitudes at a frequency of 20 kHz. Due to the relaxation of the closure stresses and the high vibrational stresses applied to the aluminum samples, the cracks began to grow Chen, J. C. (2007), meaning that the area ahead of the crack tip was being plastically deformed and would also be generating heat.

The left side of Figure 5.5 shows an image of the heat generation of a propagating crack in an aluminum sample. Image processing was again used to isolate regions of heat generation in the sample, shown on the right side of Figure 5.5. Figure 5.5 also shows some heat generation along the crack and two distinct regions of significant heat generation (indicated by white arrows) near the crack tip. The left heating region correlates to a branch in the crack. In the experiment shown, only the branch of the crack on the right side grew, indicated by the heating region on the center-right side of Figure 5.5, and indicated by the arrow on the right side of the figure. Heat generation at this location occurred past the crack tip where plastic deformations were occurring, giving strong evidence of plasticity-induced heat generation. Rabiei, Evans, and Hutchinson

Rabiei, A. (2000) and Luong Luong, M. P. (1998) present direct evidence of heat generation due to plastic deformations in samples not containing cracks.

It is likely that some heat near the crack tip also results from friction during the portion of the vibration cycle where the crack faces are in contact. Previous experiments on cracks Renshaw, J. (2008) showed that heat generation occurs along partially-opened cracks until they are fully opened. Though stresses were low and no crack growth occurred, this does not prove that plasticity-induced heat generation can not occur in a nonpropagating crack.

5.5.3 Viscoelastic heating

Viscoelastic heating of simulated delaminations has been observed in polymer composites by Reifsnider, Henneke, and Stinchcomb Reifsnider, K. L. (1980). They report that viscoelasticity is a dominant heat generation mechanisms in polymer composites. Additional viscoelastic heating is present in the vicinity of a defect due to the high stress concentrations around such defects when they are vibrated intensely, as in vibrothermographic studies. Figure 5.6 shows viscoelastic heating in a carbon fiber reinforced composite (CFRP) measured using an infrared camera. Holes were drilled in the bar shown at the bottom of Figure 5.6 to generate stress concentrations primarily above and below the holes when vibrated in the direction indicated in Figure 5.6. Applied vibrational stresses were kept low to avoid plastic deformation. When the sample containing the drilled holes was vibrated, the stress concentrations around the holes generated heat above the baseline of the excited resonance in a pattern consistent with the expected stress concentration around a stressed hole, as shown in the IR heating data in Figure 5.6. Other studies have confirmed that high vibrational stresses in materials can cause heat generation due to viscoelasticity (or material damping) Homma, C. (2006).

5.6 Conclusions

This paper presents experimental evidence of the sources of heat generation in vibrothermography that agree with, and further explain, heat generation data from other published experimental results in the field of vibrothermography. These results show that the dominant sources of heat generation in a vibrating crack can include frictional rubbing, plastic deformations, and viscoelasticity depending on the material, type of defect, and the vibrational stress level.

Frictional rubbing occurs, especially in cracks, and is evidenced by alterations or damage to rubbing crack faces. Plastic deformations in the plastic zone of a propagating crack may also occur at high vibrational stress levels and will generate additional heat beyond that of friction, especially in regions beyond the crack tip. Viscoelastic heating can also occur depending on the material and is related to the vibrated material's properties and level of applied vibrational stress. Viscoelastic heating is increased in regions of stress concentration and does not require a rubbing interface to generate heat. For typical applications of vibrothermography (nonpropagating surface cracks in metals), frictional rubbing is the primary source of heat generation.

5.7 Acknowledgements

This material is based upon work supported by the Air Force Research Laboratory under Contract #FA8650-04-C-5228 at Iowa State University's Center for NDE

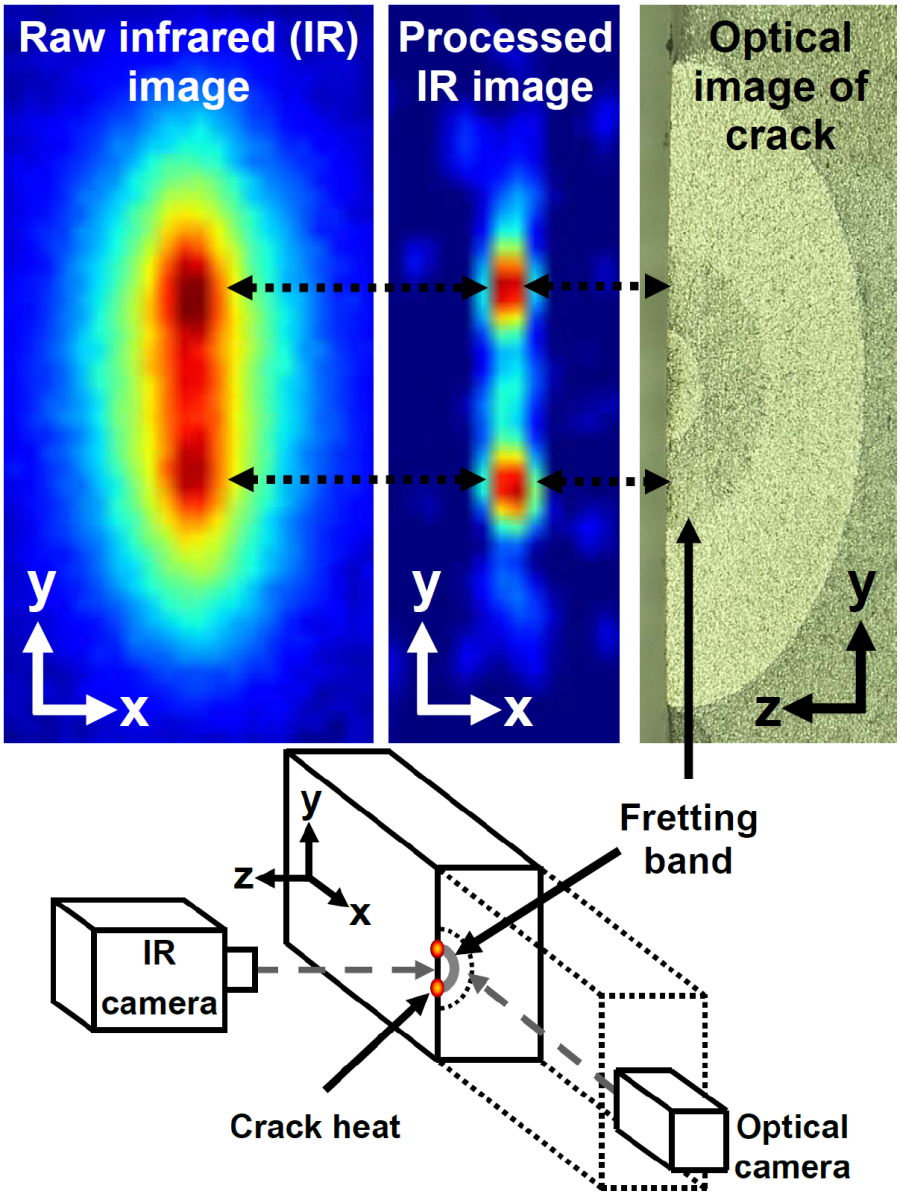

Figure 5.3 Correlation of frictional heat generation with crack face damage in titanium (Ti 6-4), (top, right) an optical image of the unvibrated half of the crack, (middle, left) raw heating data, (middle, center), processed heating data isolating regions of heat generation, (middle, right) melting and other damage observed on the crack faces, and (bottom) a schematic of the crack and sample geometry.

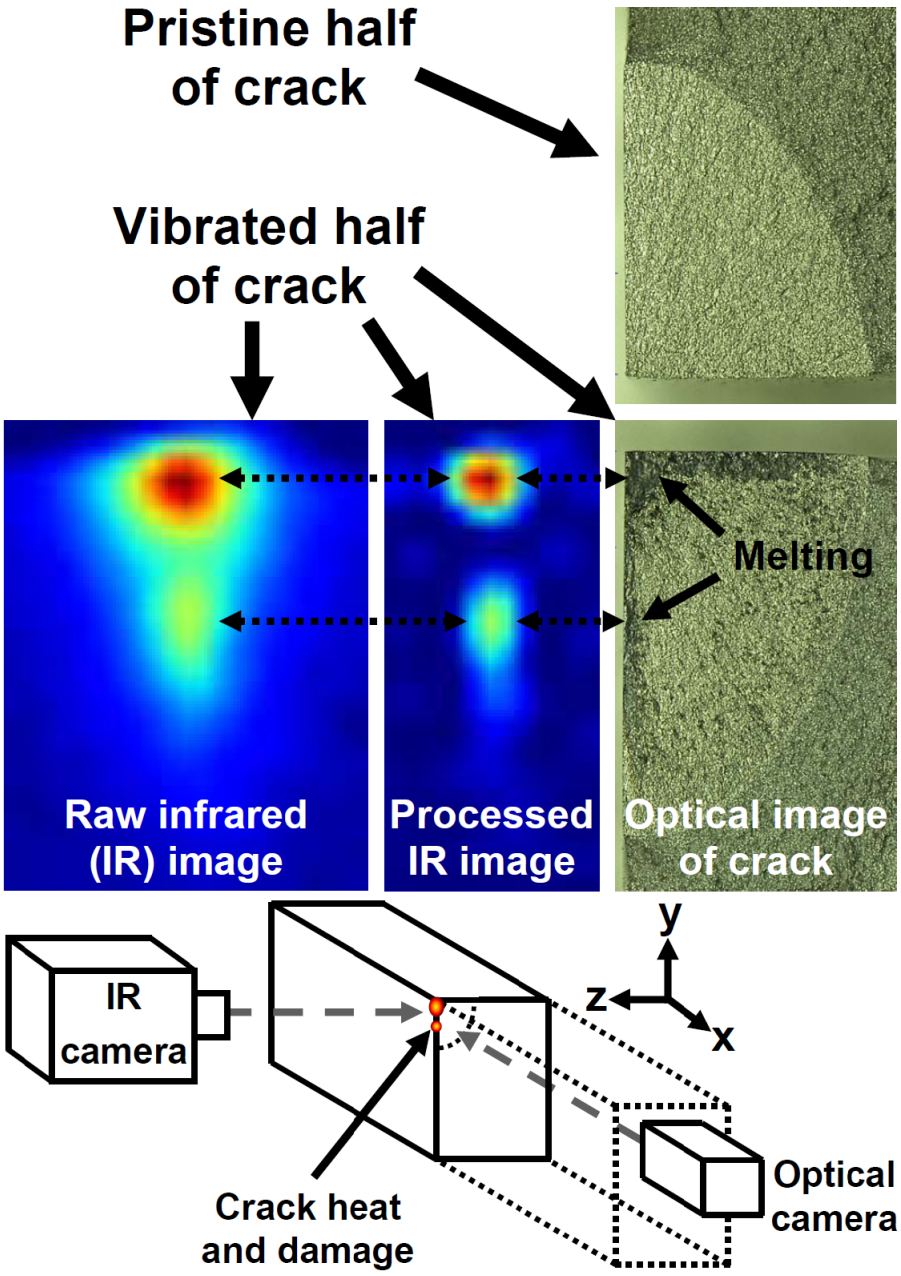

Figure 5.4 Correlation of frictional heat generation to crack face fretting in titanium (Ti 6-4), (top,left) raw heating data, (top,center), processed heating data isolating regions of heat generation, (top,right) fretting observed on crack faces, and (bottom) a schematic of the crack and sample geometry.

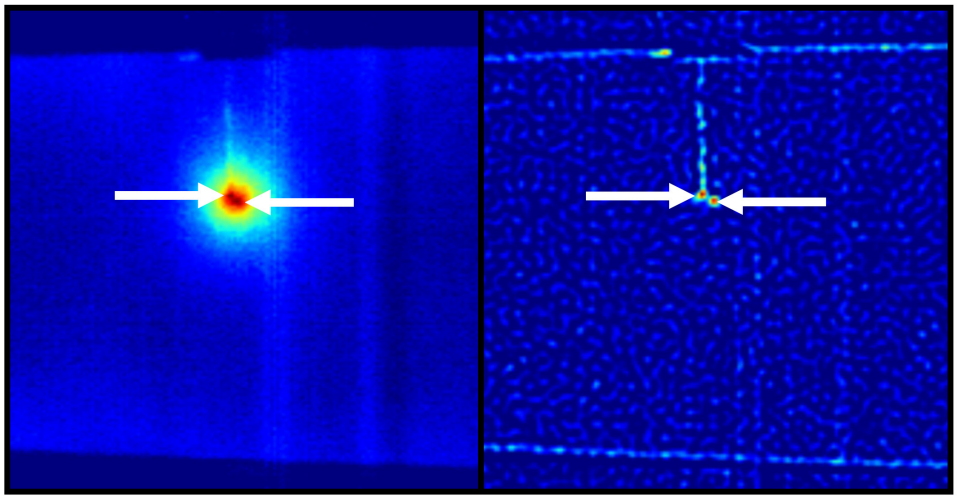

Figure 5.5 (a) Raw Infrared (IR) heating data compared to (b) processed IR data isolating regions of heat generation along the crack and at the crack tips.

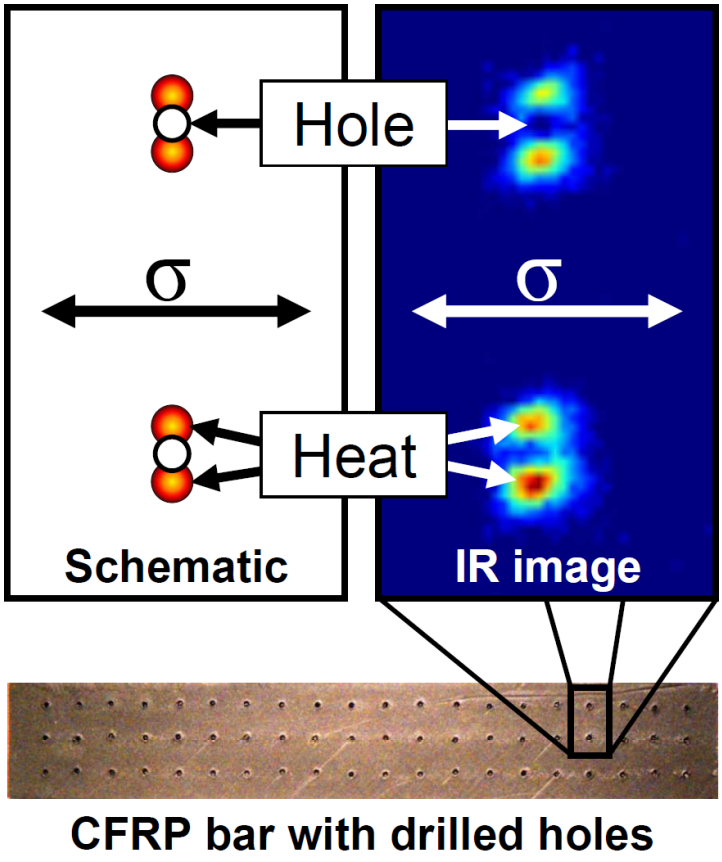

Figure 5.6 (bottom) the CFRP sample containing an array of drilled holes, (left) schematic of a CFRP sample containing drilled holes with arrows showing the direction of applied stress, and (right) observed infrared heating in the bar due to viscoelasticity and the stress concentration at the holes.

CHAPTER 6. THE EFFECT OF CRACK CLOSURE ON HEAT GENERATION IN VIBROTHERMOGRAPHY

A paper published in Review of Progress in Quantitative Nondestructive Evaluation [1]

Jeremy Renshaw [2], Stephen D. Holland, R. Bruce Thompson, and Christopher Uhl

6.1 Abstract

Vibrothermography is a nondestructive evaluation (NDE) technique that has shown great promise in detecting tight cracks that can often be missed using other NDE methods. Vibration applied to a structure containing cracks forces crack faces to rub together and generates frictional heat imaged with an infrared camera. The closure state of a crack controls the locations and magnitude of heat generation in a vibrated crack. Non-contacting regions of cracks and regions under large closure stresses generally do not rub together to generate heat. Heat is generated at contacting regions of crack faces under low closure stresses. Regions along a crack that generate heat can be modulated based on externally applied stresses. The closure state of a crack, the level of applied vibration, and externally applied stresses influence the regions of a crack that will generate heat and those that will not. Due to the nature of the heat generation process, some cracks that are not detectable using other NDE methods are readily detectable using vibrothermography.

[1]Reprinted with permission from the American Institute of Physics, 2009
[2]Center for NDE, Ames, IA 50011

6.2 Introduction

Crack closure is the process by which residual stresses force crack faces into contact. Closure stresses hold crack faces together due to a variety of mechanisms including plasticity-induced closure, roughness-induced closure, oxide-induced closure, etc. Suresh, S. (1998). Crack closure is an important parameter that affects both crack propagation rates as well as the detectability of cracks in structures. Crack closure was first observed by Elber Elber, W. (1971) and is an important parameter in understanding crack propagation. It is equally important in nondestructive evaluation (NDE) since crack closure affects the ability of NDE techniques to detect the presence and locations of cracks in structures. NDE techniques are most sensitive to open cracks since open cracks create a larger interruption in the bulk structure of a material. Open cracks have lower amounts of closure between the crack faces than tight cracks creating an effectively larger defect volume. Larger defect volumes give increased contrast in X-ray inspections, serve as fluid reservoirs for fluorescent penetrant inspections, interrupt the magnetic fields involved in eddy current inspections, leak more magnetic flux in magnetic particle inspections, and provide reflective surfaces for ultrasonic inspections. Additionally, increased closure decreases the probability of detecting and increases the probability of undersizing a detected crack Buck, O. (1983). Thus, the major NDE techniques are more sensitive to open cracks than tight cracks.

Vibrothermography, also known as Thermosonics or Sonic IR, is an NDE technique gaining increasing attention due to its ability to rapidly detect cracks, delaminations, and disbonds in structures Reifsnider, K. L. (1980). A significant advantage of vibrothermography is that it does not rely on the presence of open defect regions to interrupt the bulk structure and trigger a detectable response as do other major NDE methods. Vibrothermography instead relies on the rubbing of crack faces to generate heat. Frictional rubbing does not depend on the presence of open regions along a crack for the

inspection method to be effective. Thus, vibrothermography has the potential to detect tighter cracks with greater reliability than is possible using other NDE methods.

The method of defect detection using vibrothermography is shown in Figure 6.1. First, a part is vibrated using a transducer Chen, J. C. (2007); Holland, S. D. (2007A). The vibrations force opposing crack faces to rub together. Heat is generated at rubbing crack faces due to friction, increasing the temperature of the material surrounding the defect. An infrared (IR) camera is used to observe the outer surface of a sample for the presence of defects which are indicated by locations of local temperature changes on the surface. Thus cracks, disbonds, delaminations, and other defects with contacting interfaces may be observed due to friction-induced heat generation at the defect.

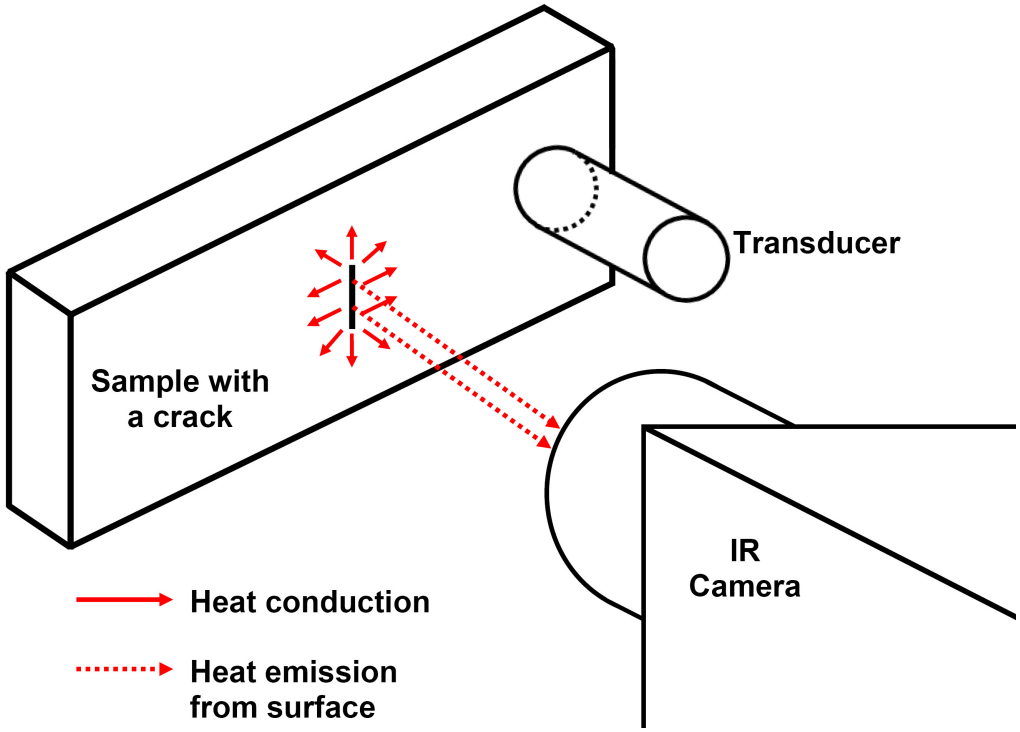

Figure 6.1 The heat generation process in vibrothermography. First, the part is vibrated causing crack faces to rub and generate heat. Heat diffuses away from the crack and is emitted from the outer surfaces. An infrared camera is used to observe the changes in surface temperature.

The amount of crack closure and the distribution of closure stresses between crack faces affect the heat generated in vibrothermography and appear to be major factors influencing both the detectability of a crack as well as determining which crack regions, if any, will generate heat due to applied vibrational stresses. Both the amount of heat generated as well as the locations within a crack that generate heat are affected by the closure state of the crack and can be modulated by applying an external load to open or close the crack Lu, J. (2007); Renshaw, J. (2008).

6.3 Theory

Crack faces may be forced into contact through a variety of mechanisms. Generally, the dominant closure mechanism is plasticity-induced closure, caused by the envelope of plastically-stretched material from the plastic zone around an advancing crack tip forcing crack faces into contact upon relaxation of the externally-applied load that grew the crack. A second important mechanism, roughness-induced closure, results from a mismatch in opposing fracture surface roughnesses giving way to additional closure stresses between crack faces. Many other closure mechanisms are possible based on the conditions to which the crack was subjected Schijve, J. (1988); Stoychev, S. (2003); Suresh, S. (1998); however, these mechanisms were not significant in the cracks studied in this paper. Closure mechanisms affect the detectability of cracks by causing crack faces to contact prematurely (under tensile or zero external load) and creating interactions between the faces of the cracks. These interactions cause closure stresses between the crack faces that can reduce or eliminate the ability of NDE techniques to detect the cracks or mask portions of the crack Buck, O. (1983, 1987).

Heat is generated in contacting regions of the crack that are under low, but nonzero closure stress. The regions of the crack that are held together too tightly to be rubbed together due to the applied vibration are referred to as locked asperities. Locked asperity

regions do not generate heat since the crack faces are not free to rub against each other. Similarly, regions of the crack that do not contact due to the applied vibration, but remain open do not heat and are referred to as open regions. Thus, heating asperities are those regions of the crack where asperities are in contact and rub due to the applied vibration which generates frictional heating. Heat generated in cracks is not uniformly generated along the surface of a crack. Different regions along a crack will heat up to varying degrees and in many cases, certain regions of a crack will not generate any heat. It is possible that heat can be generated both at the surface as well as below the surface. Figure 6.2 shows a depth profile of a semielliptical surface crack with a schematic of the crack heating as a function of the crack length and depth. Figure 6.2 shows that heat generation can occur both at the surface and below the surface, often giving rise to complicated surface heating profiles as shown in Figure 6.3. These heating profiles can be very complex depending on the amount and type of closure mechanisms acting along the crack faces; however, due to heat diffusion, these regions often blur together and create difficulties in imaging individual regions of heat generation.

Removing the effects of diffusion is not a trivial process. Heat is generated at different contacting regions of the crack and separated by small regions devoid of contact. Additionally, the contact between asperity regions is very complex and heat that is generated by these asperity regions is generated at different amounts along contacting regions. Finally, only temperature changes at the surface of a structure can be imaged, so solutions to back out specific heat generating regions and amounts of heat generated can quickly diverge. Holland and Renshaw Holland, S. D. (2009) have developed a method to remove diffusion effects in the plane of the sample surface by means of a second-order spatial derivative and two-dimensional spatial filtering. This method does not give accurate measurements of heat generation rates, but does eliminate the effects of diffusion due to surface heat propagation. Subsurface heat generation is generally lower than heat generation at the surface due to reduced crack face mobility and the

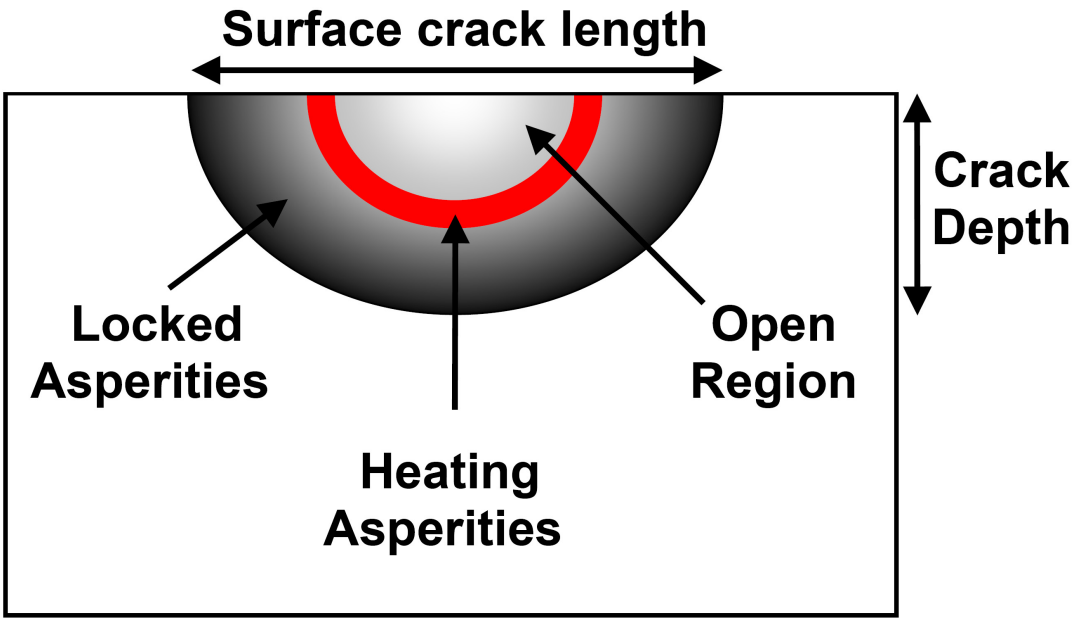

Figure 6.2 A schematic of heat generation in a vibrating crack. The figure shows a cross-sectional view of a bar containing a surface crack with a semielliptical depth profile.

additional heat diffusion length from the subsurface heat source to the surface of the part. This image enhancement method was used on a 13 mm crack as shown in Figure 6.3. The method effectively isolated regions of heat generation. It can be seen that heat is not uniformly generated along the surface of the crack. More importantly, the heat generating length of the crack shown in Figure 6.3 is 6.64 mm but the crack length is 13.51 mm. Heat generation was centered between the two crack tips but did not occur near the crack tips. This means that a large portion of the crack did not generate heat due to locking of crack face asperities from the higher closure stresses present near the crack tips. These higher closure stresses resulted from plastic deformations that occurred during the crack growth process.

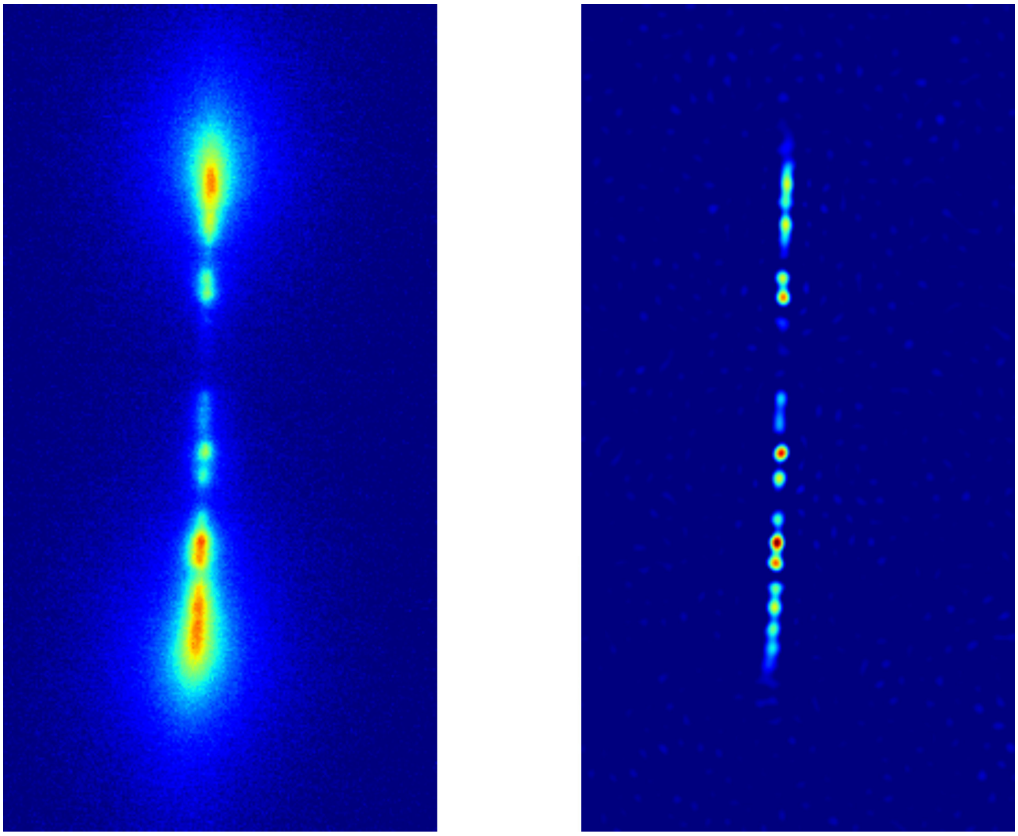

Figure 6.3 Infrared image of a crack (left) and the same image once the effects of surface heat diffusion are removed (right).

6.4 Experimental Procedure

Cracks were grown in Titanium 6Al-4V (Ti 6-4) samples to a length of about 13.0 mm under different conditions designed to grow cracks with different closure states to compare the effect of closure on the positions of heat generating regions of the cracks. The crack in Sample A was grown to have a lower closure stress than the crack in Sample B. After unloading these samples from the servohydraulic testing machine used to grow the cracks, they were placed in a bending fixture to modify the closure state on the crack faces by introducing external tensile loads to counteract the plastic closure stresses. Mounting points were selected to correspond to nodal locations of the excited vibrational resonance to minimize their effect on the sample vibration Holland, S. D.

(2008). An external tensile load was applied using the bending fixture to peel open the cracks as the samples were vibrated to generate heat on portions of the contacting crack faces. Regions of heat generation were compared versus the closure state on the cracks to determine the influence of crack closure on the regions of the crack that generated heat.

6.5 Results

Figure 6.4 shows the regions of heat generation as a function of the applied tensile loads for the two cracks. The regions of heat generation move towards the crack tips as the load is increased and away from the tips as the load is decreased. Figure 6.4 shows that as the closure state of the crack changes, so do the primary regions of heat generation along the cracks. The heat-generating regions of Sample B are closer together than those of Sample A due to the higher crack closure stresses present in Sample B.

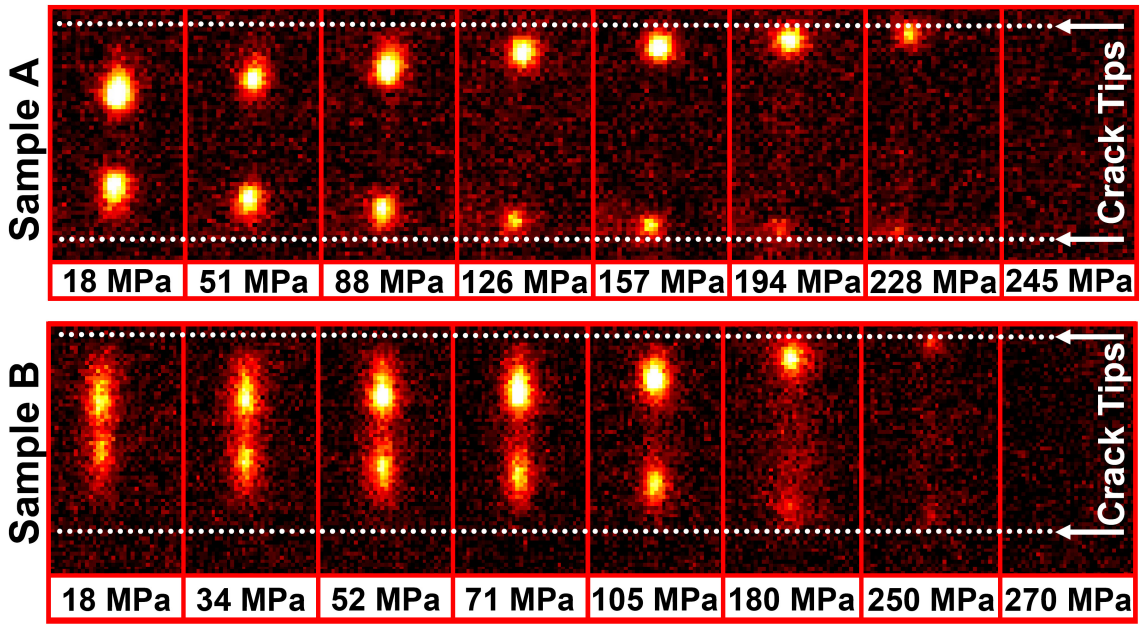

Figure 6.4 Images of infrared crack heating locations as an increasing tensile stress is applied.

Using the regions of heat generation shown in Figure 6.4, the closure stress profile along a crack can be determined Renshaw, J. (2008). Regions of heat generation indicate which portions of the crack have been opened and which portions remain locked. Figure 6.5 shows the heating regions of two cracks as a function of the applied opening stress with the crack length normalized by the total crack length, $2a$, from $-a$ to $+a$. The portion of the crack length that has been opened at a given stress level is the distance between two heat generating regions in Figure 6.4 or the portion of the crack length between two points at equal applied opening stresses on the graph in Figure 6.5. The portion of the crack that remains closed, or locked, at a given opening stress is the portion of the crack length beyond the same two points in either figure. The two horizontal lines on the graph in Figure 6.5 are measures of the crack opening stresses, or the stresses required to fully open each of the cracks. No heat is generated at the crack opening stress level since the cracks have fully opened and the opposing crack faces are no longer able to rub together to generate heat. These data have been used to measure crack opening stresses and crack closure stress profiles of cracks Renshaw, J. (2008). These data also show that the locked asperities will not generate heat until a sufficient stress is applied to overcome the static frictional forces locking the asperities together.

Comparing the two cracks shown in Figure 6.4 shows that the regions of heat generation in a tight crack occur further from the tips than in open cracks. This means that tighter cracks have a larger portion of the crack faces locked together than open cracks. These results show that the crack closure stress on a crack affects the regions along a crack that generate heat and that these locations can be modified by applying an external load on the crack. The most important parameters affecting crack detectability in a vibrothermographic inspection are the closure stress along a crack, effects of static loads, and the applied vibrational or dynamic stress level. If the applied vibrational and static stresses on a crack dominate the locking stresses - due to closure stress and static friction on the crack faces - then the crack face asperities will rub against one another

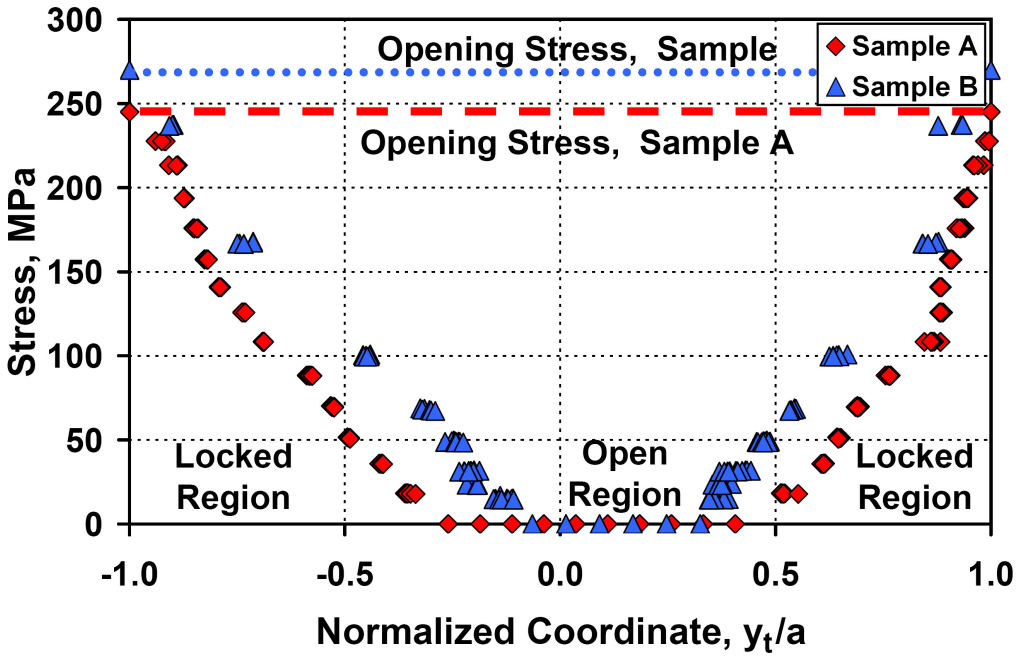

Figure 6.5 Graph showing the distance between heating regions divided by the crack length and plotted as a function of the tensile static stress applied on the crack.

and generate heat, creating a detectable infrared indication. If the closure stresses and static friction dominate the vibrational and static stresses, however, crack face asperities will remain locked and will not generate heat, causing the crack to be undetectable using vibrothermography. The presence of both open and locked regions along a crack gives rise to heating asperities as shown in Figure 6.2 and significantly increases the probability of detection of a crack. Thus, cracks with both open and locked regions will likely also have asperities that are able to vibrate and generate heat. Such cracks exhibit heat generation at lower vibrational stresses. A fully open or fully locked crack is less likely to have asperities able to generate frictional heat and are more likely to be undetectable unless very high vibrational stresses are applied. A crack that is fully open along its length, however, is rare in an NDE inspection.

Smaller cracks have lower crack opening stresses than larger cracks that are grown under identical conditions in constant amplitude (CA) loading, though the crack opening

stress is only a measure of the closure at the crack tip. Therefore, small cracks may have a sufficient closure stress along the length of the crack to lock all of the asperities together and prevent heating. Larger cracks are more likely to have larger variations in closure stresses and open regions, making them easier to find. Also, larger cracks have have more mobility and a larger fracture surface area available for heat generation. The larger surface area, larger mobility, and larger variation in closure stresses increase the probability of detection of larger cracks. Thus, defect detection with vibrothermography is dependent on the applied vibration level, the size of the crack, and the closure profile of the two opposing crack faces. These factors are important in explaining why smaller cracks are generally harder to detect with vibrothermography than large cracks and thus have lower probabilities of detection Uhl, C. J. (2009). It also explains why some cracks that can be missed with FPI and other methods (due to the lack of open regions) can be easily detected using vibrothermography, as shown in Figure 6.6.

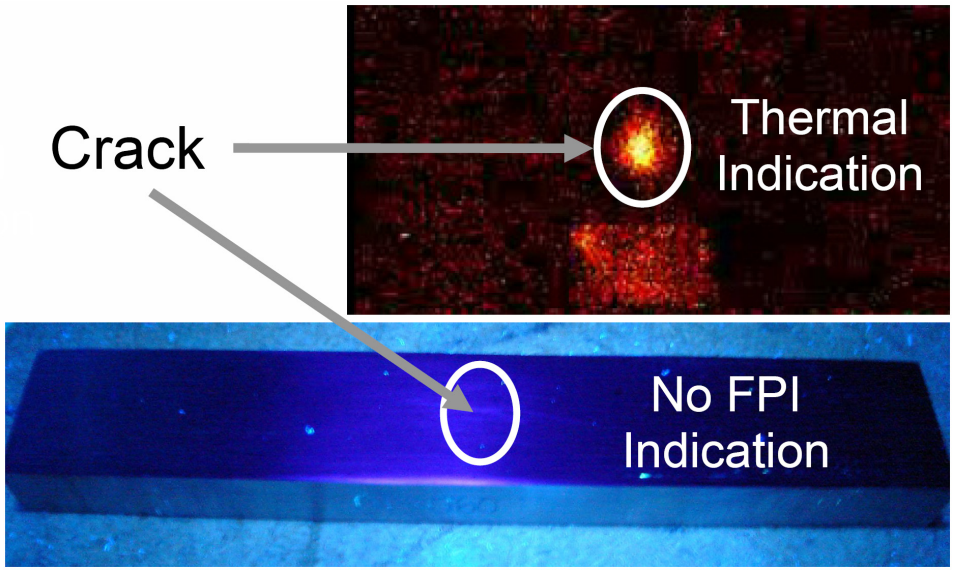

Figure 6.6 A tight 3.9 mm crack in a titanium sample heats up significantly due to vibration (above). The same crack was not detected with multiple inspections using fluorescent penetrants.

Figure 6.6 shows a 3.9 mm crack with a very small crack opening displacement,

giving it a very low defect volume. This crack remained undetectable after multiple fluorescent penetrant inspections, but readily generated heat during a vibrothermographic inspection. Despite the fact that the entire surface of the crack remained in contact, the applied vibrational stress was able to rub the crack faces together and generate heat, making the crack easily detectable. Thus, some cracks that may be missed using FPI or other inspection techniques can be detected using vibrothermography.

6.6 Conclusions

Cracks of the same size may heat differently depending on the closure stresses on the cracks as well as the influence of externally applied loads. More open cracks generate heat closer to the crack tips than tight cracks and have larger open regions that can aid crack detectability.

This paper shows how closure stresses on a crack affect the heat generation from and detectability of a crack. Larger cracks or more open cracks are generally easier to detect using NDE methods. Smaller cracks or tighter cracks are more difficult to detect with NDE methods, including vibrothermography. Vibrothermography has, however, shown great promise in its ability to detect tight cracks that cannot be detected using other methods. The detectability of a crack using vibrothermography is dependent on the amount of heat that the crack can generate. The amount of heat that is generated is related to the crack size, the crack mobility, the level of applied vibrational stress, and the interaction of the closure stresses on the crack with any externally applied loads. A deeper understanding of the heat generation process is needed to develop methods to generate more heat on crack surfaces and increase the probability of detection of cracks as well as understand the limitations associated with this NDE method. Understanding the physics of the heat generation process will help to create more accurate models of heat generation at contacting crack asperities and help vibrothermography to become a

better understood and more utilized NDE tool.

6.7 Acknowledgements

This material is based upon work supported by the Air Force Research Laboratory under Contract #FA8650-04-C-5228 at Iowa State University's Center for NDE.

CHAPTER 7. MEASUREMENT OF CRACK OPENING STRESSES AND CRACK CLOSURE STRESS PROFILES FROM HEAT GENERATION IN VIBRATING CRACKS

A paper published in Applied Physics Letters [1]

Jeremy Renshaw [2], Stephen D. Holland, and R. Bruce Thompson

7.1 Abstract

A method is described to measure crack opening stresses and closure stress profiles of a surface-breaking crack. Vibration is used to generate frictional heat by rubbing crack face asperities. Heat is generated at regions of contacting crack asperities under low, but nonzero, closure stress. Increasing force is applied to incrementally open the crack and measure the locations of crack heating as a function of applied load. Surface crack closure stresses are approximated from the heating locations as the load is varied and the crack opening stress is measured from the load required to fully open the crack and terminate heat generation.

Crack closure, the process by which crack faces contact and carry load Suresh, S. (1998), is a controlling factor of crack propagation under loading. A crack in tensile mode I loading must be opened by the crack opening stress, or the stress required to fully open a crack Elber, W. (1971), and have an additional stress applied at the tips

[1] Reprinted with permission from the American Institute of Physics, 2009

[2] Center for NDE, Ames, IA 50011

to propagate. When the tensile stress is removed, the residual plastic deformed region, formed during crack propagation due to the advancing crack tip, causes the crack faces to contact. This process is known as plasticity-induced crack closure. Closure stresses vary along the crack and can approach the material's yield stress at the crack tips Suresh, S. (1998), forcing regions near the crack tips to contact very tightly while other regions far from the tips may remain open. Many crack closure models have been developed since Elber's discovery of crack closure Elber, W. (1971), such as the work of Newman Newman, J. C. Jr. (1981, 2004). These models describe variations in closure due to crack size, location, geometry, loading, etc. Newman, J. C. Jr. (1988), and extensive experiments and numerical simulations have been done to validate these models on simple cracks McClung, R. C. (1999); Stoychev, S. (2003), however, the difficulty of accurately measuring closure regions has hindered measurements of opening or closure stresses, though ultrasonic methods have shown promise in evaluating closure regions Buck, O. (1984). Compliance techniques Elber, W. (1971); Pippan, R. (1999) are more common for measuring opening stresses, but are usually limited to measurements when strain gages are located near the wake of the crack or crack tip Hsu, C. (1999); Pippan, R. (1999); thus experiments may require numerous strain gages. This paper presents a method to measure surface crack opening stresses and estimate surface closure stress profiles based on thermographic images of closure regions.

This information is deduced from measurements of vibration-induced heat generated at contacting regions (asperities) of a crack. A sample is vibrated, causing asperities under low closure stress to rub and generate heat, which is imaged with an infrared camera (vibrothermography). Open regions of the crack are areas where crack faces do not contact; thus they cannot rub to generate heat. In other areas closer to the crack tips, closure stresses lock asperities together, preventing both rubbing and heat generation. Heat generation sites, therefore, indicate a closure transition region between open and locked asperities in the crack. Only asperities under low stress (from external loading

and closure) generate heat. Changing the external load changes the closure state of a crack and the locations of contacting asperities under low stress. In this manner, crack opening stresses and approximate crack closure stress profiles are measured by tracking locations of low-stress heat-generating asperities as a function of applied external load.

Consider a linear surface crack with a semielliptical depth profile in a bar, as shown in Figure 7.1. As the crack grows, it stretches the material around it elastically and plastically. The plastically deformed area around the crack tip forms a permanently stretched plastic zone. In constant amplitude loading, the plastic zone size increases as the crack advances, leaving behind a plastic wake of increasing size Elber, W. (1971), as seen in Figure 7.2(a). The plastic wake and plastic zone are referred to as the plastic region and represented by a series of distributed springs whose stiffness is that of the deformed material. The equilibrium length of each spring is related to the amount of permanent stretching, or the width of the plastic region under tensile load, at the spring's location.

When the load growing the crack is released, the material surrounding the plastic wake elastically contracts towards its previous noncracked configuration, compressing the plastic region around the crack. Since the plastically deformed region is larger near the crack tips than at the center of the crack Elber, W. (1971), areas closer to the crack tips are pressed together more tightly than areas further from the crack tips, as seen in Figure 7.2(b). Compressing the plastic region creates an unknown closure stress, $\sigma^{p}_{xx}(y, z)$, on the crack faces along the crack length y and depth z. Applying a tensile load reduces the compressive closure stresses on the crack faces. Once the closure stress reaches zero at a point, the crack faces at that point separate and act as free surfaces, as shown in Figure 7.2(c). Opening a portion of a crack corresponds to decompressing a set of springs until they reach their equilibrium lengths and separate. For simplicity, it is assumed the springs act independently and there is no interaction (i.e., lateral support) between springs.

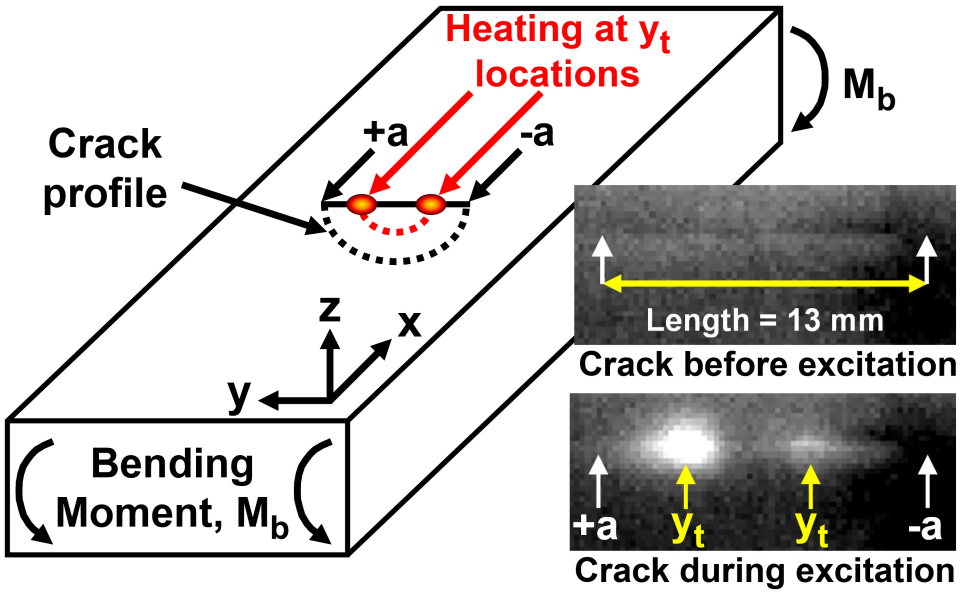

Figure 7.1 (Color online) Schematic of a crack in a test bar. The right side shows the IR images of a stationary crack (top) and the IR heating when the crack is vibrated (bottom). Crack tips are located at $\pm a$.

Locations on the surface ($z = 0$) where crack faces separate indicate a transition from closed to open and are referred to as closure transition points, y_t. Since only surface heating can be observed, this method can only obtain information about surface closure states. When a cracked sample is vibrated, asperities surrounding y_t heat up as seen on the right side of Figure 7.1 which shows experimental observations of y_t in a partially closed crack. Increasing static tensile stresses are applied in four-point bending to peel open the crack. A separate piezoelectric transducer is placed in contact with the sample to apply low amplitude vibration, generating heat at each closure transition point, y_t. Once the crack fully opens, crack faces no longer rub and no more heat is generated.

Applying a bending moment, M_b, to the bar opens the crack to a corresponding y_t. The stress σ_{xx} on the bar's surface can be approximated by combining terms representing bending stress, residual plastic stress, and a possible stress concentration,

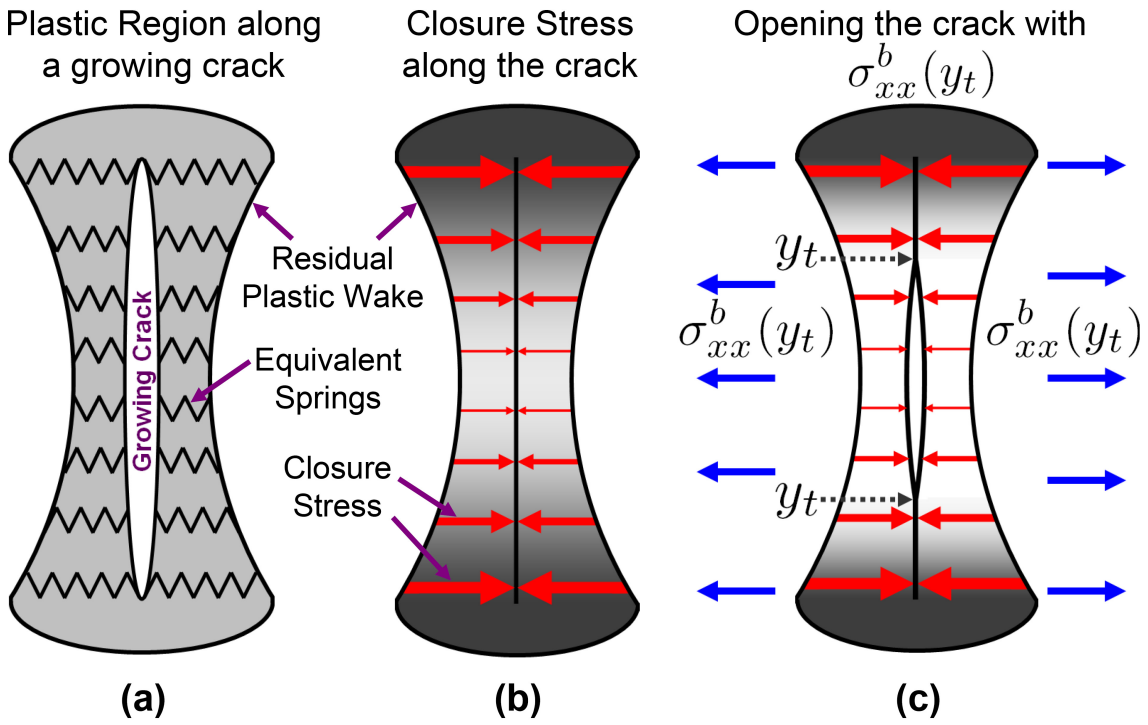

Figure 7.2 (Color online) Crack closure model showing (a) the plastic region as the crack advances, (b) closure stresses along a crack due to the compression of the plastic region, and (c) opening the crack with an applied stress to track the closure transition points, y_t, as a function of the applied load.

$$\sigma_{xx}(y) = \begin{cases} \frac{M_b c}{I} + \sigma^p_{xx}(y,0) + \frac{K^t_I}{\sqrt{y-y_t}} & y > y_t \\ 0 & y \leq y_t \end{cases} . \tag{7.1}$$

The crack at $y > y_t$ is presumed to be closed and at $y \leq y_t$ is presumed open (zero closure stress). The first term of Equation 7.1, $M_b c/I$, is the usual expression for bending stress. The second term, $\sigma^p_{xx}(y,0)$, represents the closure stress due to plasticity at y. The third term represents a possible stress concentration around the closure transition point with the normal $1/\sqrt{r}$ dependence. This term is included since the other terms do not represent the stress concentration usually found at the tip of a crack or notch. Our argument, along the lines of Dugdale Dugdale, D. S. (1960), is that there cannot be a physical stress concentration around y_t since the stress at y_t must be zero or the

crack will incrementally open or close, moving y_t to a different location where the stress would again be zero. Thus, the third term of Equation 7.1 must be zero or it would cause large variations in stress over short distances near y_t that are clearly nonphysical given the freedom of the crack to open or close. Equation 7.1 is approximate because, other than including a stress concentration term, it does not represent the effect of the modified boundary conditions as the crack opens and closes with the applied moment M_b. The bending stress at the crack is slightly higher than shown in Equation 7.1 due to the reduction in cross sectional area as the crack peels open. Higher order terms, possibly needed to fully satisfy the boundary conditions, are also neglected. Solving Equation 7.1 for $\sigma^p_{xx}(y_t, 0)$ at the closure transition point ($y = y_t$, $\sigma_{xx} = 0$), the opening and closure stresses are approximated as

$$\sigma^p_{xx}(y_t, 0) = -\frac{M_b c}{I} \tag{7.2}$$

where the term on the right, the bending stress, can be easily measured with strain gages. Equation 7.2 shows that the crack closure stress at a point y is proportional to the bending stress required to open the crack up to y (move y_t until it meets y). This method, in reality, measures the crack partial-opening stresses, but per the argument above, this gives an approximation of the closure stresses along the crack. Once the crack opening stress is reached, the crack faces completely separate and no further heat is generated. Thus, this method approximates crack closure stress profiles by tracking y_t (heating) locations as a function of the applied stress or load and directly measures the crack opening stress once the crack fully opens and can no longer generate frictional heat.

Linear surface cracks with semielliptical depth profiles were grown in bending in titanium (Ti 6-4) bars using a rectangular EDM starter notch of width 0.75 mm that was subsequently machined off. Figure 7.1 shows the coordinate system used and the

specimen geometry. The cracks were grown in a servohydraulic test machine to a length of about 13.0 mm. The crack in sample A was grown with an R-ratio (min/max stress) of 0.1 and in sample B with an R-ratio of 0.75. The higher R-ratio of sample B was intended to grow a crack of a comparable length to sample A with a higher opening stress Schijve, J. (1988) due to differences in the plastic region around the crack. Once the final crack length was reached, the samples were removed from the test machine, or given an underload, and strain gages were applied to the samples to directly measure the applied stresses in the next testing phase. After unloading the samples, both X-ray and eddy current measurements verified that the crack in sample B was a tighter crack than the crack in sample A. Hence, cracks of similar lengths with different closure profiles were compared to observe the effects of closure on heat generation in the cracks. Next, each sample was placed in a four-point bending fixture to control the applied static load and vibrated at low amplitude at its third-order flexural resonance using a piezoelectric transducer. The four-point bending mounts were placed at nodal points to minimize the effect of the mounts on the applied vibration. The samples were vibrated as the applied static load was incrementally varied to measure the change in position of the closure transition regions (y_t) with respect to the crack length as a function of the applied static stress. The combination of applied stress and vibrational stress were carefully controlled to prevent crack growth during the experiment.

Regions of heat generation were used to measure y_t locations as a function of the applied static bending stress. Figure 7.3 shows heating locations at several applied bending stresses. Note that closure transition points moved towards the crack tips with increasing static tensile stress. The location of the crack tips (at $+a$ and $-a$) are indicated by the white arrows in Figure 7.1 and the dotted lines in Figure 7.3. Heat generation occured at two y_t regions, both a short distance apart, but not at the crack tips or in the center of the crack. The open region (between the two y_t locations) and the locked asperity regions (near the crack tips) did not generate heat.

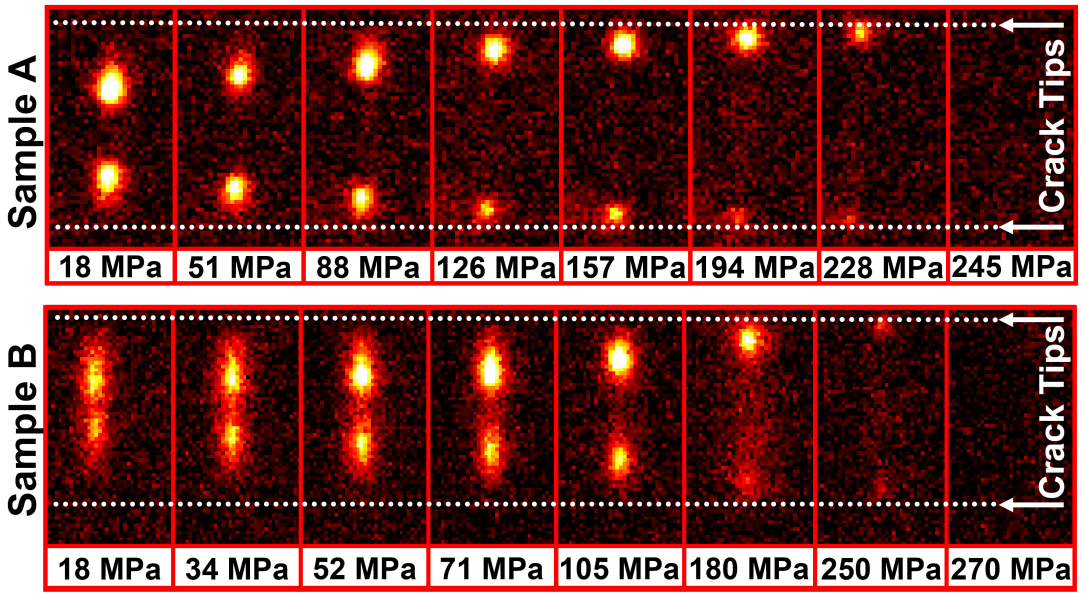

Figure 7.3 (Color online) Regions of crack heating as a function of applied bending stress. The far right images show the crack opening stress, or the applied stress required to fully open the crack and terminate heat generation.

Crack opening stresses were measured at the applied static stress required to fully open the crack faces. Once the crack faces were completely separated, they could no longer rub together to generate heat. This is indicated by the two images on the far right of Figure 7.3 where no heat generation is observed. The crack opening stress for sample A was 245 MPa and 270 MPa for sample B. Measuring the locations of heat generation in Figure 7.3 and applying Equation 7.2 gives an approximation of the closure stresses of each crack. Closure stresses versus crack lengths are plotted in Figure 7.4. Figure 7.4 shows that the crack in sample B was tighter and had a higher crack opening stress than the crack in sample A.

This paper presents a method capable of measuring surface crack opening stresses and surface closure stress profiles along a crack using frictional heat generated from vibration-induced rubbing of contacting asperities in a crack. Vibration generates heat at low-stress contacting asperities in a crack from frictional rubbing. Heat generation

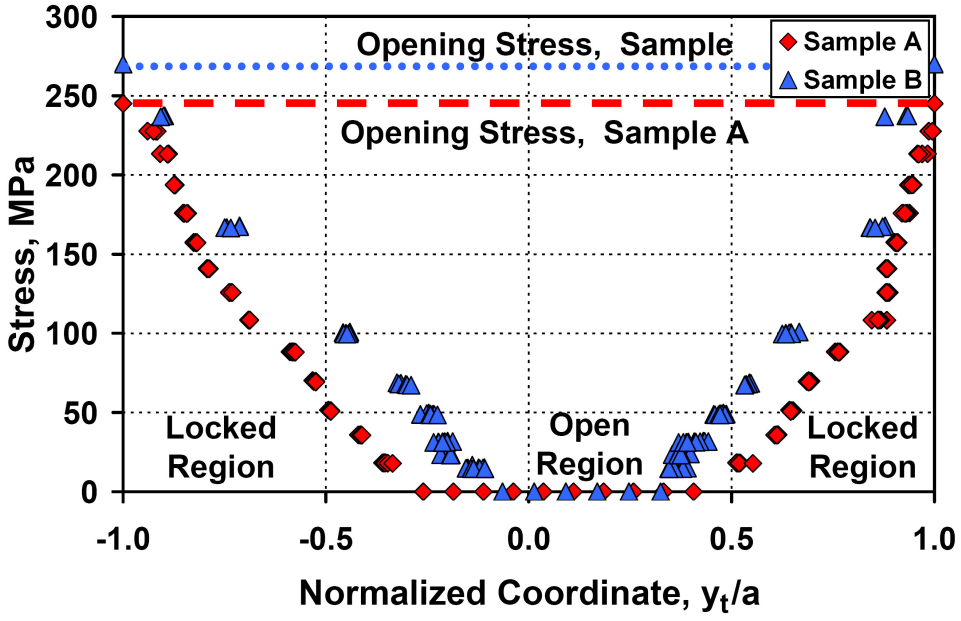

Figure 7.4 (Color online) Crack opening stresses and closure stress profiles along the lengths of two cracks calculated from measures of y_t and Equation 7.2 and normalized by y_t/a.

occurs at locations of low closure stress, referred to as closure transition points, y_t. The closure transition points are used to approximate surface crack closure stress profiles along the entire length of a crack. Opening the cracks to their tips terminated heat generation since the crack faces were no longer in contact and could not rub together to generate frictional heat. Thus, crack opening stresses were measured as the tensile stress required to open the cracks and terminate heat generation. This measurement method offers several advantages over current methods of measuring crack opening and crack closure stresses. It does not require the installation of numerous strain gages or strain gage arrays, is not dependent on the proximity of strain gages to the crack, and gives a direct measurement of the crack opening stress. Also, it can be performed after unloading a crack, as presented in this paper, or in situ during fatigue crack propagation.

7.2 Acknowledgements

This material is based upon work supported by the Air Force Research Laboratory under Contract #FA8650-04-C-5228 at Iowa State University's Center for NDE.

CHAPTER 8. VIBRATION-INDUCED TRIBOLOGICAL DAMAGE TO FRACTURE SURFACES VIA VIBROTHERMOGRAPHY

A paper to be submitted to the Journal of Applied Physics

Jeremy Renshaw [1], Stephen D. Holland, James Anderegg, R. Bruce Thompson, and Ryan J. Paul

8.1 Abstract

Vibrothermography is a nondestructive evaluation technique that uses a temperature-sensitive infrared (IR) camera to observe vibration-induced heat generation at defects, such as cracks, to locate defects within a structure. Vibrothermography has been hindered by issues of repeatability even between consecutive experimental runs on the same sample. This paper presents experimental evidence of the tribological changes that can occur on rubbing crack faces resulting from friction and heat generation. The observed changes include plastic deformation, fretting, adhesive wear, oxidation, phase transformation, and melting. These tribological damage mechanisms on the crack faces are responsible in part for the issues with repeatability in vibrothermography and can be minimized by applying vibrational stresses below a threshold.

[1]Center for NDE, Ames, IA 50011

8.2 Introduction

Vibrothermography is a nondestructive evaluation (NDE) technique used to inspect materials and structures for the presence of cracks and other defects. Defect detection is based on observations of friction-induced heat generation at vibrating defects Morbidini, M. (2006). However, the widespread application of this method has been hindered by a lack of repeatability, partly due to the fact that the vibration can cause permanent, irreversible changes to the specimen. In some extreme cases, it has been shown that the applied vibrational stresses can be sufficiently high to propagate cracks Chen, J. C. (2007); Lively, J. (2009), though no cracks studied in this paper grew as a result of the vibrational stresses. All of the observed tribological damage occurred at stresses well below those required to grow cracks.

This paper describes the tribological damage mechanisms - topographical or other physical changes to contacting asperities (crack face contact points) within a crack Hogmark, S. (1992) - that occur on rubbing crack surfaces and can produce variations in crack heating. Tribological damage is distinct from bulk material degradation that may propagate cracks or otherwise reduce the fatigue life of a structure. The vibrational stress levels used in the experiments in this paper were kept well below those required to cause bulk material damage so that the only observed physical changes occurred on the rubbing crack faces.

Modifications to the rubbing crack faces alter their frictional properties and therefore the heat generation of the crack. In general, vibration-induced heating of a crack reduces with successive vibrational excitations, as illustrated in Figure 8.1. Each heating versus vibrational stress "run" (set of data points) follows a well-defined trend, but each subsequent experimental run tends to generate less heat at the same vibrational stress levels. After about 1000 vibrational excitations, between the first and final run, the amount of heat generated reduced by more than a factor of 10. It is apparent that

something in the crack changed as a result of the applied vibration.

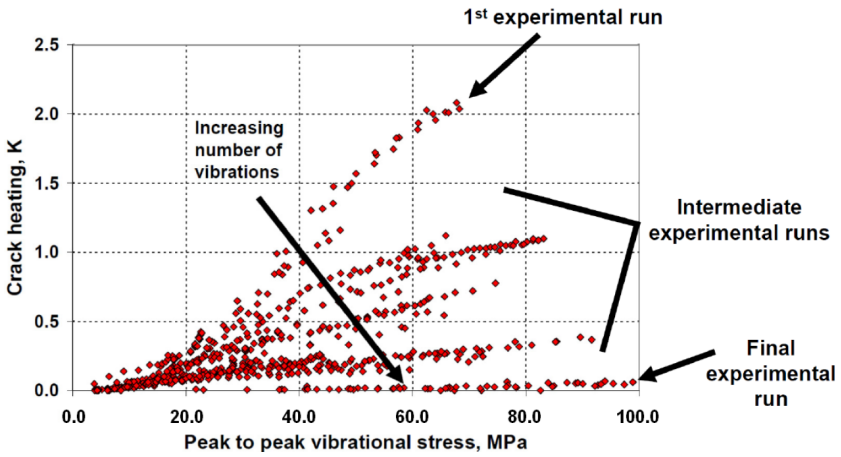

Figure 8.1 Measured crack heating as a function of the applied vibrational stress on a crack during about 1000 vibrational excitations, split up into runs of about 50 excitations, each run generally following a distinct line. Heat generation of the crack tends to decrease with an increasing number of vibrations applied to the crack. This is especially evident between experimental runs.

Occasionally, and especially with very high vibrational stress levels, a different trend is observed where measured heating may increase with successive vibrational excitations. One such example is shown in Figure 8.2. This paper focuses on determining what underlying physical mechanisms cause these variations in repeatability for vibrothermography.

8.3 Theory

Fracture surfaces (i.e. opposing crack faces) are extremely delicate. Even gentle touching, handling, or rejoining can irreparably damage the surfaces and cause difficulties in characterizing the fracture surfaces Wulpi, D. J. (1999). Moreover, it has been shown that the contact pressure between adjoining asperities alone is always sufficient to produce localized plastic flow Bowden, F. P. (1950). Vibrothermographic experiments, however, intentionally apply high-amplitude vibrations to force frictional rubbing and heat generation between crack faces so that an infrared (heat sensing) camera observing

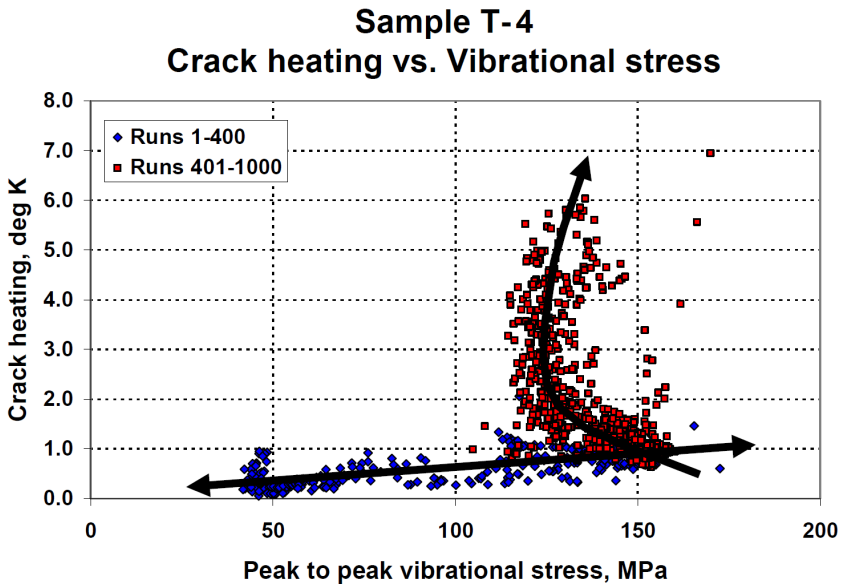

Figure 8.2 Measured crack heating as a function of the applied stress on Sample T-4. The first 400 excitations were repeatable with little scatter and followed the straight, two-way arrow in the figure. During the final 600 excitations, heat generation tended to increase with an increasing number of vibrations applied to the crack and became non-repeatable, following the one-way arrow in the figure with significant scatter.

the surface of the cracked sample can detect cracks and other defects. Thus, it is likely that the vibrational stresses, on top of stresses already approaching yield, can cause permanent changes (tribological damage) to the fracture surfaces of an interrogated crack.

Two contacting fracture surfaces may undergo a number of physical changes, or tribological damage mechanisms, due to intense frictional rubbing between asperities. The primary mechanisms are:

1. Plastic deformation - plastic deformation may occur due to stresses applied above yield on crack face asperities and is evidenced by plowing features Blau, P. J. (2009) or otherwise deformed asperities on crack faces. Plastic deformation of rubbing asperities is likely since stresses on asperities may already be at yield due to

the relatively low area of actual contact between crack faces Bowden, F. P. (1950), so any additional compressive stress will cause additional plastic deformation.

2. Fretting - fretting is a common wear mechanism that occurs as a result of contact between rubbing surfaces, such as in vibrating cracks Waterhouse, R. B. (1992). Fretting in cracks is evidenced by pull-out and tearing of crack face asperities Chen, J. C. (2007) that results from repeated oscillatory motion and is a special case of plastic deformation.

3. Adhesive wear - adhesive wear is a common damage mechanism in some materials evidenced by observations such as material transfer between rubbing interfaces and material loss from a surface due to rubbing Bowden, F. P. (1950); Ludema, K. C. (1992). Adhesive wear is an extreme case of plastic deformation.

4. Oxidation - oxidation is a phenomenon that occurs readily on the surfaces of most materials, though in many non-ferrous metals (i.e. aluminum and titanium), the thicknesses of natural oxide layers are very thin, and significant oxide layers do not form until the material is subjected to elevated temperatures in an oxygen-containing environment.

5. Phase transformation - at elevated temperatures, some materials may undergo a solid-state phase change. Some of these phase changes are reversible while others are not. Irreversible phase changes may show up as a change in the crystal structure of the material.

6. Melting - melting is an extreme case of a phase transformation and can occur due to the heat generated by intense frictional rubbing and can be evidenced by solidified droplets on rubbing surfaces or by very smooth, featureless surfaces observed using an SEM Bowden, F. P. (1950); Blau, P. J. (2009). High stresses,

rubbing velocities, and frictional coefficients as well as low thermal conductivities increase the probability of melting.

This paper presents evidence of each of these tribological damage mechanisms. It also shows that their impact on a vibrothermographic inspection can be mitigated by operating at appropriate vibrational stress levels for the inspected materials.

Large temperature rises due to friction on rubbing surfaces is a well-understood concept. Two rubbing surfaces are only in actual physical contact at a very small number of points, or asperities Bowden, F. P. (1950); Blau, P. J. (2009). These contacting asperities can therefore, undergo very large stresses and strains, even when bulk stresses and strains are low, potentially resulting in plastic deformation, fretting, and adhesive wear. When a very small area is strained or sheared quickly, it generates a large amount of heat that must dissipate. Since the asperities are small, heat transfer to the bulk material is slowed due to the conduction shape factor between the asperities and the bulk material Incropera, F. P. (2002). Consequently, even at low bulk stresses, strains, and temperatures, localized oxidation, phase transformations, and melting can also occur between rubbing asperities.

The most severe tribological damage mechanisms are thermally driven, though there is no possible direct measurement of the temperature inside of a crack. Bulk temperatures can be measured using an IR camera; however, the only possible observation of melting must be performed after the experiment is over in a scanning electron microscope (SEM) once the crack has been broken open. Melting is still very difficult to detect, even in an SEM, unless sufficiently high stresses and strains were utilized to increase the size of the melted regions to a size comparable to the fracture surface asperities.

Cowan and Winer Cowan, R. S. (1992) in the ASM Handbook on Friction, Lubrication, and Wear provide many useful formulas published by numerous authors to calculate the maximum instantaneous change in temperature reached by rubbing asperities, or as-

perity flash temperatures. Using specified dimensions and material properties, asperity flash temperatures can be estimated. A useful asperity flash temperature estimate from Cowan and Winer assuming contact between two bodies in motion is

$$T_f = \frac{0.63\mu}{2b}\left(\frac{W}{L}\right)^{0.75}\left(\frac{E}{(1-\nu^2)R}\right)^{.25}\sqrt{|V_1 - V_2|}. \tag{8.1}$$

where T_f is the asperity flash temperature, μ is the coefficient of friction, b is the thermal contact coefficient (square root of the product of density, specific heat, and thermal conductivity), W is the load, L is the characteristic length, E is the Young's Modulus, ν is Poisson's ratio, R is the equivalent radius, and V_1 and V_2 are the rubbing velocities of the two bodies (in this case, the velocities are equal and opposite, so this quantity can be taken as $\sqrt{2V_1}$) where all above quantities are as defined by Cowan and Winer Cowan, R. S. (1992). The velocity values used were estimated by taking 1/2 of the value calculated from a finite element simulation of the crack geometry at an identical normal stress and vibrational frequency as measured on a sample used in this study (Sample T-4). Values used were taken as 1/2 of that calculated in the finite element model to minimize displacement, and hence velocity, errors due to the possible displacement constraints imposed by crack closure.

Equation 8.1 was derived for a generic tribosystem, thus it is not directly applicable for any specific tribosystem, but is useful in this case to provide an order of magnitude estimate of the asperity flash temperatures. Endothermic processes, such as melting or other phase transitions, will lower the peak flash temperature in the material since they act as a heat sink. The melting temperature is considered an upper temperature limit for these calculations since the liquid is able to act as a frictional lubricant or can flow away from the rubbing interface. Either of these actions will limit the maximum interface temperature. General tribological models of frictional heat generation Blau, P. J. (2009); Cowan, R. S. (1992) take into account such factors as rubbing velocity, load (or contact

stress), coefficient of friction, density, specific heat, and thermal conductivity and various other factors when calculating approximate asperity flash temperatures. However, these models have limited accuracy due to the complicated mechanisms involved Blau, P. J. (2009); Cowan, R. S. (1992) since some parameters, such as the coefficient of friction, may increase or decrease with increasing rubbing velocity, load, and other factors Blau, P. J. (2009). Certainly, as asperities are altered from the rubbing process, the coefficient of friction and true area of contact change, further reducing the accuracy of such models. Despite these limitations, such equations are useful in obtaining an estimate of the asperity flash temperatures of two rubbing surfaces.

Using the values shown in Table 8.1 to solve equation 8.1 to obtain an estimate of the Ti 6-4 asperity flash temperatures at half of the maximum vibrational stresses and strains used in this experimental study, specifically on Sample T-4, gives approximately 7212° Celsius, which is significantly higher than the liquidus (complete melting) temperature of Ti 6-4 titanium, or 1660° C. The actual asperity flash temperatures reached are generally limited to a few degrees above the melting temperature Bowden, F. P. (1950). Regardless of the actual temperature reached by the asperities, this equation suggests that melting is likely to occur due to the large changes in pressure or load on the rubbing asperities.

8.4 Experimental Procedure

Techniques used to characterize each sample material include optical microscopy, profilometry, SEM microscopy, energy dispersive X-ray spectroscopy (EDS), and Auger spectroscopy. Optical microscopy and profilometry are useful to observe larger-scale effects, such as asperity fretting, that are sometimes visible to the naked eye through optical observations and measurements of surface profiles. An SEM, which uses a focused electron beam to image surfaces to great magnifications, is useful for characterizing many

Table 8.1 Thermal properties for titanium (Ti 6-4) including values used for the asperity flash temperature calculation, Equation 8.1. The coefficient of friction value for titanium was taken from Blau, P. J. (1992); Budinski, K. G. (1991); Friction Data Guide, (1988). The load was estimated using half of the measured normal vibrational stresses applied on crack faces Uhl, C. J. (2008). The characteristic length and equivalent radius values were estimated from SEM observations. Velocity values were estimated using 1/2 of the value calculated from a finite element simulation of an identical crack at the same vibrational stress and frequency. Other values presented are handbook values for Ti 6-4 material properties.

Property	Symbol	Value	Units
Coefficient of friction	μ	0.30	-
Thermal contact coefficient	b	6388	$\frac{N}{mKs^{0.5}}$
Load	W	687	N
Characteristic length	L	100×10^{-6}	m
Young's Modulus	E	113.8×10^{9}	N/m^2
Poisson's ratio	ν	0.342	-
Equivalent radius	R	50×10^{-6}	m
Asperity rubbing velocities	V_1 / V_2	0.13	m/s

damage mechanisms, especially those that occur on very small length scales, through comparing and contrasting observations of pristine and tribologically-damaged surfaces. An SEM equipped with EDS is useful for characterizing elements present within a sample since it can measure the spectrum of emitted X-ray photons from a sample excited using the electron beam. The presence of oxide scale on the fracture surfaces was characterized using EDS, though only qualitative measures could be obtained for light elements such as oxygen. An Auger spectrometer was used to confirm the presence of oxide scale as well as adhesive wear on rubbing crack faces. An Auger spectrometer measures energetic electrons that are emitted from an excited specimen due to internal atomic relaxations within the sample atoms.

Evaluation of the fracture surfaces must be done carefully to avoid problems with data analysis and the possibility of forming inaccurate conclusions. A common surface

evaluation technique such as profilometry by itself is not adequate since fretting will tend to increase the roughness of a surface while melting will most likely decrease the roughness and adhesive wear may cause either an increase or a decrease in roughness. It is therefore necessary to employ multiple techniques to better characterize tribological damage mechanisms that may have occurred on the mating fracture surfaces.

Two material systems were studied in this paper. The first material system was a set of titanium (Ti 6-4) bars containing fatigue cracks and the second was a set of brass samples containing cracks due to an extrusion pipe defect produced when extruding a brass billet.

The test setup used for the titanium samples consisted of a bar held in place at each end with clamps and excited near the center with a piezoelectric stack transducer Uhl, C. J. (2009). Samples were held in place using rubber pins placed at the nodes of the excited flexural vibrations. The piezoelectric transducer was used to excite high-amplitude vibrations in each sample at a specified frequency or range of frequencies. Vibrational stress amplitudes were calculated using the known resonant mode shape and measured vibration velocity Elmore, W. C. (1985); Uhl, C. J. (2009).

The test setup for the brass samples was slightly different due to the different size and shape of samples used. The samples were much smaller and could not be clamped in place, so the transducer itself was used to secure the samples in place. Samples were placed in between the transducer and a hard surface. Pneumatic pressure was applied to the back side of the transducer to hold the samples in place during vibration.

All vibrational excitations in this study had a duration of one second with at least one minute between excitations to allow both the sample and testing equipment to cool properly. Upon completing vibrational excitation on all of the samples, they were broken open to examine the tribological damage induced on the fracture surfaces. After the samples were broken open, they were carefully cleaned using an acetone bath in an ultrasonic cleaner to remove any contaminants or wear debris accumulated in the cracks.

8.4.1 Titanium

Semielliptical surface cracks were grown in bending using 11 titanium test samples (Ti 6-4). Figure 8.3 shows a schematic of the sample geometry including the meaning of the sample dimensions included in table 8.2, sample length, width, thickness, and crack length. Table 8.2 includes a brief an overview of each sample's group assignment, dimensions, and number of excitations used in testing. All cracks were initiated using a 0.75 mm wide EDM notch and an R-ratio (min/max load) of 0.5 with a maximum applied bending stress of 772 MPa in 3-point bending. The EDM notch was subsequently machined off.

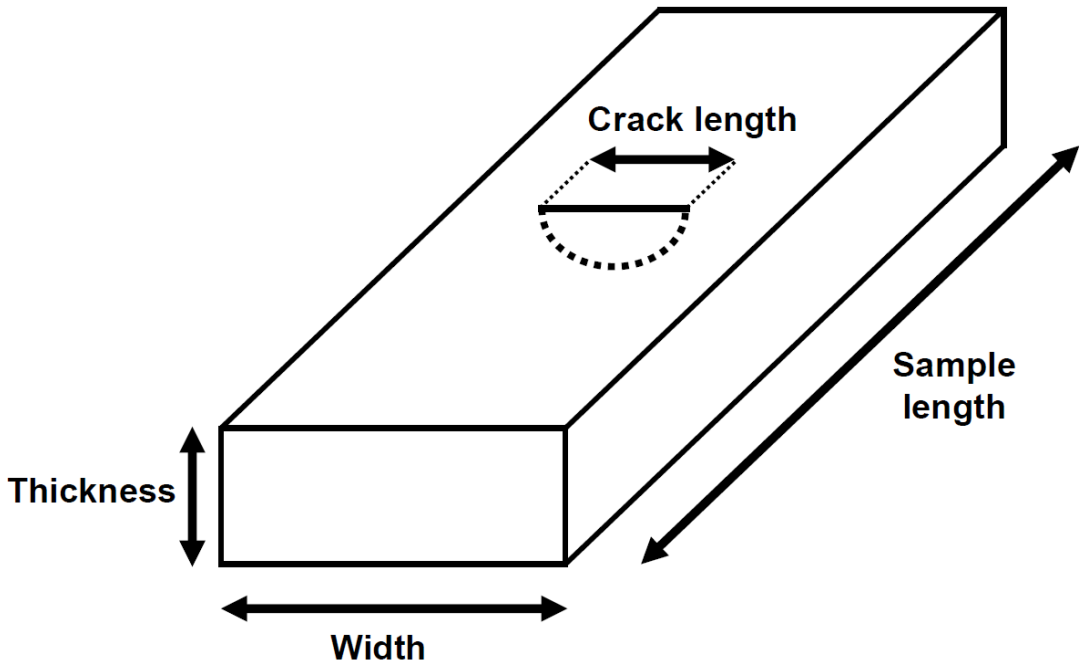

Figure 8.3 Schematic of the sample geometry used for the titanium test samples showing the important dimensions of sample length, width, and thickness as well as crack length. See Table 8.2 for each sample's dimensions.

Table 8.3 presents a brief description of the tests performed on each sample group, the purpose of each test, and the test results. Samples T-13, T-32, and T-37 in the C (CONTROL) Group were broken open immediately after fatiguing to obtain a baseline

Table 8.2 Titanium sample dimensions and vibrational excitation parameters summary

Group ID	Sample ID	Length, mm	Width, mm	Thickness, mm	Crack length, mm	Number of excitations	Maximum vibrational stress, MPa
C	T-13	154.0	25.27	6.71	8.00	0	
	T-32	153.4	25.25	6.93	8.00	0	0
	T-37	153.5	25.25	6.99	8.00	0	
G1	T-11	153.7	25.22	7.11	8.00	500	
	T-31	153.3	25.27	7.01	8.00	500	85
G2	T-8	153.9	25.30	7.21	8.01	1000	
	T-25	154.6	25.25	7.04	8.00	1000	70
	T-28	153.5	25.25	7.09	8.00	1000	
G3	T-4	153.0	25.20	7.14	8.03	0 / 1000	
	T-21	153.7	25.25	7.09	8.00	0 / 1000	175
	T-23	153.6	25.25	7.19	8.00	0 / 1000	

fracture surface of an as-fatigued pristine crack not exposed to high frequency vibration (vibrothermographic excitation). Samples T-11 and T-31 in group G1 were used to determine the most effective vibrations to induce fracture surface tribological damage. T-11 was vibrated using a frequency sweep from 0.1 to 20.0 kHz while sample T-31 was vibrated using a tone burst at 20 kHz, corresponding to a known heat generating resonance for this bar (its 5^{th} order flexural resonance) to observe whether a frequency sweep across multiple resonances or a tone burst at a single resonance results in more tribological damage to the fracture surfaces. Both samples were excited 500 times for one second each. It was found that the tone burst at resonance was much more effective at both generating heat and altering the fracture surfaces than the frequency sweep; therefore, the 5^{th} order flexural resonance was used for subsequent tests. The next three samples tested (T-8, T-25, and T-28), in group G2, were vibrated using a tone burst at their 5^{th} order flexural resonances 1000 times each to induce tribological damage from frictional heat generation. The final three samples (T-4, T-21, and T-23), in group G3, were carefully machined so that the semielliptical surface cracks that had been grown in

them were cut in half, forming two similar (nominally identical) quarter-elliptical edge cracks. One half of each crack was vibrated 1000 times to induce tribological damage on the fracture surface while the opposing half was not vibrated to serve as an as-fatigued pristine control sample for reference and comparison.

Table 8.3 Titanium Sample Tribological Damage Summary

Group ID	Tests performed	Purpose of test	Test results
C	None	Maintain pristine reference asperities	Pristine asperities maintained
G1	high amplitude frequency sweep (0.1-20.0 kHz) or 5th order flexural resonance excitation	Determine vibration type that results in tribological damage	Only resonance vibration resulted in tribological damage (fretting)
G2	70-85 MPa vibrational stress at 5th order flexural resonance	Observe if tribological damage occurs at lower vibrational stress levels	No tribological damage observed in any samples
G3	1/2 of crack unvibrated 1/2 of crack vibrated at very high amplitude 5th order flexural resonance	Observe changes to two halves of the same crack due to high vibrational stresses	No tribological damage observed on unvibrated crack half. Significant tribological damage observed on vibrated half (oxidation, melting, etc.)

8.4.2 Brass

A group of nine cracked brass samples was used to compare the effect of high-amplitude vibrations on brass versus titanium. These cracks were created due to a problem with the extrusion process used to form the samples. Figure 8.4 shows a picture of the brass samples used for testing. Due to both the lower yield stress and melting temperature of the brass alloy (905-930° C), it is expected that the brass samples were more likely to be tribologically damaged by high-amplitude vibrations than the titanium samples. As with the titanium samples, three brass samples were kept as pristine

references while the other six were vibrated. The complicated geometry of the samples only allowed for a comparison between vibrated and unvibrated samples (i.e. cracks in the brass samples could not be sectioned to examine variations within the same crack as was done with the titanium samples).

Figure 8.4 Picture of a brass sample used for testing.

Due to high heat generation in the brass samples, significant material ejection from the cracks during vibration, and clearly visible signs of crack face alteration after vibration, the brass samples were only subjected to about 100 excitations. Only 100 excitations were used to avoid masking the effects of competing tribological damage mechanisms.

8.5 Results

The geometry and rubbing conditions of vibrating cracks that were inspected using vibrothermography creates a very complicated tribosystem. Cracks can have closure stresses ranging from zero (non-contacting crack faces) Renshaw, J. (2008) to the compressional flow stress of the material (assuming an elastic-perfectly plastic material) Suresh, S. (1998). Applied vibrational stresses in the titanium samples generally ranged from 30 to 175 MPa (peak to peak) at frequencies between 15-20 kHz. Due to the specimen geometry, the cracks generated heat most efficiently when vibrated in Mode I loading (crack opening and closing). Since Mode I vibration causes crack opening and closing, as the crack faces rubbed together both the contact stress and rubbing velocity were constantly changing due to the nature of the oscillating load on the crack. In addition, the rubbing surfaces had the potential to leave and regain contact during the vibration cycle.

8.5.1 Titanium (Ti 6-4)

The control group (C) of three pristine titanium samples were examined first. They showed a regular pattern of pristine asperities as shown in Figure 8.5 due to the fatigue process used to grow the cracks. The asperities shown are typical of those found on samples T-13, T-32, T-37, and the unvibrated halves of Samples T-4, T-21, and T-23. Such asperities are also characteristic of other Ti 6-4 fatigue cracks grown under similar conditions.

Due to minute differences in each crack and small changes in the dimensions of each bar, the maximum vibrational stresses that could be applied to each of the bars using the vibrational transducer were not the same. The vibrational stresses applied to the bars with semielliptical cracks, in groups G1 and G2 (samples T-8, T-25, T-28, and T-31), ranged from 30-85 MPa peak to peak. No clear evidence of tribological damage

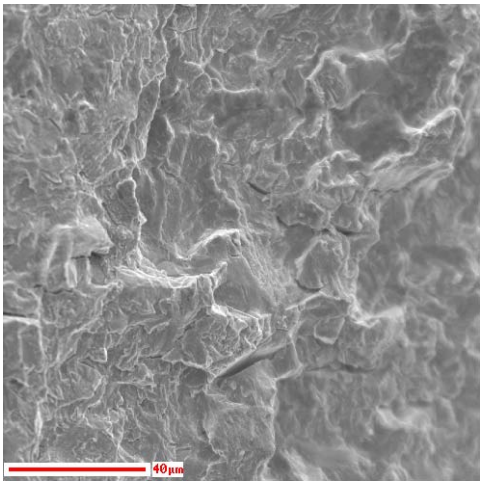

Figure 8.5 SEM image showing pristine fracture surface asperities on the unvibrated titanium (Ti 6-4) samples. Pristine asperities are evidenced by clearly-defined, or sharp, features.

was observed on the fracture surfaces of the first three samples where the maximum vibrational stresses never exceeded 70 MPa, or approximately 30 percent of the endurance limit of Ti 6-4 (240 MPa). The asperities observed on these crack faces are indistinguishable from those shown in Figure 8.5. These results are consistent with the proposed rule of thumb that vibrothermographic inspections should only employ stresses below 20 percent of the inspected material's endurance limit Ruhge (F. 2008).

Sample T-31, which was vibrated at stresses between 70-85 MPa, exhibited fretting on a portion of the crack surfaces as evidenced by the dark, labeled band in Figure 8.6. Fretting damage occurs due to repeated oscillatory motion between two bodies Waterhouse, R. B. (1992), so the observation of fretting due to vibrothermographic excitation is not surprising. Fretting damage is evidenced on fracture surfaces by an increase in surface roughness due to pull out and tearing of rubbing asperities. Asperity pull out and tearing were observed visually and the increase in surface roughness was measured using profilometry. Figure 8.7 shows an exploded view around the fretting band observed in figure 8.6 illustrating four paths (dashed lines) along which roughness data were collected using an optical profilometer. Regions 1 and 4 were just outside of

the fretting band on either side while regions 2 and 3 were just inside of the fretting band, adjacent to regions 1 and 4. Table 8.4 shows the measured surface roughness parameters of the fracture surface of Sample T-31. Roughnesses within the fretting band were approximately 60 percent higher than the roughness values just outside of the fretting band on either side. The band of fretting damage correlates to the regions along the crack where vibration-induced heat generation was observed, as shown in Figure 8.6. Previous research Renshaw, J. (2009C) has shown that the regions of a crack that generate heat are those where tribological damage is likely due to high vibrational stresses. No evidence of other tribological damage mechanisms was observed in the semielliptical cracks since the physical dimensions of the samples did not allow higher stresses to be introduced into the bars using the piezoelectric transducer.

Table 8.4 Measured surface roughnesses for Sample T-31, all dimensions are in μm and Regions 1-4 are as defined in Figure 8.7.

Roughness parameter	Description	Region 1	Region 2	Region 3	Region 4
R_a μm	Average height of profile	4.49	7.16	8.04	4.87
R_q μm	RMS height of profile	5.54	8.88	10.05	6.18
R_{max} μm	Maximum peak to valley height of primary profile in sampling length	20.97	40.18	52.56	26.56
R_c μm	Mean height of profile irregularities of primary profile	14.47	25.70	27.13	16.91
R_z μm	Mean peak to valley height of primary profile	17.90	30.16	32.63	23.25
R_p μm	Max peak height of primary profile	15.13	22.95	21.00	19.19
R_v μm	Max valley height of primary profile	11.41	18.15	32.49	14.49
R_t μm	Max peak to valley height of primary profile	26.54	41.10	53.49	33.68

The geometry of the bars in group G3 containing the quarter-elliptical cracks (semielliptical cracks that were cut in half) allowed these samples to vibrate more freely and

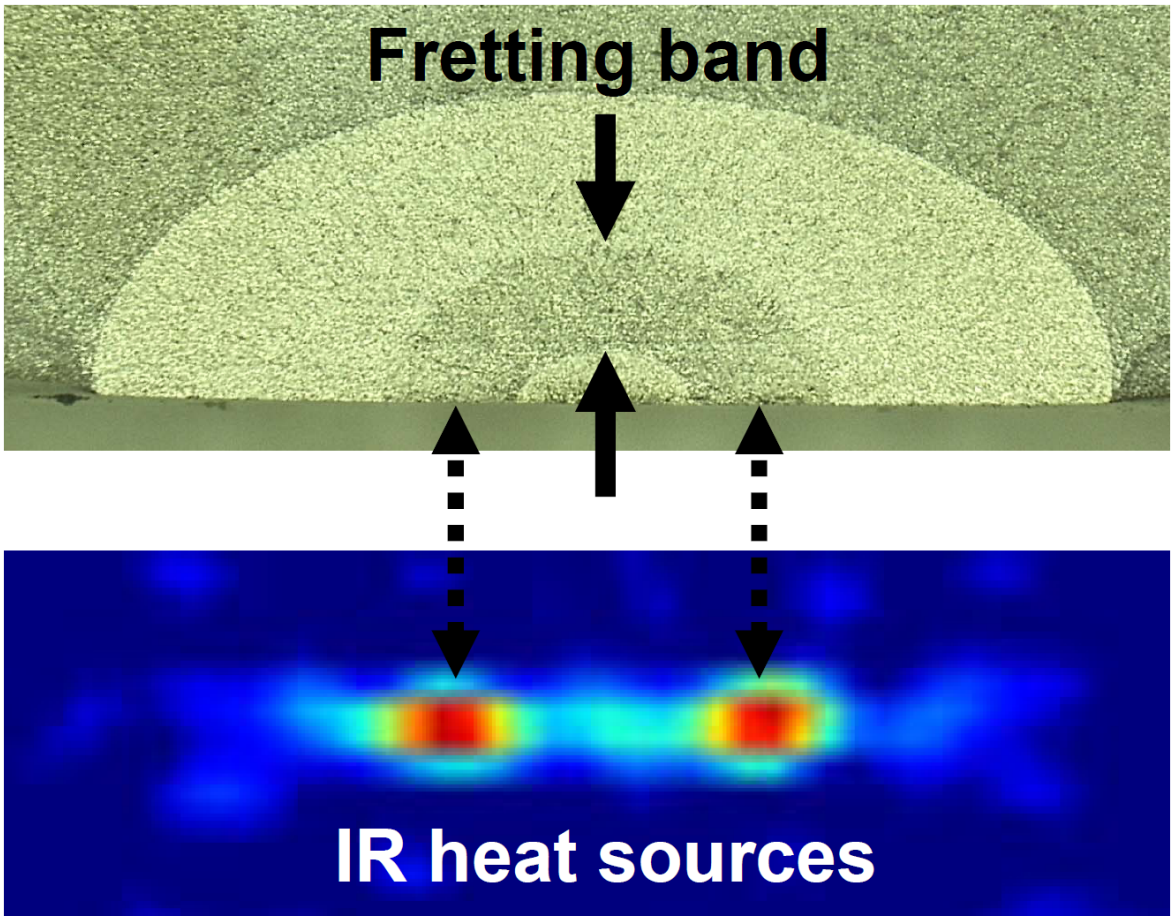

Figure 8.6 (Top) Stereo microscope image of the cross section of a vibrated crack showing a fretting band on the fracture surface. (Bottom) Processed image of surface infrared heating of the crack correlating the fretting band to the regions of heat generation along the crack.

these samples had applied vibrational stresses that approached 175 MPa, compared with 85 MPa for the samples in group G1 and 70 MPa for the samples in group G2. Due to the high vibrational stress levels, significant heat generation and additional tribological damage mechanisms were observed. The fracture surfaces for these cracks showed significant oxidation in the form of small nucleation sites of oxide scale that show up as small, light-colored dots in Figure 8.8, and are clustered into colonies concentrated on the upper-left side of the image. The presence of high levels of surface oxygen was confirmed via EDS. The oxide scale growth was limited by the one second duration of the

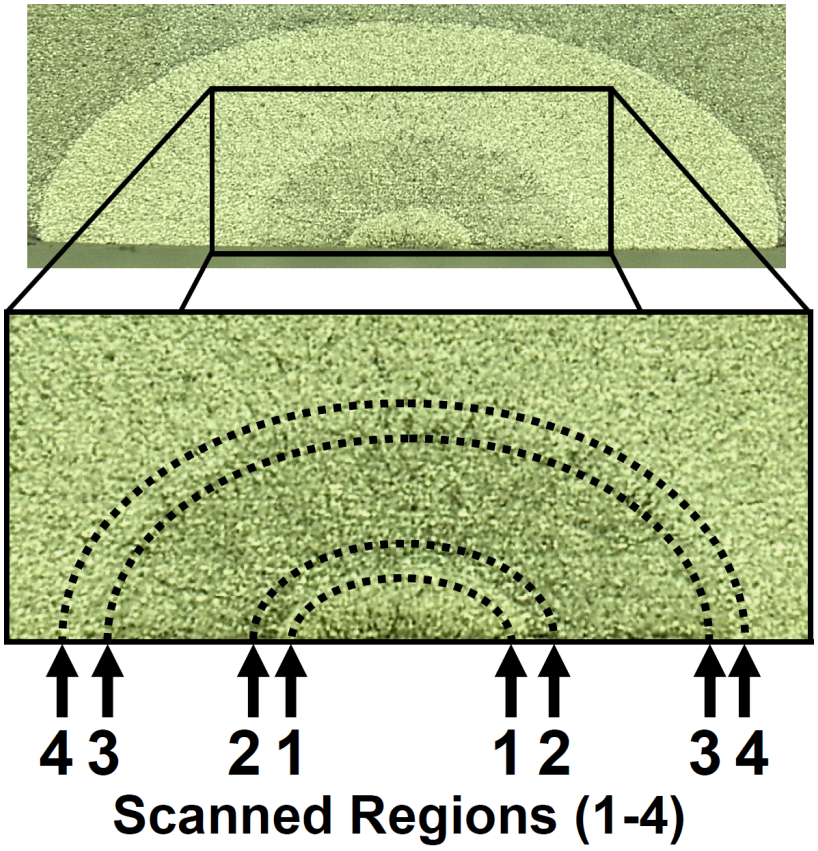

Figure 8.7 Map showing an exploded view of the fretting band shown in Figure 8.6 observed in Sample T-31. An optical profilometer was used to scan four regions along the edges of the fretting band. Regions 1 and 4 were just outside of the fretting band on the smaller radius and larger radius paths, respectively. Regions 2 and 3 were just within the fretting band on the smaller radius and larger radius paths, respectively.

vibrational excitation, resulting in numerous small oxide particle patches on the rubbing surface. The oxide levels dropped sharply with depth into the crack, consistent with the lower amounts of available oxygen deeper in the crack and lower expected heating (due to lower vibrational stress levels) closer to the neutral axis of the bar.

The large vibrational stresses in the samples generated very large stresses on the contacting asperities of the crack since stresses are amplified many times at regions of contact Bowden, F. P. (1950), such as crack face asperities. The large stresses and

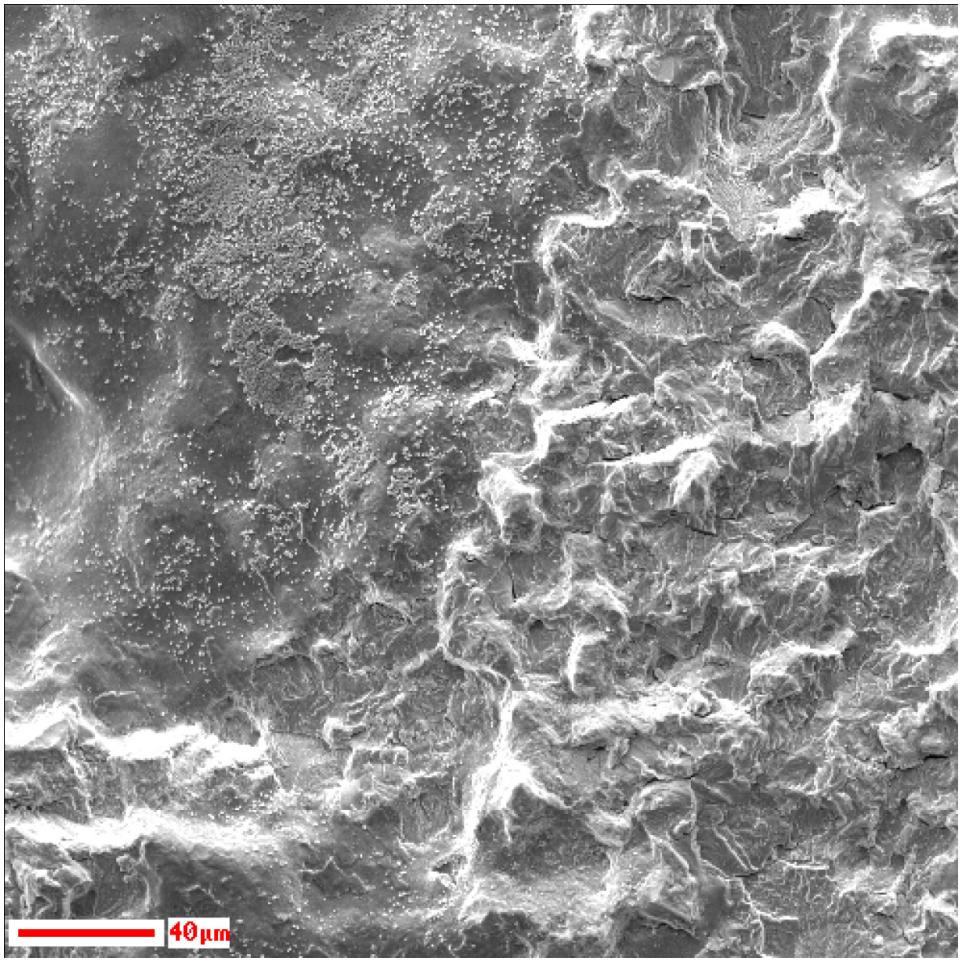

Figure 8.8 SEM image of a titanium fracture surface with numerous oxide particles (small bright dots and patches concentrated towards the upper-left region of the image).

rapidly oscillating loads caused melting on some portions of the fracture surfaces of the quarter-elliptical edge cracks in titanium, as evidenced by the very smooth, featureless surfaces shown in Figure 8.9.

8.5.2 Brass

Brass (CDA 27000) is a softer, weaker material than titanium and has a lower melting point. Thus, it is expected that similar and possibly additional tribological damage mechanisms may be observed on the brass fracture surfaces than observed in titanium.

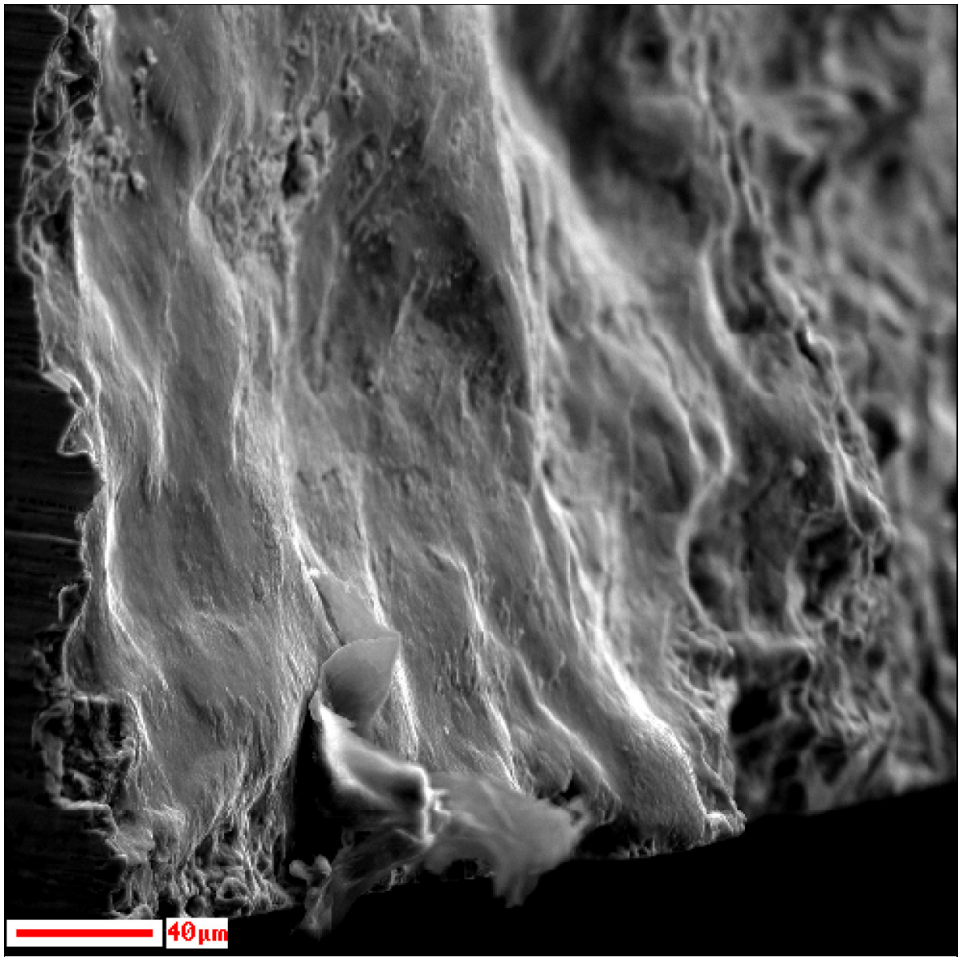

Figure 8.9 SEM image of fracture surface melting on the titanium sample, evidenced by the smooth, featureless surface.

Due to their small size and complex geometry, coupled with the difficulty of mounting the samples, it was not possible to measure meaningful vibrational stresses applied to the brass samples.

In contrast to the titanium samples, the brass samples were only excited using 100 excitations. During vibrational excitation, the IR camera observed debris ejected from the crack in the form of particles and material clouds. Figure 8.10 shows a sequence of IR images of a particle that was ejected from one of the cracks due to vibrational rubbing. After only 100 excitations, significant macroscopic changes, such as significantly larger crack openings and plastically deformed surface regions along the cracks, were observed

on the outer surface of all vibrated cracks, meaning that further vibrational excitation was not needed and could potentially mask weaker tribological damage mechanisms. Figure 8.11 is an image of typical unvibrated and vibrated crack samples that shows significant changes in a crack due to vibrational excitation. The outer surface of one side of the vibrated crack face was plastically deformed and pushed up and its crack opening displacement increased dramatically. Such initial and final states were typical of all brass samples used in this study.

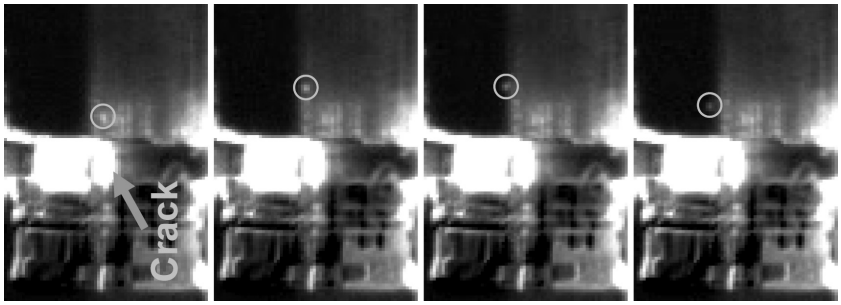

Figure 8.10 Infrared heating images showing ejected material from a crack. The gray arrow points to heat generated at the crack and the white circles indicate the ejected particle.

The reason for the dramatic change in the fracture surfaces was primarily due to material being transferred from one crack face to the other or ejected from the crack through adhesive wear. Adhesive wear occurs when asperities on a rubbing surface break off from the surface to form loose wear debris and/or adhere to the opposing surface in the form of flakes or particles Ludema, K. C. (1992). This wear debris can significantly alter wear rates and has the potential to leave the rubbing interface (i.e. eject from the crack) Hogmark, S. (1992). In this experiment, adhesive wear on the brass surfaces was so intense that significant wear debris could be observed shooting out of the cracks, as shown in the sequence of infrared images in Figure 8.10.

Figure 8.12 shows typical brass asperities from a pristine sample and Figure 8.13 shows flakes of material transferred between the brass fracture surfaces due to adhesive

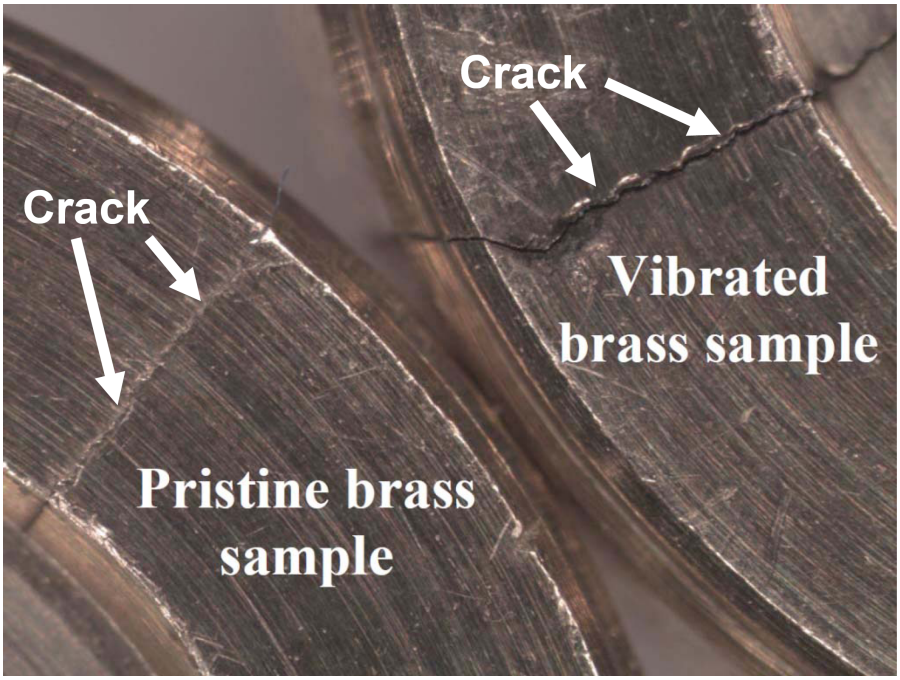

Figure 8.11 Image of a pristine crack in a brass sample (lower left) and a crack that was modified due to vibration (upper right).

wear. The pristine asperities have very distinct features while the flakes formed from adhesive wear are much smoother and have well-defined boundaries between the flakes that have an appearance similar to very fine cracks. An Auger spectrometer was used to verify that the material flakes (lighter color) were composed of brass, a good conductor, but despite being composed of brass, had a poor electrical contact to the base brass material (darker color) of identical composition, meaning that they were not well bonded to the bulk brass. The poor contact between the flakes and the base metal results in electrical charging on the flakes, giving them a lighter color when imaged.

Figure 8.14 shows that the high stresses applied to the fracture surfaces caused plastic deformation on some asperities. Plastic deformation is evidenced by the plowing features Blau, P. J. (2009) through the region, distinct boundaries of the region, and the contrast between the plastically-deformed asperities in Figure 8.14 and the pristine asperities in Figure 8.12.

Bulk temperature rises in the brass sample (about 16° C) observed with the IR camera were about twice as high as those of titanium. Due to the higher thermal diffusivity of brass compared to titanium, a larger temperature bulk temperature rise means that much more heat was being generated and that melting was likely to occur. In fact, numerous regions across the brass fracture surface exhibited evidence of melting. Figure 8.15 shows this evidence of melting, again in the form of smooth, nearly featureless regions on the fracture surfaces. These regions are very different from pristine asperities and do not have distinct plowing features associated with plastic deformation or material flakes as would be expected with adhesive wear, but instead are very smooth and featureless.

8.5.3 Effects of tribological damage on heat generation

Crack heating versus applied vibration stress data for the titanium samples were measured using the IR camera and laser vibrometer, respectively. Bulk surface temperature rises observed using the IR camera for the titanium samples due to vibration-induced heat generation reached 7 degrees Celsius at the cracks.

In general, the heating versus vibrational stress data tended to follow distinct trends for the samples exposed to lower stress levels and bulk temperatures, such as sample T-25, as shown in Figure 8.16. Heat generation for sample T-25 remained consistent and repeatable with little scatter regardless of the number of times the sample was vibrated. For samples exposed to higher stress levels, such as sample T-4 in Figure 8.2, the distinct change in heating versus applied vibrational stress is consistent with the alteration of the rubbing asperities at high vibrational stresses. Since the conditions of rubbing changed, it is apparent that heat generation due to friction would also change. It is not surprising that extreme vibration levels could cause unpredictable and highly-nonlinear changes on rubbing crack faces.

Figure 8.2 shows the temperature rise versus vibrational stress data for Sample T-4,

a sample that exhibited melting on its crack faces, showing that the general trend of heat generation tended to increase in this sample as the crack faces were progressively damaged tribologically during 1000 excitations. For clarity, the data presented are only presented in two groups, the first 400 excitations and the final 600 excitations. The first 400 excitations gave somewhat repeatable results with moderate scatter while the final 600 excitations exhibited a large amount of scatter and were not repeatable, as shown in Figure 8.2. Since there is no measurable change in the method of applying or measuring vibration or heat generation, these data gave strong evidence that something had changed within the crack due to vibrothermographic inspection which was subsequently confirmed by observing and comparing the rubbing crack faces with pristine, as-fatigued crack faces.

8.6 Conclusions

Vibrations of various amplitudes were used to cause frictional rubbing in cracks. This rubbing caused numerous changes, or tribological damage, to the crack surfaces that are believed to play a role in the lack of repeatability observed in vibrothermography. The observed tribological damage mechanisms were plastic deformation, fretting, adhesive wear, oxidation, phase transformation, and melting occurring on crack face asperities.

Though it is impossible to prevent all forms of tribological damage to a fracture surface from vibrothermography, the data presented in this paper (see Tables 8.2 and 8.3) indicate that stresses in titanium below 70 MPa, or below about 30 percent of the endurance limit of Ti 6-4 (240 MPa), do not appear to cause measurable tribological damage to the fracture surfaces. Fretting damage was observed between 30 and 40 percent of the endurance limit and severe fracture surface tribological damage was observed above 40 percent of the endurance limit. Similar damage mechanisms were observed in the brass samples, though no quantitative stress values could be obtained. The mea-

sured stress values related to damage mechanisms in titanium are obviously dependent not only on the applied vibrational stress, but also on crack growth parameters used to grow the cracks, the material system (i.e. materials other than Ti 6-4), crack closure, and crack morphology, so these stress values are not absolute tribological damage thresholds or material standards. These results are also consistent with the proposed rule of thumb to only apply stresses below 20 percent of the material's endurance limit during vibrothermographic inspection.

Applying large stresses to a fracture surface, such as during a vibrothermographic inspection, can alter the rubbing surface, possibly increasing or reducing the heat generation capability of the crack and its infrared signature in subsequent inspections. For this reason, it is important to understand the vibrational stresses that are applied to structures to avoid inducing tribological damage to the cracks.

8.7 Acknowledgements

This material is based upon work supported by the Air Force Research Laboratory under Contract #FA8650-04-C-5228 at Iowa State University's Center for NDE.

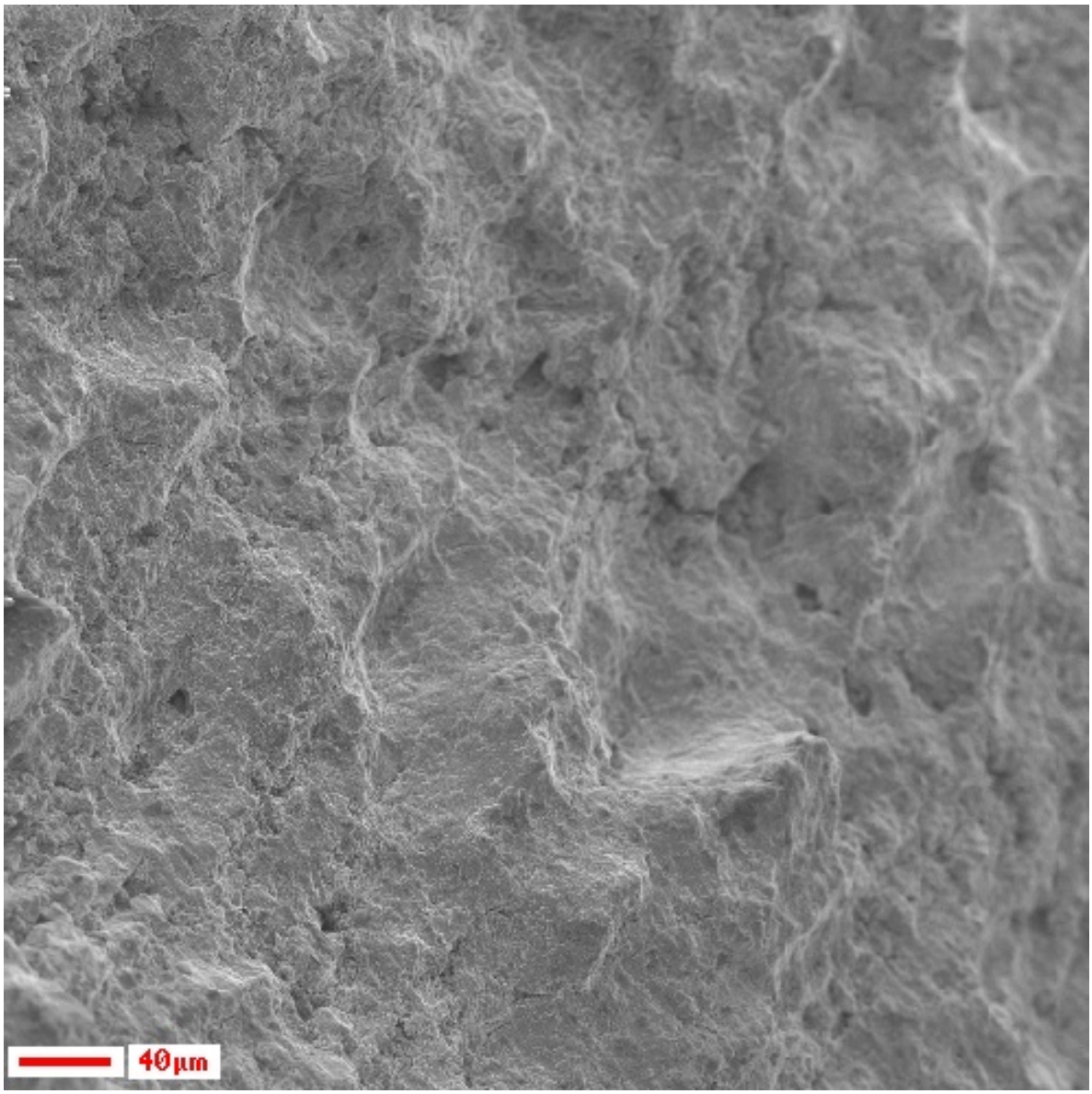

Figure 8.12 Pristine asperities of a typical brass sample.

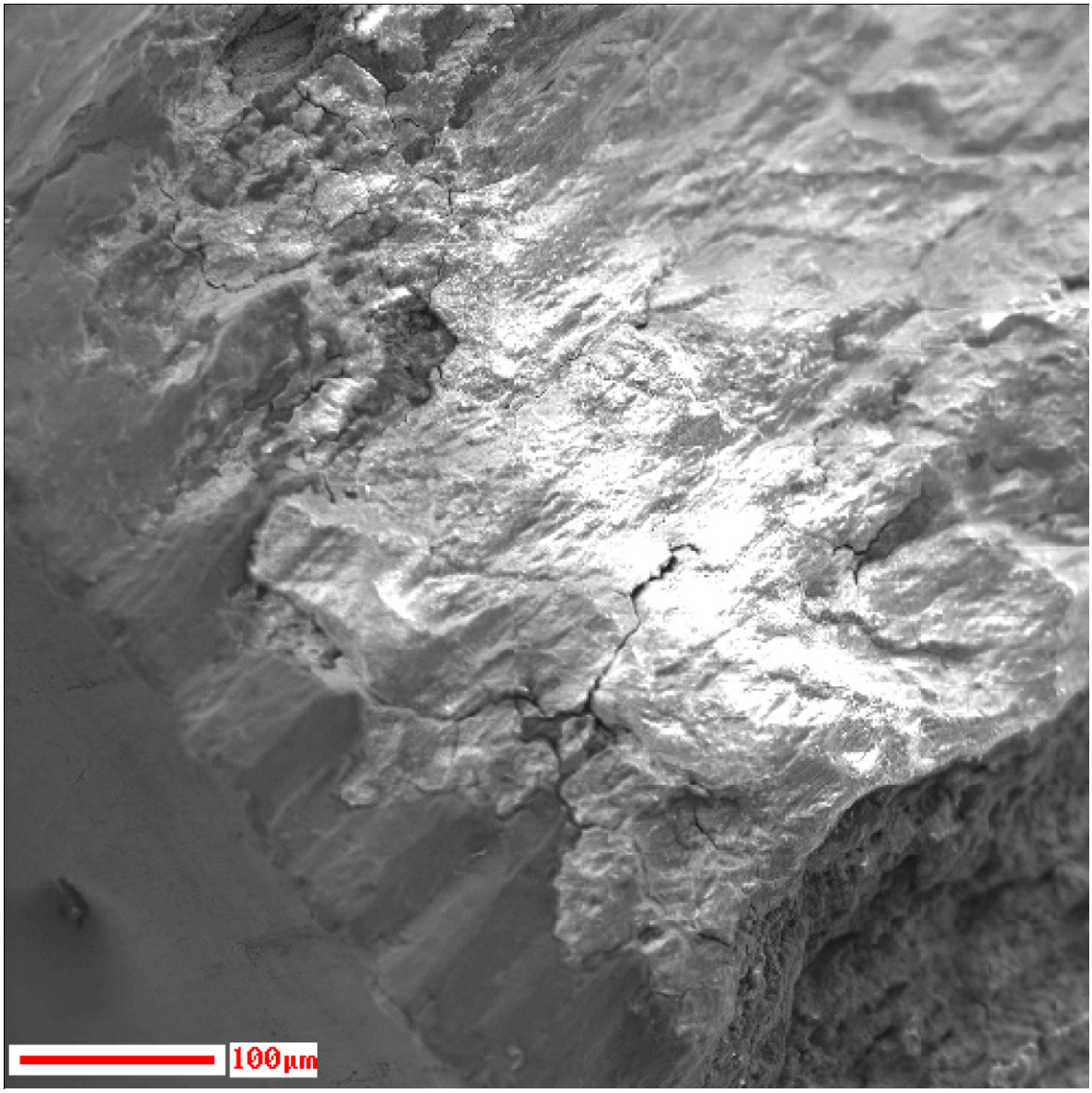

Figure 8.13 Flakes from adhesive wear loosely connected to the base brass metal.

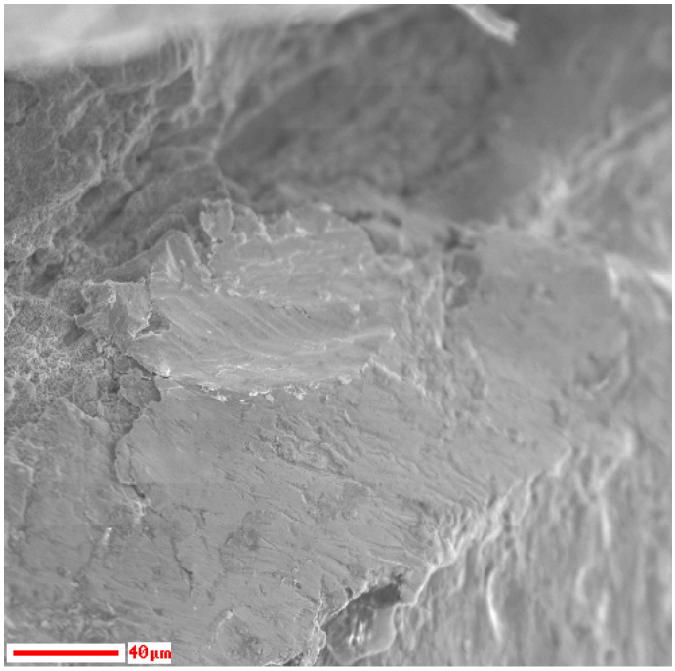

Figure 8.14 Plastic deformation on an asperity evidenced by distinct boundaries and plow marks.

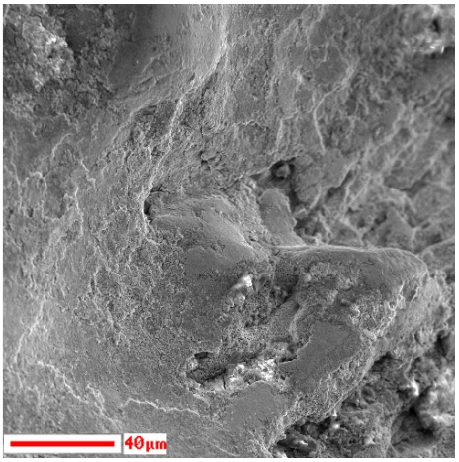

Figure 8.15 Very smooth surfaces indicative of fracture surface melting.

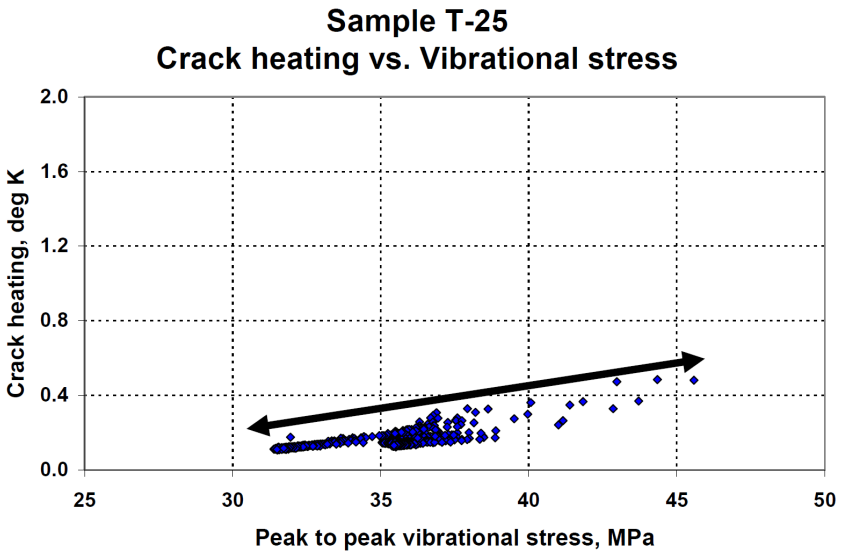

Figure 8.16 Measured crack heating as a function of the applied stress on Sample T-25. Since applied vibrational stresses were kept low, heat generation remained consistent and repeatable with little scatter regardless of the number of vibrations applied to the crack in sharp contrast with the data presented in Figures 8.1 and 8.2.

CHAPTER 9. CONCLUSIONS

Jeremy Renshaw

Vibrothermography is a useful and important NDE technique that can rapidly detect the presence and location of defects in structures. This section presents a brief overview of the conclusions relating to vibration, crack closure, synthetic defects, fracture surface damage mechanisms, and thermal properties of materials.

9.1 Synthetic Defects

Synthetic defects are artificial defects, used in place of real defects, to aid in evaluating the defect detection ability of an NDE technique. Synthetic defects, therefore, are required to qualify an NDE technique for a specific application. Typical synthetic defects used for other NDE methods are EDM notches, flat bottom holes, and teflon inserts. Of these, only teflon inserts are appropriate for limited use with vibrothermography, since they have a rubbing surface capable of generating heat; however, they can only be manufactured in composite laminates. For this reason, a new type of synthetic defect was developed for vibrothermography: viscous material-filled (VMF) synthetic defects. VMF synthetic defects generate heat with the application of vibration and are widely applicable to a variety of materials and structures.

Chapters 2 and 3 detailed a method to manufacture and test these viscous material-filled (VMF) synthetic defects. A VMF synthetic defect consists of a pre-existing or drilled hole filled with a viscoelastic material (generally honey) and capped with an emissive coating (in this case, spray paint). These defects have been tested and can

be used to image relative stresses across regions of a sample, observe mode shapes of vibration, and evaluate coverage for defects using vibrothermography.

Though these synthetic defects require further development, they are the first viable synthetic defects that can be easily manufactured and that reliably generate heat when vibrated. Future applications of the principles shown in this dissertation can be used to create coatings that can be easily applied and removed from test parts which will heat up when exposed to vibration.

9.2 Vibration Measurement

Chapter 4 dealt with calculations of the full stress and strain tensor based on measures of surface vibrations. By measuring the full three-dimensional motion across the entire surface of a sample, it is possible to calculate the internal motions and displacements of a sample. The full stress and strain tensors throughout a sample can be calculated based on a knowledge of the material properties and surface motion. Future applications of this technique are to measure the full stress and strain tensors of complicated geometrical parts as well as to apply the method to parts containing internal voids. This method allows for accurate, non-contact measures of stress, strain, and displacement in a test piece.

9.3 Heat Generation

Chapter 5 explained different sources of heat generation in vibrothermography. The primary mechanism of heat generation (in a crack) was shown to be friction between rubbing crack faces. Regions of a crack where asperity rubbing was observed, evidenced by tribological damage on rubbing asperities, were shown to correspond to heat generation sites along a crack. Crack closure affected the regions of a crack where heat can be generated by controlling which regions of a crack are open, locked, or in contact and

able to rub. The vibrational stress level also controls how much heat is generated for regions of a crack that are in contact.

Plasticity was shown to generate heat under certain circumstances, such as during crack growth or due to friction-induced plasticity on rubbing crack faces. Viscoelastic heating was also observed to generate heat due to viscous flow for a carbon fiber reinforced polymer (CFRP) composite, and to generate additional heat due to stress concentrations in viscoelastic materials.

9.4 Crack Closure

Chapters 6 and 7 focused on aspects of crack closure and fracture mechanics. Crack closure was shown to have a significant influence on the portions of a crack that generated heat and exposed a potential problem in detecting very tight cracks. It was found, however, that vibrothermography has potential to find tight cracks that can be missed using other NDE techniques since vibrothermography relies primarily on contact and motion between rubbing surfaces. A tight crack may still be missed using vibrothermography, but the probability of detecting such a crack may be higher using vibrothermography than with some other methods; for example, fluorescent penetrant inspection since there is no dependence on the volume of the defect to serve as a reservoir for the penetrant used in the inspection.

A method was developed that is able to measure crack opening stresses and crack closure stress profiles along the length of surface cracks. This method is a direct measure of the contact at the surface of a crack and images regions of contact through frictional heat generation. Resolution of closure regions is limited by the camera resolution and distance from the sample. Decreasing the distance between the IR camera and the cracked sample will increase the resolution of the camera and help to resolve smaller-scale effects such as roughness-induced closure. Measuring closure stresses using this

method provides an improved technique to measure crack opening stresses as compared to conventional techniques and provides local information along the opening of the crack. This is in contrast to conventional measures of crack opening stresses, which are derived from curve fits of stress-strain curves of a cracked sample where deviations in the stress-strain curve of a cracked sample are assumed to be caused by the opening of the crack.

9.5 Fracture Surface Modifications

Chapter 8 discusses the "tribological damage" (modifications to contacting asperities due to frictional rubbing and heat generation) that occurs on the fracture surfaces of a vibrated crack. Delicate crack faces are exposed to intense vibration, causing violent rubbing between the two contacting crack faces. Observations of tribological damage on rubbing crack faces were presented from optical microscopy and profilometry, a scanning electron microscopy (SEM), Auger spectroscopy, and energy dispersive X-ray spectroscopy (EDS) that provide evidence that vibration is responsible for the observed tribological damage. The observed tribological damage mechanisms include fretting, plasticity, oxidation, wear (primarily adhesive wear), and melting. The vibrothermographic heat generation of a crack was also observed to change in parallel with the modifications to the contacting asperities, though not in a consistent or repeatable manner. Some cracks became more efficient at generating heat while others became less efficient. Using sufficiently low vibrational stresses appeared to avoid causing measurable tribological damage to crack faces and dramatically improved repeatability.

9.6 Summary and Conclusions

Vibrothermography consists of a combination of several physical phenomena, all of which must be well understood in order to effectively implement vibrothermography as a reliable NDE technique. First, the physics of vibration must be characterized

to understand how a sample must be vibrated to provide sufficient vibrational stress throughout the sample for adequate defect inspection coverage. Second, the mechanisms of heat generation must be understood to provide limits as to what types of defects will give a response and which ones will not. Third, the thermal properties of a sample must be well understood to determine how suitable a sample is for vibrothermographic inspection.

Synthetic defects can be used for vibrothermography to further understand which structural resonances are useful for detecting defects located at specific locations within a structure. Vibrational frequency controls which resonances were excited within a structure while local vibrational amplitude determines how much a defect will heat up. Friction is the primary source of heat generation in vibrating cracks with additional heat generation possible through plastic deformations and viscoelasticity. Crack closure determines which regions of a vibrated crack would heat based on the applied vibration. Measures of heat-generating locations as a function of the applied external load provide estimates of the closure stresses on a crack. Different tribological damage mechanisms operate on cracks based on the level of applied vibrational stress. Vibrational stresses below a certain level do not appear to have a significant effect on the rubbing surfaces, whereas higher vibrational stresses cause permanent changes (tribological damage) to the crack surfaces and may adversely affect future defect detectability. Locations of heat generation can be mapped to locations of damage on fracture surfaces, giving strong evidence that heat generation is primarily frictional.

Vibrothermography has significant potential as an NDE technique and will be an industrially useful tool in the near future. To achieve this goal, future work in the area of vibrothermography should focus on continuing to improve understanding of inspection coverage analysis, the relationship between vibration and heat generation, and creating useful statistical models for vibrothermographic defect detection. Preliminary work on inspection coverage analysis was presented in this work and is an important topic that

must be addressed for each situation where vibrothermography is a candidate inspection method. Since defect detection is dependent on the position of the defect within excited vibrational modes in a structure, an understanding of the vibrational stresses and strains throughout an inspected structure must be known for a robust inspection. Basic physical mechanisms of heat generation have been elucidated in a series of controlled experiments, which in conjunction with an understanding of structural vibrations helps to understand when and how a defect will be detected using vibrothermography. Such information is necessary to construct accurate and valid models for defect detectability that can be used for statistical purposes. There is still more work that must be done to improve our understanding of vibrothermography before it can be accurately modeled, but once developed, vibrothermographic models would be a critical step for defining the limits of when vibrothermography would be an accurate and reliable inspection method versus when it would fail. Once sufficient knowledge is obtained about vibrothermography, it could find widespread application in industry and could enhance, or potentially replace, other NDE methods.

APPENDIX A. EXPERIMENTAL PROCEDURE FOR MANUFACTURING SYNTHETIC DEFECTS FOR VIBROTHERMOGRAPHY

The following procedure outlines the steps necessary to manufacture viscous material-filled (VMF) synthetic defects in a sample. The process is simple and results in synthetic defects that generate a significant amount of heat when exposed to vibration. The process is most efficient when manufactured in batches to create multiple synthetic defects in parallel.

Sample preparation

Samples may be prepared using a single synthetic defect or an array of defects. These defects are easily produced, though the process may be time-consuming. The selected locations for the synthetic defects should be located in an regions where it is possible to drill holes or where accessible holes already exist. The holes used in this study were drilled to a depth of about 5.0 mm using a 1.17 mm diameter (0.046 in) drill bit, though there is no set minimum or maximum size for the holes. Smaller holes will be more difficult to fill with honey, but an array of smaller holes has the potential for better vibrational coverage resolution. Larger holes will be easier to fill with honey, but will result in reduced resolution. The size of the holes should be determined based on the particular need of an experiment. A 1.17 mm diameter hole is shown in Figure A.1. Holes must be drilled to a depth that is less than the thickness of the material, but

greater than or equal to two times the hole diameter, if possible. The depth of the hole determines the amount of viscous fluid that the synthetic defect may hold.

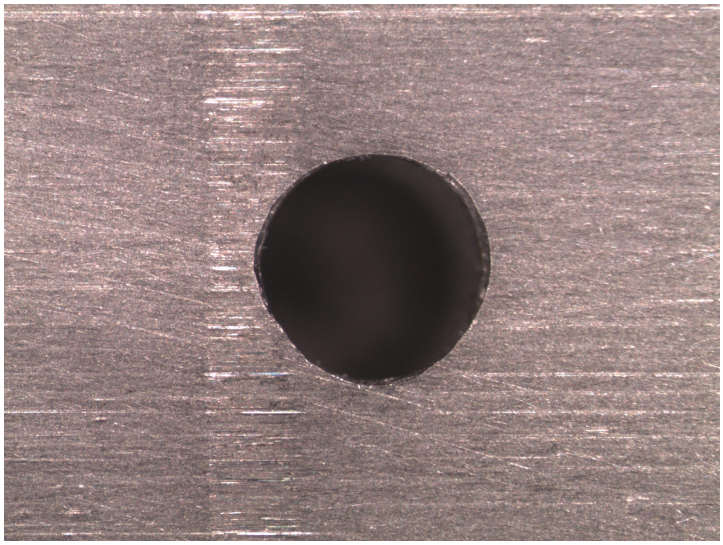

Figure A.1 Figure showing a drilled hole that will be used as a synthetic defect.

Once the holes have been drilled, grind or sand the top surface of the holes to remove the lip at the surface of the sample caused by the drilling process. The presence of this lip prevents proper surface cleaning and increases the difficulty of producing the synthetic defects. Once the lip has been removed, use compressed air to clean the residual metal dust and chips out of the drilled holes. Residual metal chips or dust may contaminate the synthetic defect and alter its performance.

Applying a viscous fluid

Several materials have been tested for use in synthetic defects including honey, shear wave couplant, CA glue (superglue), and several adhesives (3M products: #72, #75, and repositionable #77). Honey was shown to be the most versatile, easiest to apply, and most effective at generating heat. It is also chemically inert, inexpensive, and easy

to remove. Though another more suitable material may be found in the future, honey appears to be well suited for such an application.

Once the holes have been prepared, apply the honey in moderation to the surface. The honey will not enter into the hole, but traps the air inside the hole, causing a noticeable reflection inside the diameter of the hole when viewed under a stereo microscope as can be seen in Figure A.2. This reflection is important in determining if a drilled hole contains air or if it is partially or fully-filled with honey. All subsequent steps should be done while observing the hole under illuminated magnification, preferably with a stereo microscope, at 16 times magnification or higher.

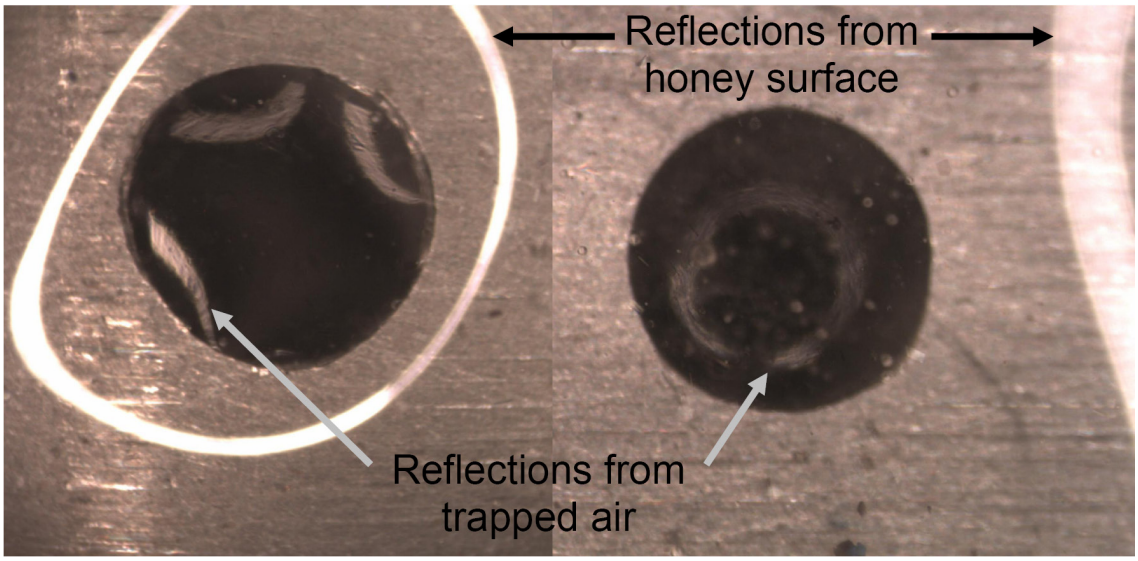

Figure A.2 Figure showing reflections of incident light that can be used to determine if a hole contains an air bubble has been filled with honey.

Honey will not readily enter the drilled holes on its own, so it is necessary to force the trapped air out of the holes and cause the honey to enter the holes. This is done by pushing a thin rod (in this case, a paperclip of 0.83 mm diameter was used) into the hole after the hole has been covered with honey. The rod should enter the hole vertically and should contact one side of the hole as it is pushed down into the hole. This will force a

single large air bubble to exit the hole on the opposite side of the inserted rod as seen in Figure A.3. If the rod is not carefully inserted, multiple air bubbles may leave the hole from different sides and create difficulties in forcing all of the air out of the holes and honey into the holes.

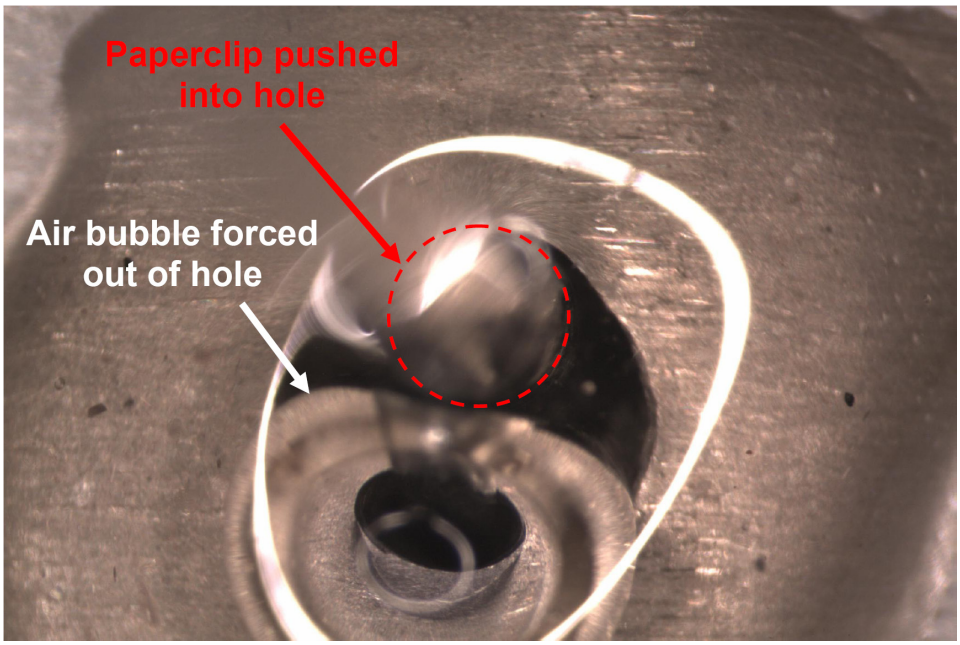

Figure A.3 Insert the paperclip into the drilled hole to force the air bubble out of the hole to allow the honey to enter.

Once a single air bubble has been displaced from the hole and is trapped in the honey, push the inserted rod in the hole around so that it acts as a barrier between the air bubble and the hole as shown in Figure A.4. Remove the rod slowly and observe the behavior of the honey and the air bubble. Ensure that the air bubble does not return into the hole (i.e. the size of the air bubble does not change), but that the hole fills with honey. Some air may enter the hole despite these and other precautions. If part or all of the air bubble does re-enter the hole, repeat the same process to remove the air bubbles until the hole has been completely filled with honey. Often, small air bubbles will remain trapped inside the hole. As long as these bubbles are less than 20 percent of the diameter of the hole, they will not have a significant effect on the behavior of the

synthetic defect.

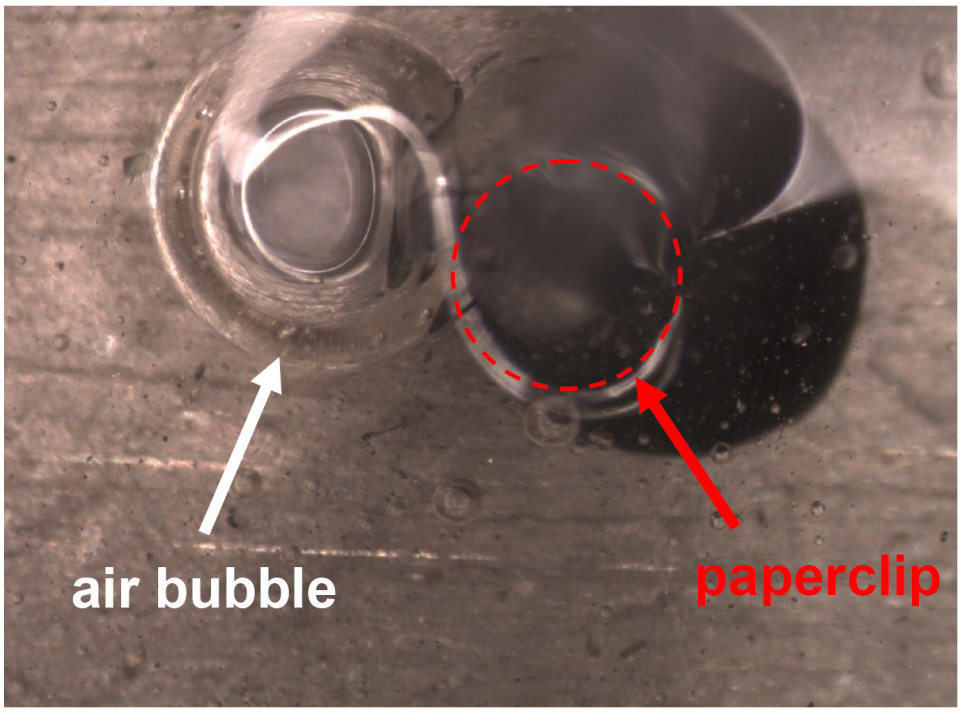

Figure A.4 Isolate the air bubble from the hole and slowly remove the paperclip to prevent the air from re-entering the hole as the honey fills the hole.

The process to check if a hole has been filled with honey is relatively simple and straightforward, though it may take some experience to master. The presence of an air bubble in the hole beneath the honey creates a reflection when viewed under the stereo microscope. When the hole is completely filled with honey, however, it is not reflective and the hole appears dark as shown in Figure A.5. Experience is important in identifying these reflections to determine if a hole has been properly filled with honey or not.

Finishing the defect

Once the holes have been filled with honey, it is necessary to clean the excess honey from the surface. Use a straight edge to scrape off the bulk of the excess honey from the surface. To clean the small remaining residue of honey, use a damp cloth and gently

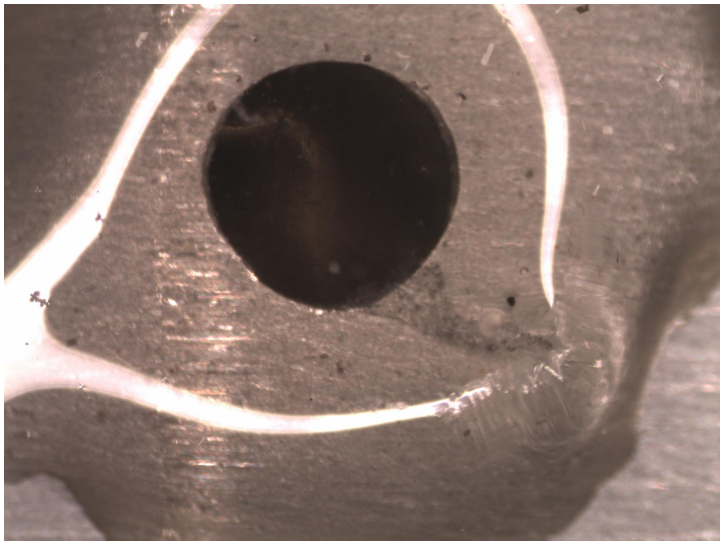

Figure A.5 Figure showing the honey-filled synthetic defect. Note that the hole shows no internal reflection, contrasted with Figure A.2, indicating that little to no air has re-entered the hole and that the synthetic defect is nearly complete.

wipe the surface and be careful to avoid sucking honey out of the filled holes. Allow the surface to dry before continuing.

Once the excess honey has been removed and the sample is dry, spray on an emissive coating to trap the honey in the holes. Alternative adhesive tape coatings may also be used, if appropriate.

Measurement

As a viscous fluid, the honey heats up when subjected to shearing motion. This means that the honey will heat up more in regions that have higher vibrational motion. Vibrate the sample at different resonant frequencies or using a frequency sweep to excite multiple frequencies to observe the patterns or profiles of heat generation. Using the heating profile of an array of synthetic defects, it is possible to obtain information about structural mode shapes of a sample and their respective frequencies of excitation.

Considerations when using honey

One important item to be aware of when using honey for synthetic defects is that it has a tendency to crystallize over time while in storage. It is possible to decrystallize the honey without stripping the coating. Heat the honey to a temperature of 60 deg C (140 deg F) for 30 minutes. This will cause the honey to decrystallize and be ready for use. Allow the sample to cool to room temperature before commencing experiments. Do not heat the honey using a microwave oven as this can also alter the sugars in the honey and possibly degrade its performance as a viscous material for synthetic defects.

Removing honey from a synthetic defect

Removing honey from a synthetic defect is quite simple since honey is water soluble. First, clean off the emissive coating from the surface to expose the honey. Place the sample into a water bath in an ultrasonic cleaner and clean it for 30 minutes. Since honey is water soluble, the ultrasonic vibrations should effectively clean the honey from the holes. If the honey is not completely removed after the first cleaning cycle, repeat as necessary.

APPENDIX B. EXPERIMENTAL PROCEDURE FOR COLLECTING 3-D STRESS AND STRAIN TENSORS IN A VIBRATING BAR

The following procedure outlines the steps necessary to measure the full stress or strain tensor in a bar through measures of surface vibrations.

Sample Preparation

The sample used was a titanium (Ti 6-4) bar with dimensions of 152.4 mm X 25.4 mm X 12.7 mm (6.00 in. X 1.00 in. X 0.50 in.). An M8 hole was drilled and tapped 6.35 mm from the bottom edge and halfway between the two sides of the 152.4 X 25.4 mm face as shown in Figure B.1. A set screw was tightened into the hole such that the sample could be mounted securely to the transducer Holland, S. D. (2007A).

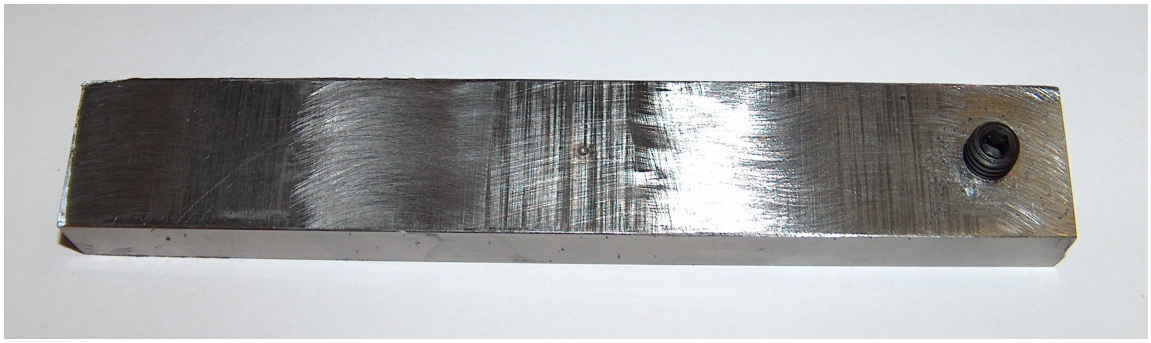

Figure B.1 Figure showing the drilled and tapped hole used for mounting the transducer.

The laser vibrometer uses the Doppler shift in the laser beam reflected back to the

vibrometer to measure vibrations parallel to the direction of the beam. Thus, it is important to reflect back as much of the incident beam as possible. For this reason, the entire sample surface was covered in retroreflective tape to maximize the laser beam reflection returning to the vibrometer. Gloves should be worn when applying the tape to prevent contaminating the tape's surface. It is also important to avoid air bubbles forming under the surface of the retroreflective tape when applying it to a surface. The tape should be applied up to the edges of the samples to maximize the scannable area of the sample. One method to maximize the scanned area is to apply a piece of tape that is larger than the scannable area and then cut off the excess tape using a utility knife.

The program that controls the motion control system generates a discretized grid of points across the surface of the sample to be scanned. The discretization process will also only generate points if they lie greater than a specified threshold from the sample edges. Points that lie at the sample edges often have poor reflective properties, so staying a minimum distance away from these regions helps to minimize the number of poorly reflecting points and increases the quality of the data.

The scanfacets.py controlling program will refocus the laser if the reflections in an area are too small, resulting from either poor tape reflectivity in that region or if the tape does not cover the scanned region of the surface. If the tape does not cover a certain region, the program will try to refocus the laser to obtain the maximum reflection, but if the reflection is below the minimum threshold the point will be thrown out, its velocity set to zero, and the laser will continue to the next point on the surface. Such regions should be cleaned after the scan has terminated to get rid of any contamination on the surface. These points should also be rescanned later to improve the overall quality of the data.

This experiment needs to maximize the scannable area of the sample, so the transducer is used for vibrational excitation and as the mounting location. The transducer will, however, still shadow some regions of the sample which then cannot be scanned

for vibration measurement. Due to the scanning procedure, the laser will still try to scan these regions, however, it is requisite that no reflection is received when the laser is trying to measure areas of the sample surface masked by the transducer. Covering the transducer in black electrical tape is an effective means of eliminating reflections from the transducer. Thus, the vibration data will only include data from the vibrated sample and not the transducer.

Alignment

The alignment of the sample in the motion control system is critically important. Measures of distance require an accuracy of less than 1/2 of a millimeter are needed with angular accuracy of the mirror within 1/3 of a degree for proper alignment. The alignment process may take several hours, but if not done properly, will produce very poor quality data, require that the measurement is redone with improved alignment, and that all measurement errors are tracked down and corrected.

A set screw is tightened into the sample so that the sample can be mounted rigidly to the transducer for proper vibrational excitation. The transducer should be mounted as tightly as possible to the sample. Do not be concerned about the rotational orientation of the transducer with respect to the sample, only that the two are tightly fastened together. Their respective alignment is not critical since it is possible to rotate the transducer independently. Next, mount the transducer tightly to the turntable. The transducer tip and sample should be located near the center of the turntable to minimize the effect of measurement errors in its location as the turntable is rotated. Once the transducer and sample are in place, turn on the pressure using the Dataguzzler program (see Dataguzzler manual for additional information). The applied pressure should be at least 400 kPa (max 600 kPa) to reduce the risk of rotational motion of the transducer during vibrational excitation. The transducer should be aligned so that the sample bar

is perfectly vertical along both the front/back faces and the side faces. Measure the orientation of the bar using the y-axis of the motion control stage by scanning the laser up and down along the outside edges of the sample. Rotate the turntable 90 degrees to measure the side face of the sample and repeat the sample edge scan using the vibrometer and y-axis motion control stage. Realign the sample as necessary until it is perfectly vertical to within the measurement accuracy for both the front/back and side faces.

Next, it is necessary to measure all of the vectors associated with the motion control system and measurement setup (i.e. x, y, z locations of the motion control stages, center of rotation of the turntable, distances on the mounting plate, etc.). Several important vectors are described in Table B.1. The first step is to define a global origin. Once the origin has been defined, all static offsets of the sample, measuring equipment, and motion control stages must be measured in the x, y, and z directions. For this step, all motion control equipment must be positioned at the defined zero location for that stage. Thus, any motion in that stage can be added to the base vector. Record these values as accurately as possible in a laboratory notebook and enter them in the boundaryscan.py program. It is very important to keep track of any and all reference points and vectors used in this experiment. Every single vector is important and if not measured properly, can require that the entire experiment be restarted and that all of the vectors are remeasured to track down any errors, resulting in a significant loss of time. Meticulous measurement precision and careful checking will help to avoid problems down the line.

Alignment Verification

It is necessary to validate the different measured vectors before initiating any experiments. Due to the three-dimensional nature of the experiment, some errors will not show up until the final stages of testing and can be extremely time-consuming to track

down. Many errors require that the entire experiment is started over using the corrected alignment. To prevent such mistakes, it is recommended that the scanfacets.py program is started for several different facets, and stopped after it performs the outline trace of the region to be scanned. Repeat for facets in different directions and both with and without the mirror. If all of the outline boundary scans are all correct, then it is appropriate to start the experiment and begin taking data. If the outline trace does not scan the correct facet, the correct region of the facet, or there appears to be some other error, discontinue experimentation, track down the alignment problem, and verify that the proper alignment has been achieved before beginning to take any data.

Experimental Considerations

It is necessary to run several Python scripts to be able to run the data collection successfully. These scripts are outlined in the next sections. They must interface with Dataguzzler while the experiment is running, so the Dataguzzler program must be running before the scripts are used. Dataguzzler is also used for defining the measured vibration channel specified in the scanfacets.py program. A typical vibrational excitation pulse (frequency sweep from 0.1 to 20 kHz) is defined as follows:

awg:sweep arb 100 20000 .2 .201 .209 .21

Consult the Dataguzzler manual for the details of the excitation parameters. It is also necessary to define a measurement channel for the script files to use. The default name is "vib_crop" and can be defined as follows:

MATH:DEF vib_crop=CROP(Vibrometer,[0.20,0.25])

Again, consult the Dataguzzler manual for the meaning of each of these terms. Make sure that the measurement channel is defined using the proper vibrometer (Vibrometer or Vibrometer2). If this is not done, the experiment must be completely restarted using the proper vibrometer. Just because a laser beam is scanning the correct area does not mean

that the correct laser vibrometer is being used for the experiment. Unfortunately, this type of error will likely not be noticed until the post-processing stage and is thus a very time-consuming mistake. To help avoid such problems, verify that the vib_crop channel is recording the proper data by manually checking the waveform using the Dataguzzler scope display after a test excitation. Verify that the vib_crop channel continues to collect data for a sufficient time after the excitation pulse to allow the vibrations to die out for sufficient zero-padding of the data (important for improved analysis using Fourier Transforms). A low amplitude excitation pulse is best for repeatable measurements. Generally, specifying an input voltage of 0.10 V to 0.25 V is sufficient for high-quality, repeatable data. Decreasing the amplitude below 0.1 V gives a lower signal to noise ratio while increasing the voltage above 0.25 V decreases the measurement repeatability. Avoid amplitudes above 1.0 V for an experiment such as this since large numbers of high-amplitude excitations in rapid succession could overheat and damage the transducer.

Configuration

Boundary vibration measurement collection is controlled by two configuration files: `bnd_fixed_<date>_<run>.cfg` (fixed) and `bnd_var_<date>_<run>_<scan_index>.cfg` (variable). The former includes parameters that will remain fixed throughout the measurement process, such as specimen mounting and most of the fundamental unit vectors. The latter includes parameters that will vary, such as the incident laser direction ($\hat{l}$), mirror presence (mirror used or mirror not used), mirror orientation, and turntable position.

These files are interpreted as Python scripts that assign values to global variables. The `variable` configuration file can assume that `fixed` has already executed, but cannot change values assigned by `fixed`. Neither file should contain nontrivial computation.

Procedure

1. Define specimen coordinates and mount specimen on turntable

   (a) Identify the reference point on specimen (preferably a corner).

   (b) Define orthogonal $\hat{a}$, $\hat{b}$, and $\hat{c}$ axes on the specimen.

   (c) Mount the specimen on the turntable and align so that the specimen is perfectly vertical as specified in the alignment section above.

   (d) Locate the reference point within the turntable coordinates relative to the turntable reference. Record this value in the proper configuration file as `rdp_syf`

   (e) Evaluate $\hat{a}$, $\hat{b}$, and $\hat{c}$ in terms of turntable coordinate vectors. Record this value in the proper configuration file as `ahat_syf`, `bhat_syf`, and `chat_syf`.

2. Determine a set of facets (triangular or quadrilateral) that covers all of the visible surfaces on the sample.

   (a) Number the facets and measure their dimensions.

   (b) Evaluate the specimen coordinates (relative to the specimen reference) of all of the corners of each facet. Record this value in the proper configuration file. Each facet should be appended to FacetCornersList.

   (c) Select values for `ElementSpacing` (the spacing between elements) and `MinEdgeDist` (the closest distance the laser is allowed to come to any of the borders of a facet). Record this value in the proper configuration file

   (d) Use the tesselatefacets.py script file to tesselate the facets and save them to disk (these are saved in the .facet files)

   (e) Evaluate the tesselation using the readfacets.py script file. Adjust the parameters as necessary and rerun tesselatefacets.py script until the desired

tesselation is achieved. The previous .facet file must be deleted before tesselatefacets.py can be run again.

3. Check the calibration of the motion control system

   (a) Re-zero motion control system if necessary.

   (b) Carefully orient the vibrometer in the $-\hat{z}$ direction.

   (c) Verify that the laser points in the $-\hat{z}$ direction. Move the z-stage in the $\pm\hat{z}$ direction and adjust the vibrometer positioning to verify that vibrometer spot position remains fixed on the specimen as the z-stage moves. This verifies that $\hat{l} = -\hat{z}$. Record the $\hat{l}$ direction in the variable config file (lhat = (0.0,0.0,-1.0)), check that mirrorpresent=False, and that vib_standoff_n is reasonable (near a maxima, consult the vibrometer user manual for standoff distances).

   (d) Use moveto.py to move to calculated position for a front-facing facet corner (preferably the reference point) on the specimen. If the laser spot is not at the correct position, determine what coordinate or vector needs to be adjusted. Record the corrections in the proper configuration file.

   (e) Repeat step (3d) for several other front-facing facet corners elsewhere on the specimen.

   (f) Adjust the large, stainless-steel mirror to exactly 45°, set `phi = 45` and `mirrorpresent=True` in the variable config file (You may need to increase `vib_standoff_n`).

   (g) Check several corner points on the specimen as done previously. Adjust any necessary parameters. Record the corrections in the proper configuration file.

   (h) Move to the calculated position for the center of the front face. Autofocus the vibrometer, read out the focal position with Dataguzzler using the

VIB:FOCUSPOSITION? command and verify that its output is approximately 1909 ±40. This will ensure that the vibrometer standoff distance is acceptable.

4. Figure out how to obtain at least three linearly independent incident laser vectors for each point on each facet. This will require at least three scans per facet (more if some points are shaded during a scan). Sketch out ideas in a lab notebook for future reference during both measuring and analyzing the data.

5. Configure dataguzzler with the necessary excitation and measurement parameters (i.e. frequency sweep parameters, excitation amplitude, vib_crop channel definition, etc.). Save this configuration in a .set file.

6. Adjust the turntable, mirror, and aim the laser vibrometer as required for one (or more) of the scans identified in (4)

   (a) Once the vibrometer has been aimed, move the vibrometer measurement point to a reference location on the surface of the specimen.

   (b) Use the laserdirecfind.py script to evaluate the exact direction of the laser vibrometer.

   (c) Record the new orientations in the variable configuration file.

7. Execute the scanning program, scanfacets.py, specifying the configuration files to use and which facets to scan for each measurement run.

   (a) The scanning program will begin by outlining the boundaries of the target facets. Verify that no cables are at risk of snags as the motion control system scans around the facets.

   (b) The scanning program will report the number of points to scan which can be used for an estimate of the completion time.

8. Repeat steps (6)-(7) to complete all of the required scans identified in step (4).

9. Run the `boundaryscanverify.py` program, which will evaluate the scan coverage, inform you of failed measurement points, and evaluate the condition number for each facet. The condition number is ratio of the maximum singular value over the minimum singular value of the single value decomposition (SVD) of the matrix formed by assembling the incident laser vectors as rows. The condition number is ideally less than 2 and should always be less than 3.5.

10. Perform any additional scans to reduce the condition numbers as necessary.

Postprocessing

Postprocessing will transform the collection of files from the various scans into a single composite data file in which the vector velocities have been resolved into cartesian components. The resulting data file will be structured as follows:

- `VIBRDATA` chunk
  - `SNAPSHOT` chunk containing first a `METADATA` chunk containing one `METDATUM` per scalar parameter in the `fixed` configuration file, then one `GUZZNWFM` per vector/matrix/array parameter in the `fixed` configuration file. Metadata is ignored. All distances are presumed to be in mm.
  - `SNAPSHOT` chunk containing "typical" waveforms that should have remained constant throughout the test (i.e. Awg, ArbGen, XducerVoltage, XducerCurrent, XducerForce, etc.). This will be empty.
  - A `VIBFCETS` chunk containing one `VIBFACET` chunk for each facet that contains:

* A `SNAPSHOT` chunk with metadata containg the scalar parameters of the facet, plus one `GUZZNWFM` per vector parameter of the facet (e.g. Meas3DCoords, etc.).
* An optional series of `GUZZNWFM` chunks, one per element of the facet for which waveform data was collected. Each `GUZZNWFM` is either:
  - A `GUZZNWFM` chunk named VIBXYZ, which contains metadata specifying the coordinates of the center of the element, the area of the element, and the coordinates of the corners of the element. In addition, there should be the usual waveform metadata, plus n*3 data which contains the $\hat{a}$, $\hat{b}$, and $\hat{c}$ velocities in (m/s) as functions of time for the measured point, or
  - A `GUZZNWFM` chunk named VIBNORMAL, which contains metadata specifying the coordinates of the center of the element, the area of the element, and the coordinates of the corners of the element, and the normal vector from the center of the element to the laser vibrometer. In addition there should be the usual waveform metadata, plus n data elements which contain the normal velocity in (m/s) as a function of time for the measured point.

Waveform Metadata

Table B.1 lists additional metadata entries for the saved waveforms.

Table B.1 Waveform Metadata

Metadatum Name	Type	Description
FacetNum	Integer	Facet # measured (0..n-1)
ElementNum	Integer	Element # measured within the facet
r_target_a	Floating point	$\hat{a}$ coordinate of the vector from the specimen reference position to the target point for this measurement
r_target_b	Floating point	$\hat{b}$ coordinate of the vector from the specimen reference position to the target point for this measurement
r_target_c	Floating point	$\hat{c}$ coordinate of the vector from the specimen reference position to the target point for this measurement
r_actual_a	Floating point	$\hat{a}$ coordinate of the vector from the specimen reference position to the actual point for this measurement
r_actual_b	Floating point	$\hat{b}$ coordinate of the vector from the specimen reference position to the actual point for this measurement
r_actual_c	Floating point	$\hat{c}$ coordinate of the vector from the specimen reference position to the actual point for this measurement
e_laser_a	Floating point	$\hat{a}$ coordinate of the unit vector in the direction of the laser incident on the specimen surface
e_laser_b	Floating point	$\hat{b}$ coordinate of the unit vector in the direction of the laser incident on the specimen surface
e_laser_c	Floating point	$\hat{c}$ coordinate of the unit vector in the direction of the laser incident on the specimen surface

APPENDIX C. EXPERIMENTAL PROCEDURE FOR MEASURING CRACK OPENING STRESSES AND CRACK CLOSURE STRESS PROFILES FROM VIBRATION-INDUCED HEAT GENERATION AT CONTACTING REGIONS OF CRACKS

The following procedure outlines the steps necessary to measure surface crack closure stress profiles in cracks as well as the surface crack opening stress (note that both are surface measures only). Following the procedure outlined below will result in an accurate estimate of the surface closure parameters of a crack.

Sample Preparation

After the crack has been grown, clean the sample surface using an acetone bath in an ultrasonic cleaner for 30 minutes. Wipe the surface dry with a clean cloth upon removal. Apply an emissive coating to the surface of the sample using the procedure outlined at the CNDE Thermography lab's wiki site:

https://thermal.cnde.iastate.edu/lab/Emissive coating tips and tricks

Cover the regions of the sample that should not be coated with a removable tape. Apply a coating to the surface of the sample that will improve the emissivity of the surface and be thin enough to minimize the lag time from thermal conduction through the coating. Generally, a flat, black spray paint is sufficient to improve the emissivity of

a specimen to a reasonable value. Remove any excess coating by removing the tape.

If the sample surface requires additional cleaning, use a cloth dipped in acetone, but be very careful to avoid stripping or damaging the emissive coating in regions near the crack. Next, clean the strain gage mounting locations. After cleaning, mount the strain gages on the surface of the sample. Be careful to place strain gages away from both mounting pin locations and the crack since the stress fields around these locations can be quite complex and can interfere with the measurements. The strain gages should be placed halfway between the crack and the inner mounting pin (of a four-point bend configuration) on each side of the bar (exactly opposite of one another) as shown in Figure C.1. Two gages on opposite sides of the bar are used to obtain an average strain measurement (of the absolute strain values) for better measurement accuracy and to provide accurate data in case one of the strain gage becomes damaged or delaminates from the sample surface during the experiment. Use superglue to mount the strain gages to the sample surface while the sample is in an unstressed state. Align the strain gage grid to measure the strain (and convert to stress) in the sample parallel to the normal closure stresses of the crack. Superglue is recommended for mounting the strain gages to the base metal since it provides a rigid mounting that is stable over long periods of time and is easily removed using acetone. Consult a strain gage user manual regarding best practices for mounting strain gages.

Next, prepare the strain gage wires for soldering. Use electrical tape to hold portions of the wires in place such that when they are soldered to the soldering pads, any external stress on the wires will be carried by the tape and not the fragile soldering pad. Ensure that the strain gage wires will not interfere with the pin mounting locations for the application of the four-point bending load. Next, solder the connecting wires to the pads on the strain gages to connect their outputs with the measurement equipment. Calibrate the output of the strain gages with the measurement equipment to be able to measure tensile and compressive strains. Consult the instruction manual of the measurement

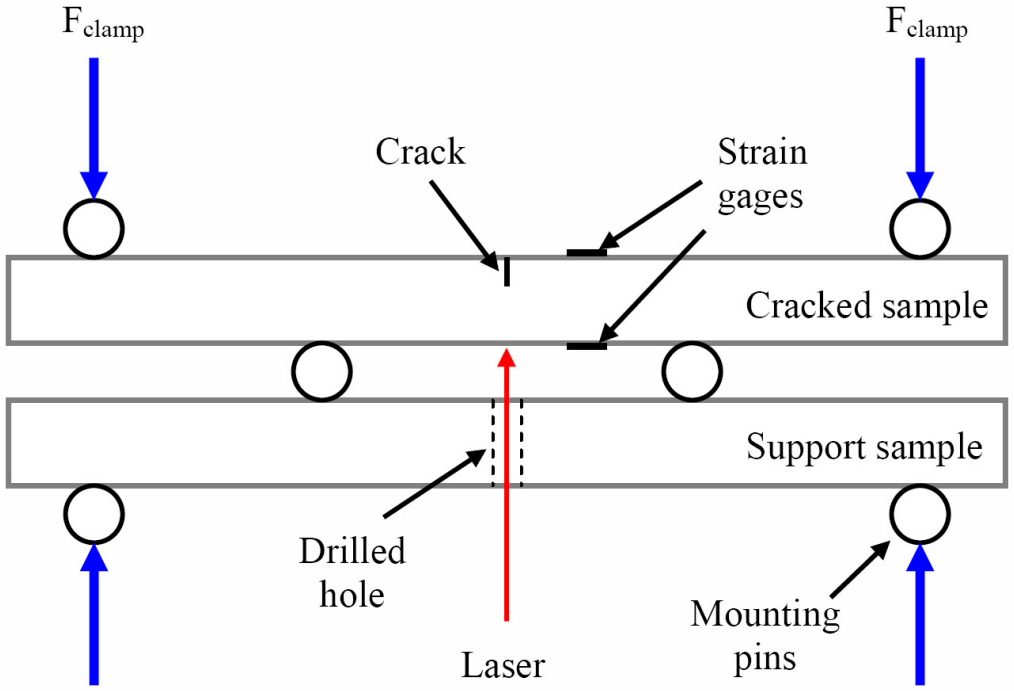

Figure C.1 Figure showing the mounting configuration for crack closure measurements.

equipment to ensure proper usage and calibration.

Prepare a second sample by drilling a hole completely through the bar specimen at the location corresponding to the crack in the first specimen. This sample bar will be used as a backing to the first specimen as shown in Figure C.1 and the hole is used so that the vibrometer can be used to measure vibrations on the back surface of the measurement sample, immediately opposite of the crack which would otherwise be blocked by the backing specimen.

Sample Mounting

Four-point bending is used to obtain a uniform bending stress between two center mounting pins (See Figure C.1 for mounting pin locations), or in this case, in the region around the crack. This setup avoids potential problems such as measurement sensitivity

due to the location of the strain gages along the sample. Using a four-point bend apparatus also avoids the complicated stress fields present near the center mounting pin in a three-point bending configuration.

To secure the sample in place, use a piece of double-sided tape at each mounting pin location. The tape serves two purposes. First, it helps the mounting pins to stay in place while the sample is positioned in the mounting setup. Second, it helps to keep the sample from walking out of the mounts due to the vibrational excitation, especially when the applied bending stresses are low, meaning that the mounting pins are not holding the sample in place as firmly.

Bending stresses are applied to the samples via two clamps. The use of two clamps allows for large stresses to be applied in a controlled fashion. Six mounting pins and two bars are required to apply the four-point bending load. Figure C.1 shows a top view of how the pins are arranged and how the four-point bending load is applied. When applying loads, apply small, incremental loads to both sides of the apparatus using a torque wrench. If a large stress is applied to one side, this will cause non-uniform bending stresses and can cause the inner mounting pin on the opposite side from where the load was applied to fall out of the mounting setup, creating a three-point bending configuration which is offset from the crack. As long as the torque that is applied on each side is approximately the same and applied in small incremental loads, these problems should be minimized.

The mounting pins used for this experiment should be a hard material, such as a high-strength steel. The rubber mounting pins used for typical vibrothermography experiments should not be used in this experiment. Using hard pins will prevent significant deformation that would occur with soft mounting pins and allow higher stresses to be applied.

To mount the samples in the experimental apparatus, first place all of the mounting pins in their locations as shown in Figure C.1 and use double-sided tape in between

the mounting pins and the metal piece. This will help to keep the pins in place when placing the bars into the experimental apparatus. Press the mounting pins into the tape so that they remain in place due to the adhesion of the tape. To move the sample bars and mounting pins into the clamps, it is beneficial to have two or more people to ensure proper alignment and positioning of the bars in the apparatus.This can be a delicate operation and adjustments may need to be made once the sample is nearly in place. Such adjustments are difficult to do with only one person. Once the bar is in place, begin to tighten the mounting clamps until a minimum stress of about 18-20 MPa is reached. Stresses below 18 MPa are insufficient to keep the sample in place when vibration is applied.

Until the clamping stress is at least 50 MPa, be careful to apply vibrational stresses that are sufficiently low so as to avoid problems with the sample moving into a different alignment or walking out of the grips but high enough to generate sufficient heat to be able to detect contacting regions in the crack.

Experimentation

Place the piezoelectric transducer on the side opposite of the crack located exactly behind one of the inner mounting pins. This mounting configuration avoids problems associated with the transducer obscuring the IR camera's view or causing distracting reflections, but still effectively transfers vibration through the mounting pin to the cracked sample. Place the laser vibrometer behind the sample and shine the beam through the hole cut in the back sample as indicated in Figure C.1. The laser beam should be aligned as close to normal as possible to the back surface of the cracked sample. Such a mounting configuration will allow the IR camera to have an unobscured view of the sample surface, allow for easy access to the strain gages, prevent the mounting pins from damaging the strain gages, and provide a standardized and accurate experimental method for crack

closure measurements.

Use the Dataguzzler program to control the data capturing process. It is best to apply small vibrational amplitudes first and then increase the vibrational stress until distinct regions of heat generation are observed. This will avoid generating massive amounts of heat along large areas of the cracks and will help to pinpoint heat-generating locations. It is also important to only apply small vibrational stresses once the crack is nearly or fully open. This will prevent or mitigate the problem of propagating the cracks during an experiment. To date, no cracks have been grown using this method, but crack lengths should be measured using optical profilometry (or a method with comparable accuracy) at 1000X magnification before and after testing to verify that crack propagation has not occurred.

Measurement accuracy

The accuracy of these measures is affected by the ability to accurately measure both stress data and heating data. Stress data are measured by converting the measured strain to a stress using the Young's Modulus of the material. Heating locations are taken as the center point within the region that generates heat. Alternatively, image processing can be used to isolate regions of heat generation Holland, S. D. (2009). The primary factors that influence measurement accuracy in this experiment are as follows:

1. Distance from the IR camera - the closer the camera is to the sample, the more accurately the camera will be able to measure heat at the contacting asperities.

2. Crack length - longer cracks will cover a larger number of pixels in the IR camera, giving increased accuracy.

3. Strain gage - the mounting condition and location of the strain gage(s) can affect the measurements since stress fields near the crack and mounts will be complicated

and can be significantly higher than the nominal applied stress.

4. Strain gage calibration - the strain gage calibration can influence the accuracy of the data since an improperly calibrated strain gage will not give accurate data.

Typical measurement accuracies along a crack will be 100 to 200 μ using the standard vibrothermography setup Uhl, C. J. (2009). Higher measurement accuracy can be obtained by using different lense attachments for the IR camera.

Alternative measures

Typical closure stress measurements have been taken by tracking vibration-induced heat generation while the crack is under a tensile, crack-opening bending load until the crack fully opens, terminating heat generation. Alternative measures of crack closure can be made while applying a compressional bending load to determine the compressional stress required to close different portions of a partially-open crack.

Another measurement that can be done using this method is to apply an increasing tensile static load while tracking locations of heat generation and then tracking these same locations as the tensile load is reduced to zero to measure the hysteresis in the crack opening due to applied opening and closing stresses.

Another variation of this experiment can be made using a tensile test machine to apply uniaxial tension to a cracked specimen (instead of four-point bending) to open the crack. Such a test setup would be more difficult than the ones described previously since it will require a powerful load cell, such as an Instron or MTS machine, and requires moving the entire vibrothermography measurement system to the location of the load cell. Despite these complications, such an experiment will likely provide minimal, if any, improvement in the accuracy of the measurement. Due to the complicated stress fields near the mounting pins of a three-point bending configuration and varying bending

moment along the sample, it is recommended that a three-point bending configuration is not used to measure crack closure parameters using this technique.

BIBLIOGRAPHY

Achenbach, J. D., *Reciprocity in Elastodynamics*, 90-94, 2003.

Blau, P.J., "Appendix: Static and Kinetic Friction Coefficients for Selected Materials," *ASM Handbook Volume 18: Friction, Lubrication, and Wear Technology*, 10th ed., ASM International, Materials Park, OH, pp. 70-75, 1992.

Blau, P.J., Friction Science and Technology, 2nd edition, CRC Press, New York, pp. 119-126, 2009.

Bovsunovsky, A.P., "The mechanisms of energy dissipation in the non-propagating fatigue cracks in metallic materials," *Engineering Fracture Mechanics* Volume 71, pp. 2271-2281, 2004.

Bowden, F.P. and Tabor, D., "The Friction and Lubrication of Solids," Oxford University Press, 1950.

Buck, O., Skillings, B.J., and Reed, L.K., "Simulation of closure: effects on crack detection probability and stress distributions," *Review of Progress in Quantitative Nondestructive Evaluation*, D.O. Thompson and D.E. Chimenti, Eds., Vol 2A, pp. 345-352, 1983.

Buck, O., Thompson R.B., and Rehbein, D.K., "The Interaction of Ultrasound with Contacting Asperities: Applications to Crack Closure and Fatigue Crack Growth," *Journal of Nondestructive Evaluation*, pp. 203-212 (1984).

Buck, O., Rehbein, D.K. and Thompson, R.B., "Crack tip shielding by asperity contact as determined by acoustic measurements," *Engineering Fracture Mechanics*, Vol 28, No. 4, pp. 413-424, 1987.

Budinski, K.G., *Proceedings of Wear of Materials*, American Society of Mechanical Engineers, 1991, pp. 289; modified ASTM G 98 galling test procedure.

Burger, C.P., *Handbook on Experimental Mechanics*, edited by A. S. Kobayashi, 260-276, 1987.

Chen, J.C., Kephart, J., Lick, K. and Riddell, W., "Crack growth induced by sonic IR inspection," *Nondestructive Testing and Evaluation* Volume 22:2, pp. 83-92, 2007.

Clark, R., Dover, W.D., and Bond L.J., "The effect of crack closure on the reliability of NDT predictions of crack size," *NDT International* Vol. 20, No. 5, pp 269-275, 1987.

Cowan R.S. and Winer, W.O., "Frictional heating calculations," *ASM Handbook Volume 18: Friction, Lubrication, and Wear Technology*, 10th ed., ASM International, Materials Park, OH, pp. 39-44, 1992.

DiMambro, J. Ashbaugh, D.M. Nelson, C.L. and Spencer, F.W., "Sonic Infrared (IR) Imaing and Fluorescent Penetrant Inspection Probability of Detection (POD) Comparison," *Review of Progress in Quantitative Nondestructive Evaluation*, D.O. Thompson and D.E. Chimenti, Eds., Vol 26A, pp. 463-470, 2007.

Dugdale, D.S. *Journal of the Mechanics and Physics of Solids*, Vol 8, pp. 100-104 (1960).

Elber, W., "The Significance of Fatigue Crack Closure," *Damage Tolerance in Aircraft Structures*, ASTM STP 486, pp. 230-242, 1971.

Elmore W.C. and Heald, M.A., "Physics of Waves," (Dover Publications, Inc., New York, NY, 1985), pp. 114-122.

General Magnaplate Corporation, "Friction Data Guide," 1988; TMI Model 98-5 slip and friction tester, 1.96 N (0.200 kgf) load, ground specimens, 54 % relative humidity, average of five tests.

Han, X., Zeng, Z., Li, W., Islam, M.S., Lu, J., Loggins, V., Yitamben, E., Favro, L.D., Newaz, G. and Thomas, R.L., "Acoustic chaos for enhanced detectability of cracks by sonic infrared imaging," *Journal of Applied Physics*, Volume 95:7, 3792, 2004.

Han, X., Zeng, Z., Li, W., Islam, M.S., Lu, J., Loggins, V., Favro, L.D., Newaz, G.M. and Thomas, R.L., "Importance of acoustic chaos in sonic IR imaging NDE," *Review of Progress in Quantitative Nondestructive Evaluation*, D.O. Thompson and D.E. Chimenti, Eds., Vol 23A, pp. 496-500, 2004.

Henneke, E.G., Reifsnider, K.L. and Stinchcomb, W.W., "Vibrothermography: Investigation, Development, and Application of a New Nondestructive Evaluation Technique," U.S. Army Research Office Final Report DAAG29-82-K-0180, pp. 22, 1986.

Hogmark, S., "Surface Damage," *ASM Handbook Volume 18: Friction, Lubrication, and Wear Technology*, 10th ed., ASM International, Materials Park, OH, pp. 177-183, 1992.

Holland, S.D., "First measurements from a new broadband vibrothermography measurement system," *Review of Progress in Quantitative Nondestructive Evaluation*, D.O. Thompson and D.E. Chimenti, Eds., Vol 26A, pp. 478-483, 2007.

Holland, S.D., Renshaw, J. and Roberts, R. "Measurement of dynamic full-field internal stresses through surface laser Doppler vibrometry," *Applied Physics Letters*, Vol. 91, Issue 13, 2007.

Holland, S.D., Uhl, C.J. and Renshaw, J., "Toward a viable strategy for estimating vibrothermographic probability of detection," *Review of Progress in Quantitative Non-*

destructive Evaluation, D.O. Thompson and D.E. Chimenti, Eds., Vol 27A, pp. 491-497, 2008.

Holland, S.D. and Renshaw J., "Physics-based infrared image enhancement for thermography," *NDT&E International*, under review, 2009.

Homma, C., Rothenfusser, M., Baumann, J. and Shannon, R., "Study of the heat generation mechanism in acoustic thermography," *Review of Progress in Quantitative Nondestructive Evaluation* D.O. Thompson and D.E. Chimenti, Eds., (American Institute of Physics, Melville, NY, 2006) Vol. 25, pp. 566-573.

Hsu, C., Chan, K.K. and Yu, J. *Advances in Fatigue Crack Closure Measurement and Analysis*, ASTM STP 1343, R.C. McClung and J.C. Newman, Jr., Eds., pp. 285-303 (1999).

Incropera, F.P., DeWitt, D.P., Bergman, T.L. and Lavine, A.S., "Fundamentals of Heat and Mass Transfer," 5th edition (John Wiley & Sons, 2002).

Kame, N. and Yamashita, T., "Simulation of the spontaneous growth of a dynamic crack without constraints on the crack tip path," *Geophysical Journal International* **139(2)**, 345-358, Nov. 1999.

Kobayashi, S., "Elastodynamics," *Computational Methods in Mechanics* Vol. 3 *Boundary Element Methods in Mechanics*, edited by D. E. Beskos, 1987.

Lively, J., Ouyang, Z., Brasche, L., Holland, S.D., Eisenmann, D.J., Bantel, T. and Hassan, W., "Status of FAA studies in thermal acoustics," *Review of Progress in Quantitative Nondestructive Evaluation*, D.O. Thompson and D.E. Chimenti, Eds., Vol 27B, pp. 1551-1558, 2008.

Lively, J., Ouyang, Z., Holland, S.D., Eisenmann, D.J., Meeker, W. Brasche, L., Renshaw, J. Uhl, C.J., Li, M., Bantel, T., Lawless, B., Ford, D., Patton, T., Smith, K., Singh, S. and Hassan, W., "Thermal acoustic studies of engine disk materials," FAA Report, to be published, 2009.

Lu, J., Han, X., Newaz, G., Favro, L.D. and Thomas, R.L., "Study of the effect of crack closure in Sonic Infrared Imaging," *Nondestructive Testing and Evaluation*, Vol. 22:2, pp. 127-135, 2007.

Ludema, K.C., "Sliding and Adhesive Wear," *ASM Handbook Volume 18: Friction, Lubrication, and Wear Technology*, 10th ed., ASM International, Materials Park, OH, pp. 236-241, 1992.

Luong, M.P., "Fatigue limit evaluation of metals using an infrared thermographic technique," *Mechanics of materials*, Vol 28, pp 155-163, 1998.

McClung, R.C. and Newman, J.C. Jr., Eds., *Advances in Fatigue Crack Closure Measurement and Analysis*, ASTM STP 1343, 1999.

Morbidini, M., Cawley, P., Barden, T., Almond, D. and Duffour, P., "Prediction of the thermosonic signal from fatigue cracks in metals using vibration damping measurments," *Journal of Applied Physics 100*, 104905 (AIP, Melville, NY, 2006).

Newman, J.C. Jr, *Methods and Models for Predicting Fatigue Crack Growth under Random Loading*, ASTM STP 748. J.B. Chang and C.M. Hudson, Eds., pp. 53-84 (1981).

Newman, J.C. Jr. and Elber, W., Eds., *Mechanics of Fatigue Crack Closure*, ASTM STP 982, 1988.

Newman, J.C. Jr. and Phillips, E.P., *Journal of ASTM International* Vol 1, No 8., pp. 1-19 (2004).

Pippan, R., Riemelmoser, F.O. and Bichler, C., *Advances in Fatigue Crack Closure Measurement and Analysis*, ASTM STP 1343, McClung, R.C. and Newman, J.C. Jr., Eds., pp. 41-56 (1999).

Rabiei, A., Evans, A.G. and Hutchinson, J.W., "Heat generation during the fatigue of a cellular Al alloy," *Metallurgical and Materials Transactions A* Volume 31A, 2000, pp. 1129-1136.

Reifsnider, K.L., Henneke, E.G. and Stinchcomb, W. W. "The Mechanics of vibrothermography," *Mechanics of Nondestructive Testing*, ed. Stinchcomb, W.W. (Plenum Press, New York, 1980), pp. 249-276.

Renshaw, J., Holland, S.D., and Thompson, R.B., "Measurement of crack opening stresses and crack closure stress profiles from heat generation in vibrating cracks," *Applied Physics Letters*, Vol 93, Issue 8, 2008.

Renshaw, J., Holland, S.D. and Barnard, D.J., "Viscous material-filled synthetic defects for vibrothermography," *NDT&E International*, Vol 42, Issue 8, pp. 753-756, 2009.

Renshaw, J., Holland, S.D., Thompson, R.B. and Uhl, C.J., "The effect of crack closure on heat generation in Vibrothermography," *Review of Progress in Quantitative Nondestructive Evaluation*, D.O. Thompson and D.E. Chimenti, Eds., Vol 28A, pp. 473, 2009.

Renshaw, J., Holland, S.D., Chen, J.C., Thompson, R.B. and Zhang, W., "The origin of heat generation in vibrothermography," under review *Physical Review B*.

Renshaw, J., Holland, S.D., Anderegg, J., Thompson, R.B. and Paul, R., "Vibration-induced tribological damage to fracture surfaces via vibrothermography," in preparation, 2009.

Ruhge, F., Presentation at the 28^{th} annual Review of Progress in Quantitative Nondestructive Evaluation special technical session on thermography and thermosonic NDE, Wednesday, July 23, 2008, University of Illinois-Chicago, Chicago, IL.

Schijve, J., "Fatigue crack closure: Observations and technical significance," *Mechanics of Fatigue Crack Closure*, ASTM STP 982, Newman, J.C. Jr. and Elber, W., Eds., pp. 22, 1988.

Shepard, S.M., Ahmed, T. and Lhota, J.R., "Experimental Considerations in Vibrothermography," (SPIE Thermosense, 2004).

Stoychev, S. and Kujawski, D., "Methods for crack opening load and crack tip shielding determination: a review," *Fatigue Fract Engng Mater Struct*, Volume 26, pp. 1054-1067, 2003.

Suresh, S., "Fatigue of Materials," (Cambridge University Press, New York, NY, 1998).

Uhl, C.J., "Relating crack heating to vibration for vibrothermography," (MS thesis, Iowa State University, 2008).

Uhl, C.J., Holland, S.D., and Renshaw, J., "Vibrothermographic crack heating: a function of vibration and crack size," *Review of Progress in Quantitative Nondestructive Evaluation*, D.O. Thompson and D.E. Chimenti, Eds., Vol 28A, pp. 489, 2009.

Waterhouse, R.B., "Fretting Wear," *ASM Handbook Volume 18: Friction, Lubrication, and Wear Technology*, 10th ed., ASM International, Materials Park, OH, pp. 242-256, 1992.

White, J.W. Jr. and Doner, L.W., "Honey composition and properties," Beekeeping in the United States, Agricultural Handbook Number 335, 1980.

Wulpi, D.J., "Understanding How Components Fail," (ASM International, Materials Park, OH, 1999).

Zhang, W. and Testa, R.B., "Closure effects on fatigue crack detection," ASCE *Journal of Engineering Mechanics*, Volume 125(10), pp. 1125-1132, 1999.